NUMERICAL AND EXPERIMENTAL INVESTIGATION OF AN ANNULAR DISC WITH RADIAL CRACKS

By

N. KARUPPAIAH

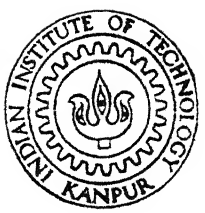

DEPARTMENT OF MECHANICAL ENGINEERING

INDIAN INSTITUTE OF TECHNOLOGY KANPUR

February, 1991

NUMERICAL AND EXPERIMENTAL INVESTIGATION OF AN ANNULAR DISC WITH RADIAL CRACKS

A Thesis Submitted
in Partial Fulfilment of the Requirements
for the Degree of
MASTER OF TECHNOLOGY

By
N KARUPPAIAH

to the
DEPARTMENT OF MECHANICAL ENGINEERING
INDIAN INSTITUTE OF TECHNOLOGY KANPUR
February, 1991

Dedicated

to my beloved

PARENTS

15/2/91

CERTIFICATE

This is to certify that this work entitled," **NUMERICAL AND EXPERIMENTAL INVESTIGATION OF AN ANNULAR DISC WITH RADIAL CRACKS** " by N. Karuppaiah has been carried out under our supervision and has not been submitted elsewhere for a degree.

Dr.P.M. Dixit,
Assistant Professor,
Department of Mech. Engg.,
I.I.T., Kanpur.

Dr.K. Ramesh,
Assistant Professor,
Department of Mech. Engg.,
I.I.T., Kanpur.

15th February 1991.

ACKNOWLEDGEMENT

I am very grateful to Dr K Ramesh for his consistent inspiration, valuable guidance and willingness to help at all times.

I am also very grateful to Dr P.M.Dixit for his methodical guidance and systematic training imparted.

I am very thankful to Shri K.G.Shastry for his help at Graphics enabling this thesis to be colourful.

I express my thanks to Messrs. R.C Maurya, K K. Bajpai, D N Sarkar, S L Srivastava, Sudhir Srivastava and other ESA Laboratory Staff for extending valuable assistance in carrying out the experimental work.

I extend my thanks to all my friends who made my stay here a very lively and pleasant one.

I am very grateful to V.R.D E , Ahmednagar for having sponsored me to do this course

And I fondly recollect the immense love and care and meticulous nurture by my parents. Words can never express my indebtness towards them.

- N KARUPPAIAH

CONTENTS

ABSTRACT

The problem of determining the stress distribution in a plate, which contains straight radial cracks originating from its outer boundary or from the boundary of a circular hole inside and which is subjected to a prescribed loading is one of great importance. For instance, plane stress analysis of radial cracks in an annular disc subjected to centrifugal and/or thermal loading is important to extend the use of Fracture Mechanics in designing practically important class of structures such as bladed disc assemblies, flywheels, clutch plates etc

One of the most important Fracture Mechanics parameter to be determined in such cases is the Stress Intensity Factor (S I.F) The present Thesis deals with the determination of S I F. for different crack lengths and number of cracks emanating from inner/outer surfaces of annular discs of different b/a ratios subjected to centrifugal loading by Finite Element Method (FEM) The program developed is also capable of finding S.I.F for discs subjected to thermal loading. Further, the Temperature distribution in a Clutch plate of an Automobile has been found using FEM and Finite Difference Methods (FDM). The concept of cyclic symmetry is used to reduce the problem size and Potter's algorithm has been used for the solution Attempts have been made also to evaluate S.I.F for rotating annular disc experimentally using the Photo-elastic coatings and Strain-gauge techniques.

LIST OF TABLES

LIST OF FIGURES

CHAPTER 1

INTRODUCTION

1.1 Introduction:

A majority of large scale failures in diverse structures such as storage tanks, pressure vessels, pipe lines, bridges, ships, turbines, generator rotors, flywheels, rocket motors, aircraft etc., have been invariably traced to the presence of cracks originating from a site of stress concentration These cracks develop and grow to critical sizes that bring about complete fracture at loads that were by no means anywhere near the critical load of the structure in the uncracked condition Fracture Mechanics is primarily concerned with the strength of cracked structures or components of a machine It provides a methodology by which one can characterise the strength of a structure in the presence of cracks

1.2 The Radial Crack Problem and the Present Work:

The problem of determining the stress distribution in a plate, which contains straight radial cracks originating from its outer boundary or from the boundary of a circular hole inside and which is subjected to a prescribed loading is one of great importance. For instance, plane stress analysis of radial cracks in an annular disc subjected to centrifugal and/or thermal loading is important to extend the use of Fracture Mechanics in designing practically important class of structures such as bladed disc assemblies, flywheels, clutch plates etc. Similarly, the plane strain problem is relevant to the study of the action of internal pressure in the interior of hollow cylinders of large wall thicknesses with radial cracks originating from the inner surface.

One of the most important Fracture Mechanics parameter to be determined in such cases is the Stress Intensity Factor (S.I.F.). The problem of cracks emanating from inner boundary of

an annular disc with internal pressure has been previously studied for large number of cracks [1-7] The present Thesis deals with the determination of S.I F for different crack lengths and number of cracks emanating from inner/outer surfaces of annular discs of different b/a ratios, subjected to centrifugal loading by Finite Element Method (FEM). The program developed is also capable of finding S.I F for discs subjected to thermal loading Further, the Temperature distribution in a clutch plate has been found using FEM and Finite Difference Methods (FDM). The concept of cyclic symmetry is used to reduce the problem size and Potter's algorithm has been used for the solution. Attempts have been made also to evaluate S I F for rotating annular disc experimentally using the Photo-elastic coatings and Strain-gauge techniques

1.3 Thesis Layout:

Chapter 2 discusses the Finite Element Formulation of the problem of Plane Elasticity It discusses the suitable choice of the element to model the inverse square root singularity required for elastic analysis of crack It also describes the method to calculate S.I.F. The Post-Processor developed, to present the output data pictorially have also been discussed S.E.N. specimen subjected to tensile loading has been modelled using the crack-tip element chosen and its different contours obtained through the Post-Processor have been displayed.

Chapter 3 explains the Potter's solution algorithm to solve a problem which is cyclically symmetric.

Chapter 4 discusses the evaluation of S.I.F. in the case of a rotating annular disc with radial cracks S I F.'s calculated numerically for different cases have been presented graphically. $\sigma_r, \sigma_\theta, (\sigma_1-\sigma_2), (\sigma_1+\sigma_2), u_r$ and u_θ contours developed through the Post-Processor have been displayed for one set of inner and outer cracks

Chapter 5 discusses the evaluation of S.I.F in the case of an annular disc with radial cracks subjected to thermal loading It also discusses the application of FEM and FDM techniques to find the Temperature distribution in an Automobile Clutch plate A sample problem has been solved and the results are presented graphically

Chapter 6 discusses the experimental methods using Strain Gauges and Photo-elastic Coatings to determine the S I F 's of a S E N. specimen and a Rotating disc with radial cracks Isochromatics in such cases, observed through the Polariscope are also displayed.

CHAPTER 2

FINITE ELEMENT FORMULATION OF PLANE ELASTICITY

2.1 Introduction

In this chapter, the general finite element formulation for elastic bodies with cracks in a state of plane stress/strain subjected to body force, surface force and thermal loading is discussed Formulation of the eight noded isoparametric crack-tip element is discussed in detail. The value of Stress Intensity Factor (S.I F) is calculated for a Single Edge Notched (S.E N.) specimen by F.E.M. using the crack-tip element. The results compare well with analytical solution

2.2 Problem of Plane Elasticity

Consider a linear elastic solid of uniform cross-section and dimension 'h' in the z-direction This 3-dimensional problem could be simplified to a 2-dimensional problem under two different conditions, one, when the thickness 'h' is very small compared with lateral dimensions (say, in x,y directions) and the other when the thickness 'h' is very large These are called plane stress and plane strain problems respectively when subjected to further conditions as described below .

2.2.1 Plane Stress

When a thin disc is subjected to support conditions and external forces on the lateral boundary which are in the plane of the disc and which do not vary across the thickness as shown in Fig 2.1, the body is said to be in a state of plane stress

For plane stress problems, the above assumptions imply that all the associated stresses with the z-direction are negligibly small. i.e.,

$$\sigma_{zz} = \tau_{xz} = \tau_{yz} = \emptyset \qquad (2\ 1)$$

and the remaining stresses are independent of z

2.2.2 Plane Strain

When a cylindrical/prismatic body is subjected to support conditions and external forces which have no components along the axis of the cylinder/prism (in z direction) and the remaining components do not change along the axis, as shown in Fig 2.2, the body is said to be in a state of plane strain

For plane strain problems, all strain components associated with the z-direction are zero, i.e,

$$\epsilon_{zz} = \epsilon_{xz} = \epsilon_{yz} = \emptyset \qquad . \quad (2\ 2)$$

and the remaining components are independent of z. Then, it is enough to analyse only a slice of the body

Although ϵ_z is non-zero in plane stress problems and σ_z is present in plane strain problems, these components can be eliminated from the governing equations.

2.3 Governing Equations of Plane Elasticity Problems

2.3.1 Strain-Displacement relation

When the deformation is small, the total strain in a body in case of plane elasticity problems can be expressed in terms of the following strain-displacement relations.

$$\epsilon_x = \partial u/\partial x,\ \epsilon_y = \partial v/\partial y,\ \tau_{xy} = \partial u/\partial y + \partial v/\partial x, \qquad ..(2.3)$$

where u & v are displacement components in x & y directions respectively.

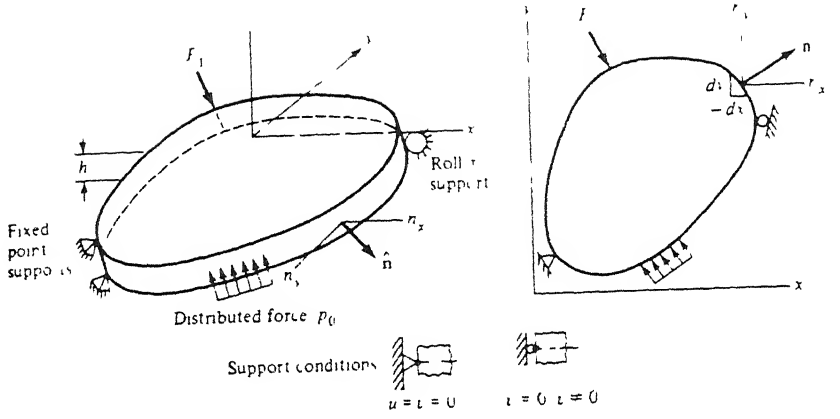

FIG 2.1 Problem of Plane Stress in Plane Elasticity

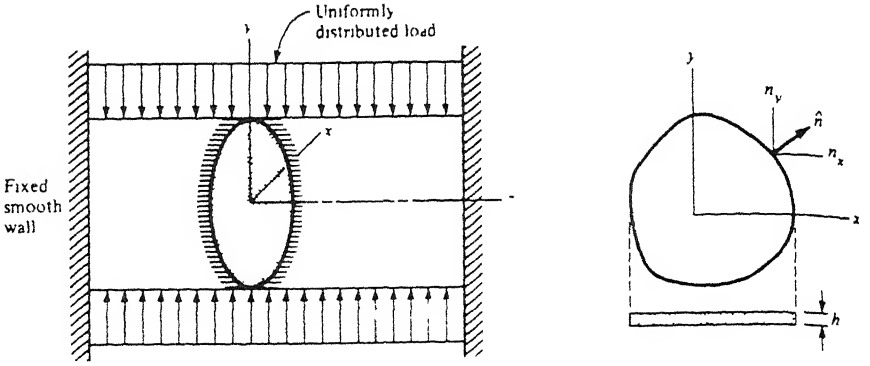

FIG 2 2 Problem of Plane Strain in Plane Elasticity

In the Matrix form, we have

$$\{\epsilon\} = [L]\{u\} \qquad (2\ 3a)$$

where the strain vector $\{\epsilon\}$, the displacement vector $\{u\}$ and the operator matrix [L] are given by

$$\{\epsilon\} = \begin{Bmatrix} \epsilon_x \\ \epsilon_y \\ \tau_{xy} \end{Bmatrix}, \quad [L] = \begin{bmatrix} \partial/\partial_x & \emptyset \\ \emptyset & \partial/\partial_y \\ \partial/\partial_y & \partial/\partial_x \end{bmatrix}, \quad \{u\} = \begin{Bmatrix} u \\ v \end{Bmatrix} \qquad (2\ 3b)$$

The total strain at a point in a body is the sum of two parts mechanical strain due to stress and thermal strain The strain due to temperature change even in the absence of stress is called thermal strain. For an isotropic material, symmetry arguments show that the thermal strain must be a pure expansion or contraction with no shear-strain componenets referred to any set of axes. For moderate temperature change, the thermal strains due to a change in temperature from T_o to T can be expressed as

$$\begin{aligned} (\epsilon_x)_o^t &= \alpha(T-T_o) \\ (\epsilon_y)_o^t &= \alpha(T-T_o) \\ (\gamma_{xy})_o^t &= \emptyset \end{aligned} \qquad \ldots(2.4)$$

where α is the coefficient of linear expansion.

2.3.2 Stress - Strain Relations

Simplifying the three-dimensional equations relating stress to the mechanical strain for a linear isotropic material in the case of plane stress problem ($\sigma_z = \emptyset$), we get

$$\sigma_x = \frac{E}{1 - v^2}[v(\epsilon_x - \epsilon_{xo}) + (\epsilon_y - \epsilon_{yo})]$$

$$\sigma_y = \frac{E}{1 - v^2}[v(\epsilon_x - \epsilon_{xo}) + (\epsilon_y - \epsilon_{yo})]$$

$$\tau_{xy} = \frac{E}{2(1 + v)}\gamma_{xy} \qquad \ldots(2.5)$$

where 'E' is the Young's modulus and 'v' is the Poisson's ratio

In the Matrix form, these equations can be written as

$$\{\sigma\} = [D]\ (\{\epsilon\} - \{\epsilon\}_o) \qquad ..(2.5a)$$

where,

$$\{\sigma\} = \begin{Bmatrix} \sigma_x \\ \sigma_y \\ \tau_{xy} \end{Bmatrix} \qquad . (2.5b)$$

is the stress vector,

$$\{\epsilon_o\} = \begin{Bmatrix} \alpha(T-T_o) \\ \alpha(T-T_o) \\ \emptyset \end{Bmatrix} \qquad (2.5c)$$

is the thermal strain vector &

$$[D] = \frac{E}{1-\nu^2} \begin{bmatrix} 1 & \nu & \emptyset \\ \nu & 1 & \emptyset \\ \emptyset & \emptyset & 1-\nu/2 \end{bmatrix} \qquad . .(2\ 5d)$$

is the elasticity matrix for plane stress

Similarly, we get the stress-strain relations for a plane strain problem ($\epsilon_z=\emptyset$). These equations can also be put in the Matrix form as

$$\{\sigma\} = [D]\ (\{\epsilon\} - \{\epsilon_o\}) \qquad ...(2.6)$$

where,

$$[D] = \frac{E}{(1+\nu)(1-2\nu)} \begin{bmatrix} 1-\nu & \nu & \emptyset \\ \nu & 1-\nu & \emptyset \\ \emptyset & \emptyset & 1-2\nu/2 \end{bmatrix} \qquad ...(2.6a)$$

is the elasticity matrix and

$$\{\epsilon_o\} = (1+\nu) \begin{Bmatrix} \alpha(T-T_o) \\ \alpha(T-T_o) \\ \emptyset \end{Bmatrix} \qquad ...(2.6b)$$

is the thermal strain for Plane Strain problems.

2.3.3 Equilibrium Equation

Force equilibrium of an infinitesimal particle gives rise to the following equilibrium equations

$$\frac{\partial \sigma_x}{\partial x} + \frac{\partial \tau_{xy}}{\partial y} + F_x = \emptyset \qquad \ldots (2.7a)$$

$$\frac{\partial \tau_{xy}}{\partial x} + \frac{\partial \sigma_y}{\partial y} + F_y = \emptyset \qquad \ldots (2.7b)$$

where F_x & F_y are the body forces along the x & y directions respectively.

2.3.4 Boundary Conditions

Formulation of a solid mechanics problem is not complete without the boundary conditions The typical boundary conditions are as follows First, the total boundary Γ is divided into two parts, i e

$$\Gamma = \Gamma_u \cup \Gamma_t \qquad \ldots (2\ 8)$$

i) Displacement boundary conditions

Displacement components are specified on Γ_u

$$u = u^*$$
$$v = v^* \qquad \ldots (2.8a)$$

ii) Stress boundary conditions

Stress components are specified on Γ_t

$$T_x = T_x^*$$
$$T_y = T_y^* \qquad \ldots (2.8b)$$

where the surface traction components (T_x, T_y) are related to the stress tensor components $(\sigma_x, \sigma_y, \tau_{xy})$ by the relation

$$\begin{bmatrix} \sigma_x & \tau_{xy} \\ \tau_{xy} & \sigma_y \end{bmatrix} \begin{Bmatrix} n_x \\ n_y \end{Bmatrix} = \begin{Bmatrix} T_x \\ T_y \end{Bmatrix} \qquad \ldots(2\ 8c)$$

where n_x and n_y are the components of the unit outward normal

Thus, the formulation of a typical plane elasticity problem consists of

i) Strain-Displacement relations (Eq.(2.3a))
ii) Stress-Strain relations (Eq (2 5a))
iii) Equilibrium equations (Eqs (2.7a-b))
and iv) Boundary conditions (Eqs (2 8a-b))

Even though these equations are linear, they are quite difficult to tackle analytically, especially when the geometry of the domain is complicated. The alternate method to solve a Solid-Mechanics problem is to minimise the total potential

2.4 Total potential energy

The total potential is given by

$$I = \int_V U dV - \int_V \{F\}^T \{u\}\, dV - \int_A \{T\}^T \{u\}\, dA \qquad ..(2.9)$$

where $\{F\} = \begin{Bmatrix} F_x \\ F_y \end{Bmatrix}$ is the body force vector . .(2 9a)

$\{T\} = \begin{Bmatrix} T_x \\ T_y \end{Bmatrix}$ is the surface force vector ...(2.9b)

and U is the strain energy density given by

$$U = \tfrac{1}{2} \{\sigma\}^T \{\epsilon\}$$
$$= \tfrac{1}{2} \{\epsilon\}^T [D] \{\epsilon\} - \{\epsilon\}^T [D] \{\epsilon_o\} \qquad \ldots(2.10)$$

The most widely used method for minimization of the total potential is the Finite Element method as described below.

2.5 8 noded isoparametric element

The unique description of the displacement within each element in terms of nodal values at boundary points or internal points of the element is the basic step in any displacement finite element formulation and can be expressed as

$$\{u\} = [N]\{u\}^e \qquad .(2\ 11)$$

where $\{u\}$ is the displacement vector,
$[N]$ is the shape function matrix,
$\{u\}^e$ is the nodal displacement vector of the element.

If the order of the shape functions chosen to describe the element geometry are identical to those used to prescribe the independent variable, then the element is termed isoparametric. A typical isoparametric element is shown in Fig.(2 3). The functional property of the interpolation function 'N_i' is that its value in the natural co-ordinate system is unity at node 'i' and zero at all other nodes For a two dimensional 8-noded element, a quadratic variation of the displacement and geometry are assumed for which interpolation functions N_1 to N_8 are given in Appendix A Thus, it has 16 displacement degress of freedom, two degrees of freedom at each node. Cartesian co-ordinates x , y and 2natural co-ordinates r_i, s_i are related as follows .

$$x = N_1x_1 + N_2x_2 + \ . \ + N_8x_8 \qquad .. \quad (2.11a)$$
$$y = N_1y_1 + N_2y_2 + \ ... \ + N_8y_8 \qquad ... \quad (2.11b)$$

Similarly, the displacements expressed in nodal values are :

$$u = N_1u_1 + N_2u_2 + \ . \ + N_8u_8 \qquad . . \quad (2.11c)$$
$$v = N_1v_1 + N_2v_2 + \ ... \ + N_8v_8 \qquad .. \quad (2.11d)$$

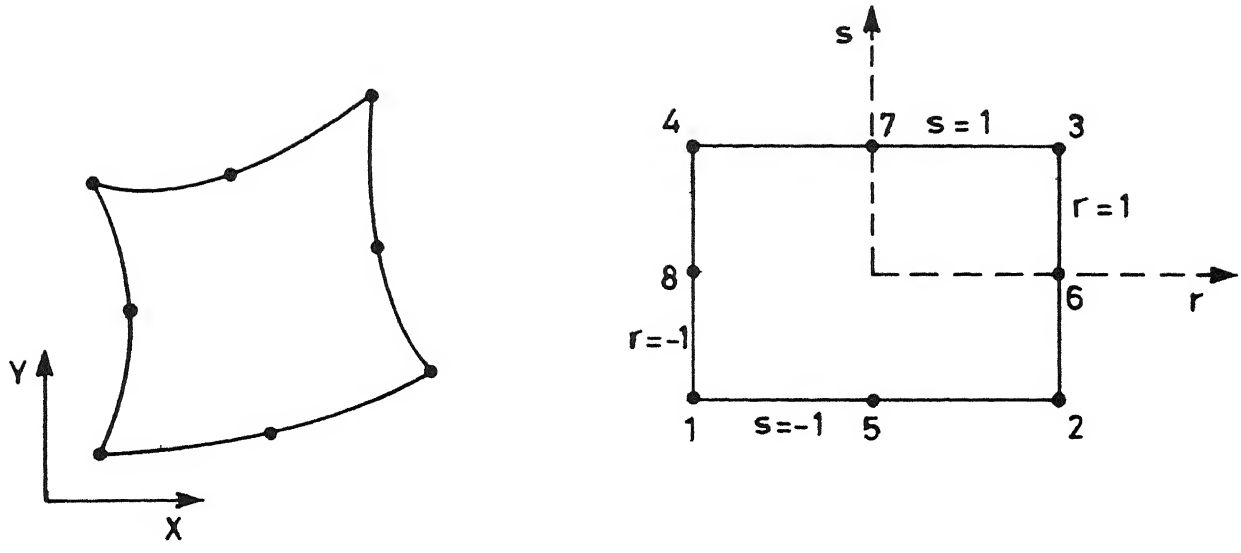

Fig. 2.3 Isoparametric transformation for a quadratic element from global to normalised co-ordinates.

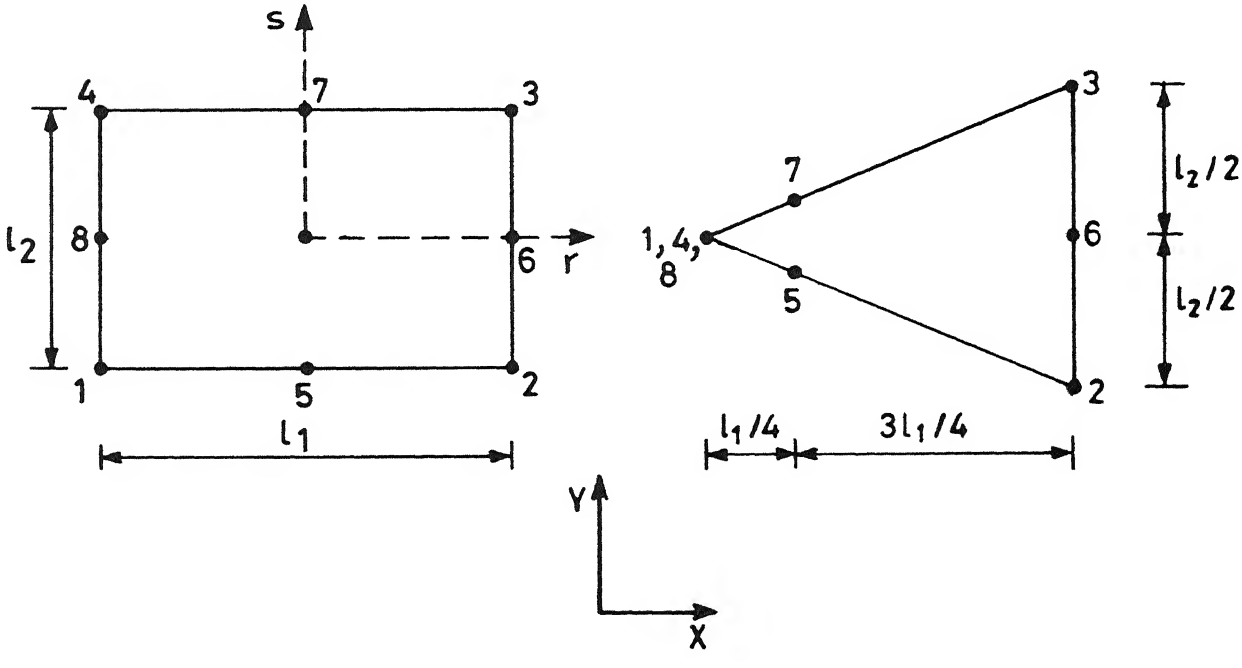

Fig 2.4 2-D triangular element with mid sides nodes at quarter point from rectangular isoparametric element.

Therefore, the shape function matrix [N] and the nodal displacement vector $\{u\}^e$ can be written as

$$\{u\}^e = \begin{Bmatrix} u_1 \\ v_1 \\ . \\ u_8 \\ v_8 \end{Bmatrix} \qquad (2\ 12a)$$

$$[N] = \begin{bmatrix} N_1 \ \emptyset \ N_2 & . & . N_8 \ \emptyset \\ \emptyset \ N_1 \ \emptyset & & \emptyset \ N_1 \end{bmatrix} \qquad (2.12b)$$

When the discretisation (2.11) is substituted in the Eq (2 9) for total potential, we get

Total potential

$$I = \sum_{e=1}^{n_e} (\tfrac{1}{2}\{u\}^{eT}[K]^e\{u\}^e - \{u\}^{eT}\{f_t\}^e - \{f_b\}^{eT}\{u\}^e) - \sum_{b=1}^{n_b} (\{f_s\}^{bT}\{u\}^b) \qquad (2.13a)$$

where n_e is no. of area elements & n_b is no. of boundary elements &

$[K]^e$ = element stiffness matrix

$$= \iint [B]^T[D][B]\ t\ dxdy \qquad ..(2\ 13b)$$

$\{f_b\}^e$ = Element Body force vector

$$= \iint [N]^T\{F\}\ t\ dxdy \qquad ...(2.13c)$$

$\{f_t\}^e$ = Element Thermal force vector

$$= \iint [B]^T[D]\{\epsilon_o\}\ t\ dxdy \qquad ...(2\ 13d)$$

& $\{f_s\}^e$ = Element surface force vector

$$= \int [N]^T \{T\}\, t\, db \qquad (2\ 13e)$$

The above expression for I can be written in terms of the Global Matrices as

$$I = \tfrac{1}{2} \{U\}^T [K] \{U\} - \{F_b\}^T \{U\} - \{F_t\}^T \{U\} - \{F_s\}^T \{U\} \qquad (2.14)$$

where {U} is the Global displacement vector and the Global Matrices [K], $\{F_b\}$, $\{F_t\}$, $\{F_s\}$ contain the contributions from all the elements Minimization of the expression (2.14) with respect to {U} gives,

$$[K]\{U\} = \{F\} \qquad (2\ 15)$$

where $\{F\} = \{F_b\} + \{F_t\} + \{F_s\}$ (2 15a)

2.6 Crack-tip Element Formulation

2.6.1 Elastic Singularity at the Crack-tip

Linear elastic fracture mechanics is based on the concept that the stress tensor (σ_{ij}) near the crack tip (taken as origin of the polar co-ordinate system) is given by the Westergaard solution in the form given by Irwin (Broek [1]),

$$\sigma_{ij} = K\,(2\pi r)^{-\frac{1}{2}}\ f_{ij}(\theta) \qquad (2.16)$$

where, K is the Stress intensity factor and designated as K_I, K_{II}, and K_{III} for the fracture modes I, II, & III respectively $f_{ij}(\theta)$ represents the distribution of stress and depends on the mode of fracture.

The above expression shows that at the crack-rip, singular stress field exists and it is popularly known as inverse square root singularity.

Any finite element procedure should take into account this fact while modelling the crack tip Earlier investigators used CST (constant strain triangle) element of very small size of the order of 1/100 (l is the crack length) near the crack-tip to model the strain gradient appropriately However, in the last few decades many new elements have been proposed by different investigators which take care of the inverse sequare root singularity and one can afford to use larger size elements near the crack tip Elements based on classical solution displacement fields, polynomial displacement fields and Isoparametric concepts as well as hybrid formulation are reported in the literature

Among the above elements quarter-point singular elements are very popular essentially due to the availability of the quadratic isoparametric serendipity element in almost all general purpose programs

2.6.2 Historical Overview of Quarter Point Elements

Barsoum [8] and Henshell and Shaw [9] have independently demonstrated that the inverse square root singularity characteristic of linear elastic fracture mechanics can be obtained in the two-dimensional 8-noded isoparametric element (Q8) when the midside nodes near the crack tip are placed at the quarter-point. This concept was subsequently extended to plate bending and shell fractures by Barsoum [10].

Barsoum [11] then showed that the triangular element formed by collapsing one side of the Q8 led to far better results than the rectangular element. Freese and Tracey [12] have shown that the natural isoparametric triangle (NIT) and the collapsed quadrilateral perform equally well If the side opposite to the crack tip is curved, then there is a substantial deterioration in the SIF calculation from the collapsed quadrilateral, and no change in the NIT. Such a discrepancy is caused by the fact that a collapsed 8-node quadrilateral does not actually degenerate into a NIT.

The extension of the quadratic isoparametric quarter-point element to cubic isoparametric was proposed by Pu et al [13] Yamada et al [14] extended the concept of the 8-noded isoparametric element to the variable numbering element

Hibbitt [15] proved that the singular rectangular element has a singular stiffness while the triangular one does not, and that in the collapsed quadrilateral element the singularity prevails along the two sides only, while it is omnipresent inside the triangular element He attributed to this difference the better results achieved by the triangular element as reported by Barsoum [11] He also demonstrated that a variety of stress singularities (1/n) can be achieved by isoparametric elements with a polynomial approximation of order n In a recent paper Ying [16] has shown that in his investigation Hibbitt [15] erroneously concluded that the strain energy of a rectangular quarter-point element is singular, but that, as previously known, the singularity is along the edges and diagonal only. Also discussed by Ying [16] is the error associated with the location of the 'quarter point' of a singular element This was further elaborated by Barsoum's [17] discussion of the previous work, where he has shown that the error in estimating the SIF is one order of magnitude smaller than the discretization error in locating the 'quarter point' Hence, the exact location of the midside node is not crucial as long as the discretization error is small. Also, by having multiple independent nodes (of a collapsed Q-8 element), Barsoum [18] has shown that small-scale yielding (characterized by 1/r singularity) could be modelled

Lynn and Ingraffea [19] generalized the concept of the quarter-point singular element, and have shown that by varying the placement of the side node, between quarter and mid-point, one can control the point where singularity is to occur (between the corner node and infinity, respectively). This led to the introduction of the transition element which, when inserted

around the singular elements, resulted in improved SIF calculations as 1/a ratio is decreased. Again, Hussain et. al [2Ø] extended the concept of quadratic transition element to cubic transition elements

Lynn and Ingraffea [19] investigated both the effect of the 1/a (element length over total crack length) and aspect ratio of the singular elements. An optimum ratio of 1/a = Ø.25 was reported, while it was found that the aspect ratio effect was relatively unimportant Another detailed investigation of the optimum quarter-point element size was carried out by Ingraaffea and Manu, [21] where 1/a was varied from Ø.2 to Ø Ø3 in both two and three-dimensional analyses The errors in the two-dimensional results varied from 8 percent for 1/a = Ø.2 to -1 percent for 1/a = Ø Ø3

An assessment of the quarter-point elements (in pressure vessel fracture analysis) was offered by Barsoum [22] for both two and three dimensional analysis Three sources of modelling errors, associated with the quarter-point elements, were discussed: (a) those associated with the type of quarter-point element, triangular or rectangular, (b) those associated with the configuration of the element boundary, straight or curved; and (c) those associated with the location of the 'quarter point' node. Barsoum [22] indicates that (a) triangular elements are to be preferred over the quadrilateral ones (whether collapsed or not); (b) the sides of the element should not be curved; and (c) a perturbation of the 'quarter point' node by e, leads to an error in calculating the stress intensity factor of ge, where g is the ratio of crack tip element to crack length

Harrop [23] qualitatively discussed the optimum size of quarter-point crack tip elements He indicates that the singular element can represent the stress singularity and a constant finite stress term only Thus, any singular element which is 'too large' cannot represent nonlinear (and non-singular) stress variation in a structure On the other hand, by using a

singular element which is 'too small', the error in representing the finite stress term decreases, but the region of the mesh representing the stress singularity also decreases This source of error would still hold even if transition elements were used. He thus pointed out that some crack tip element size has to be optimum, and concluded that ' . it is clearly impossible to recommend a particular crack tip element size suitable for all situations.'

Saouma and David Schwemmer [24] conducted a parametric numerical evaluation of the 'quarter-point' singular elements for 272 test cases The modified parameters were the order of the integration, aspect ratio, number of elements surrounding the crack-tip, use of transition elements, the singular element length over the total crack length, and the symmetry of the mesh around the crack tip Based on their analysis the following recommendations were made for the 'best usage' of the quarter-point singular element It is claimed that the SIF calculations are within 10 % of the analytical result

1 Use (2x2) reduced integration scheme.
2. Use at least four (in pure mode I problems) singular elements around a crack tip
3. Have the internal angles of all the singular elements, around the crack tip approximately equal to 45 degress.
4 Unless an excessive small l/a ratio is used little improvement is achieved by using transition elements.
5 For problems, with uniform non-singular stress distribution, little improvement is achieved by using small l/a.
6 For problems where a non-singular stress gradient is expected, l/a should be less than 0.5.

These recommendations were taken as guidelines for using the Q-P elements in the present work.

2.6.3 Quarter Point Element Implementation Consideration

Singular triangular element is obtained by collapsing the nodes 1,4 and 8 and moving the nodes 7 and 5 to the quarter point as shown in Fig (2 4). Thus, globally the nodes 1,4 and 8 are assigned the same co-ordinates and the same node number Barsoum [18] has shown that by assigning different node numbers for nodes 1,4 and 8 globally, one can simulate 1/r singularity which is prevalent in elastic-perfectly plastic problem

2.6.4 Stress Intensity Factor Calculation

One of the most important param eter to be determined in fracture mechanics analysis is the SIF It is a function of the loading on the cracked configuration and of the size and shape of the crack and other geometric boundaries It has the dimension of stress * √(length). Crack tip opening displacement (CTOD) method has been used to evaluate SIF In CTOD method, displacement u_c at the quarter point of the singular element on the face of the crack is noted and the following relation [6] is used to calculate the S I F.

$$K_I = \frac{E\, u_c}{(1+v)\,(1+K)} \,(2\pi/r)^{1/2} \qquad \ldots(2.17)$$

where,

r is the distance from the crack tip,

and K = (3-v)/(1+v) for plane stress and

= (3-4v) for plane strain

2.7 Post Processor [25]

Postprocessor displays the output data in a meaningful way The deformed structure can be displayed, either superimposed on its undeformed state or contours of stress, displacement can be plotted.

The procedure for plotting the contours is simple Each element is divided into a number of triangles (in the present case, six) such that vertices of the triangles are the nodes. The element is so divided that the triangles do not overlap each other The program assumes linear variation along the sides of the triangle Depending upon the value for which contour is plotted, the point is located on each sides of the triangle, if present. These points are joined together to form the contour in that triangle The program also has the fill option. In this, the zone between two successive contours is filled with a suitable colour The program developed can use 256 different colours and the range of each coloured contour is also displayed.

The plotting of displacement contours is straight forward since in the displacement formulation of FEM, the results obtained directly give these values at the nodes. For plotting contours of stress, one has to evaluate these, based on displacement values In some cases transformation to global cartesian will be required

As stresses are not accurate on the element boundary [26], they have been calculated at the gauss points of each elements. These stresses are extrapolated to the corner nodes by the following relation,

$$[\sigma]_C = [T]\,[\sigma]_g$$

where $[\sigma]_C$ is stress at corner nodes,

$[\sigma]_g$ is stress at gauss points,

and

$$[T] = \begin{bmatrix} 1+(\sqrt{3}/2) & -0.5 & 1-(\sqrt{3}/2) & -0.5 \\ -0.5 & 1+(\sqrt{3}/2) & -0.5 & 1-(\sqrt{3}/2) \\ 1-(\sqrt{3}/2) & -0.5 & 1+(\sqrt{3}/2) & -0.5 \\ -0.5 & 1-(\sqrt{3}/2) & -0.5 & 1+(\sqrt{3}/2) \end{bmatrix}$$

is the transformation matrix

The values of stress components at midside nodes are averages of the values at the corner nodes adjacent to the midside nodes

i.e ,

$\sigma_5 = (\sigma_1 + \sigma_2)/2$
$\sigma_6 = (\sigma_2 + \sigma_3)/2$
$\sigma_7 = (\sigma_3 + \sigma_4)/2$
$\sigma_8 = (\sigma_4 + \sigma_1)/2$

The nodes which lie on more than one element will have different values of stress corresponding to each element The value averages over all the elements to which the node belongs is considered as the stress at that node.

2.8 EVALUATION OF S.I.F. IN AN S.E.N. SPECIMEN

In order to test the 8-noded isoparametric quadrilateral crack-tip element, the problem of Single Edge Notched (S E.N.) specimen subjected to tensile loading is taken and its S.I F.(K_I) is evaluated The mesh chosen for the problem is shown in Fig (2.5)

The stiffness matrix discussed in Sec.(2 5) is referred to cartesian co-ordinates Due to symmetry of the problem, at 11-21 & 267-272, Y-displacement is suppressed and at nodes 253-265, X-displacement is suppressed. To impose the Force boundary condition, the product of the applied stress (σ) and element length on which the stress is applied, is distributed in the ratio 1/6 : 1/6 . 2/3 for two corner nodes and mid-side node respectively

The assembled stiffness matrix in banded form is solved by the Gaussian Elimination method. C T O D method has been used to calculate the S.I.F.

Analytically, the value of S.I.F. for S E.N. specimen is given as,

$$K_I = (1.1215 - 0.23 (a/w)) \sigma \sqrt{\pi a}$$

where a/w is the ratio of the crack length to width of the specimen

The results from both the methods are compared in Tab.(2 1). Various contours such as $(\sigma_1-\sigma_2)$,$(\sigma_1+\sigma_2)$,σ_x,σ_y,τ_{xy}, u_x,u_y and deformed mesh, developed through the Post-processor are shown in Figs (2.6-2 11). These figures validate the correctness of the crack-tip element used

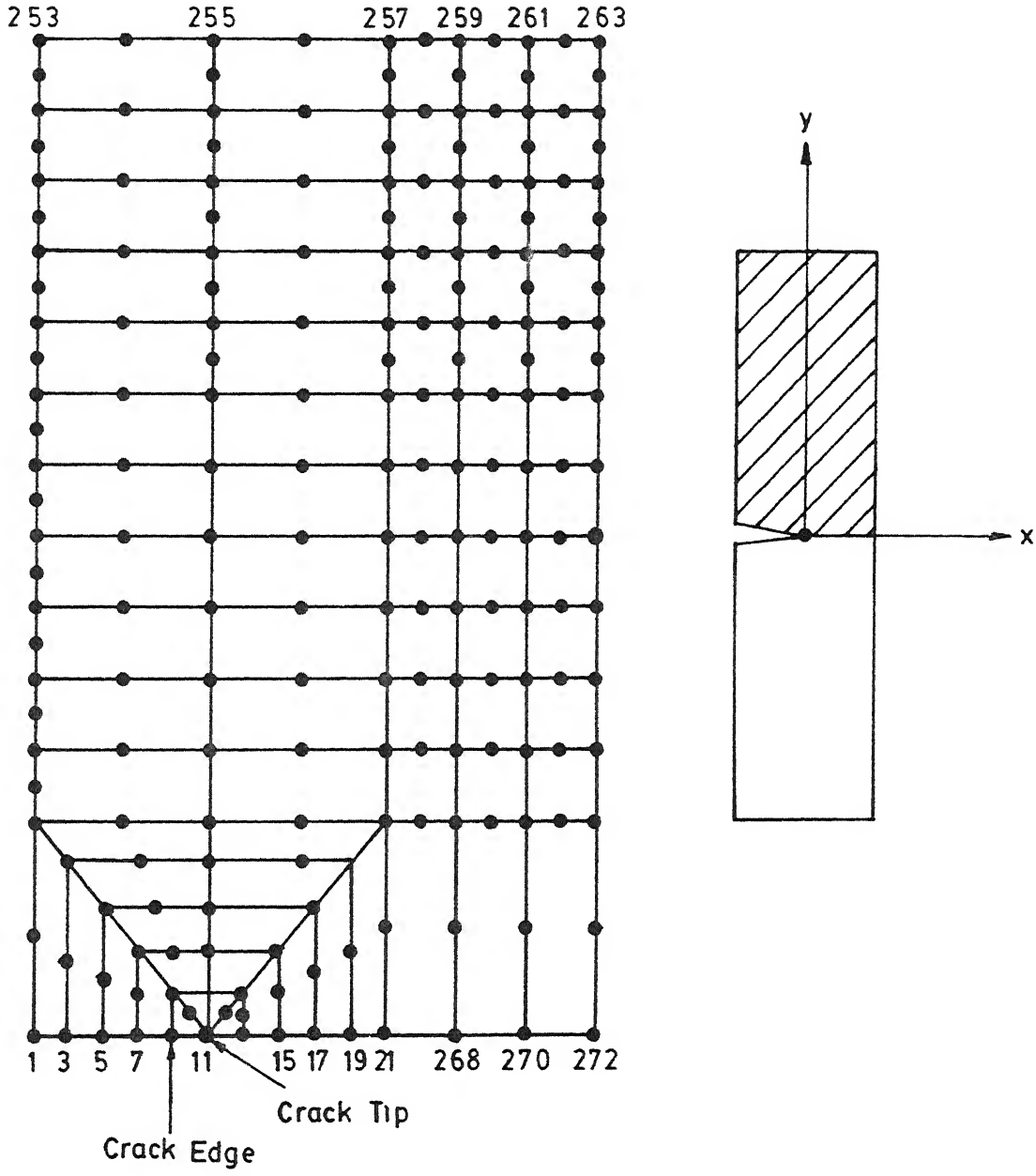

FIG. 2·5 MESH FOR S.E.N. SPECIMEN

S. No	Method	S.I F (MPa√m)
1	Analytical	478
2	F.E.M	489

Table 2.1 S.I.F's for S.E.N. Specimen

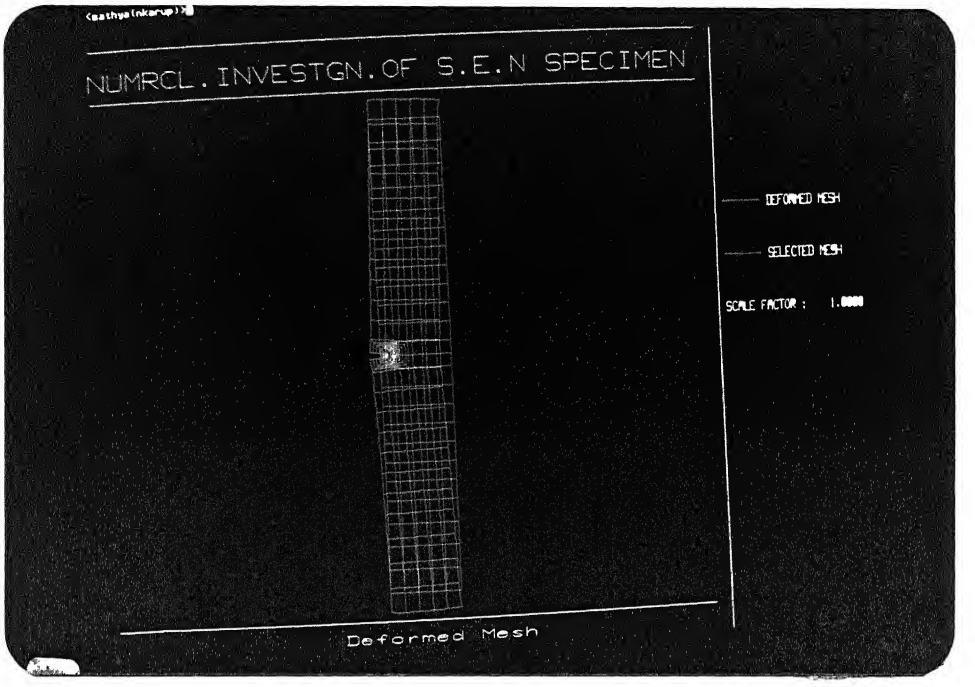
NUMRCL.INVESTGN.OF S.E.N SPECIMEN
DEFORMED MESH
SELECTED MESH
SCALE FACTOR : 1.0000
Deformed Mesh

FIG 2 6

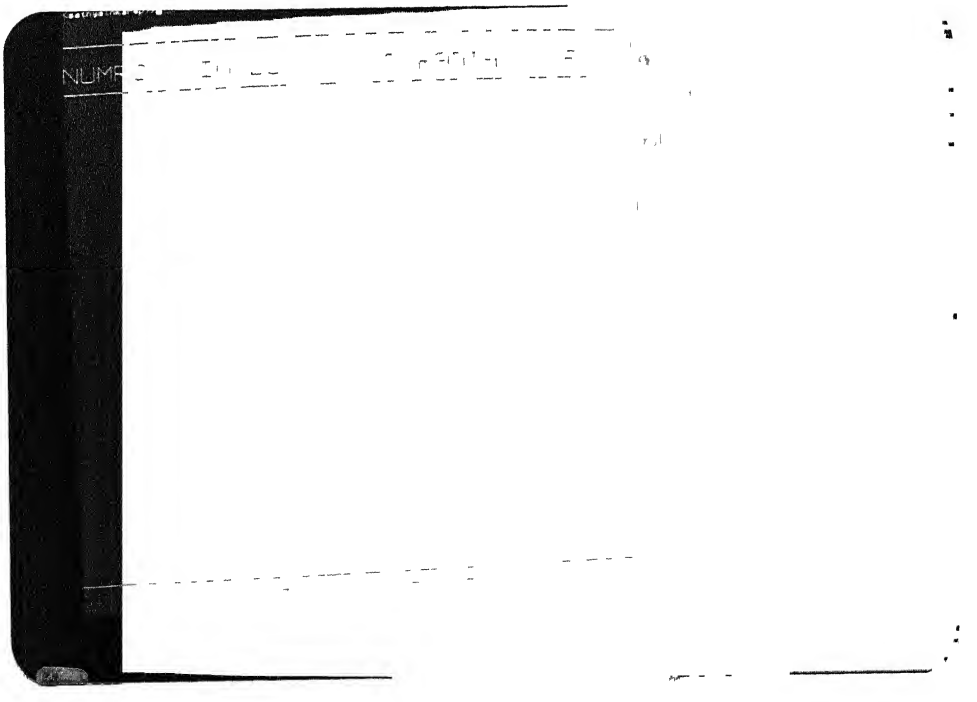

FIG 2 7

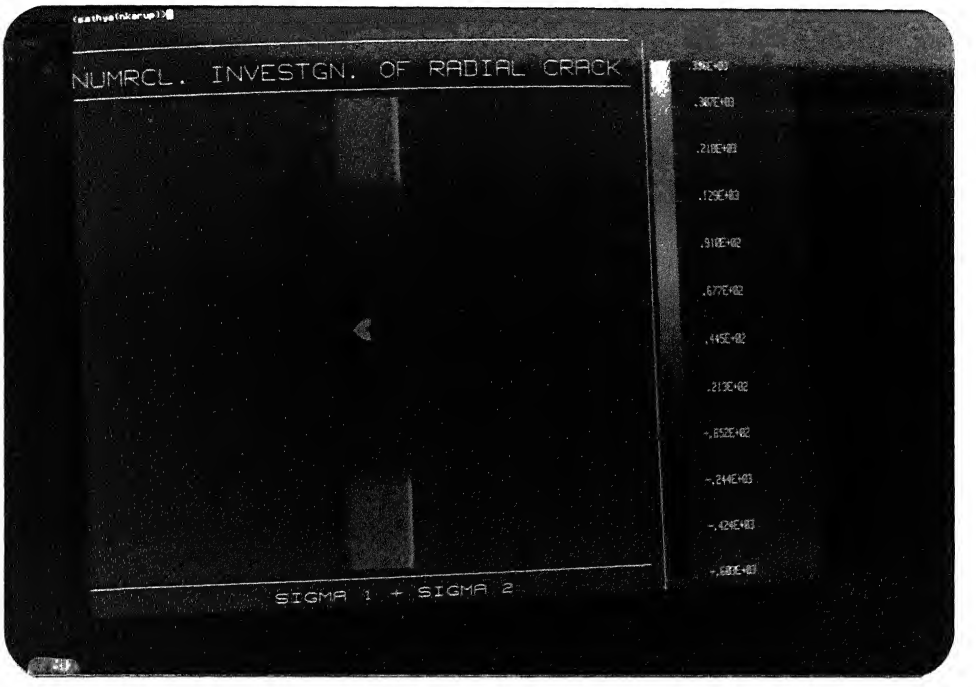
NUMRCL. INVESTGN. OF RADIAL CRACK
SIGMA 1 + SIGMA 2

FIG 2 8

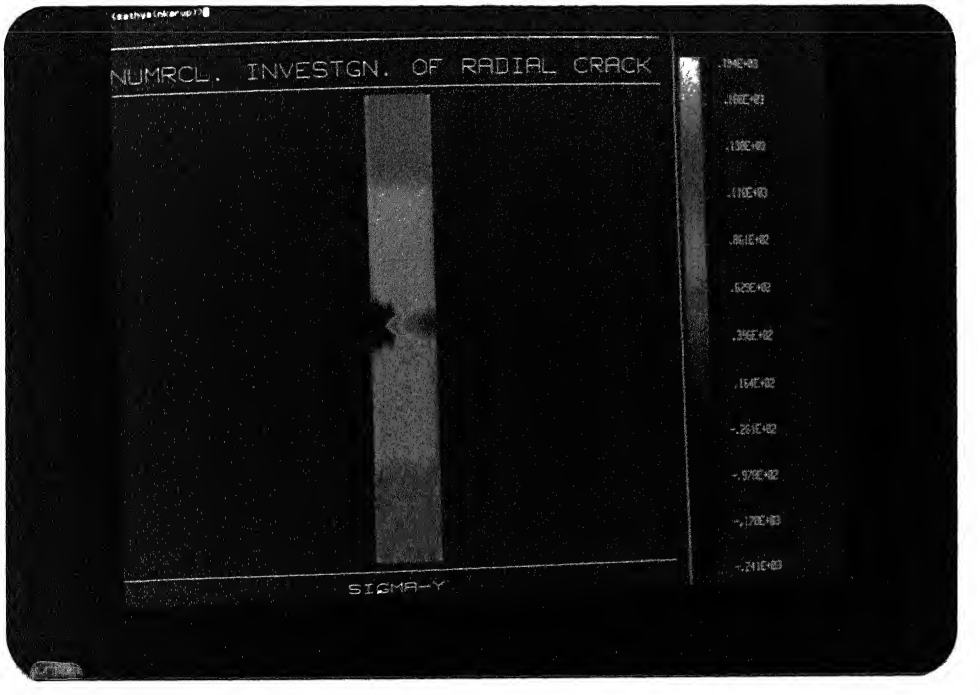
NUMRCL. INVESTGN. OF RADIAL CRACK
SIGMA-Y

FIG. 2.9

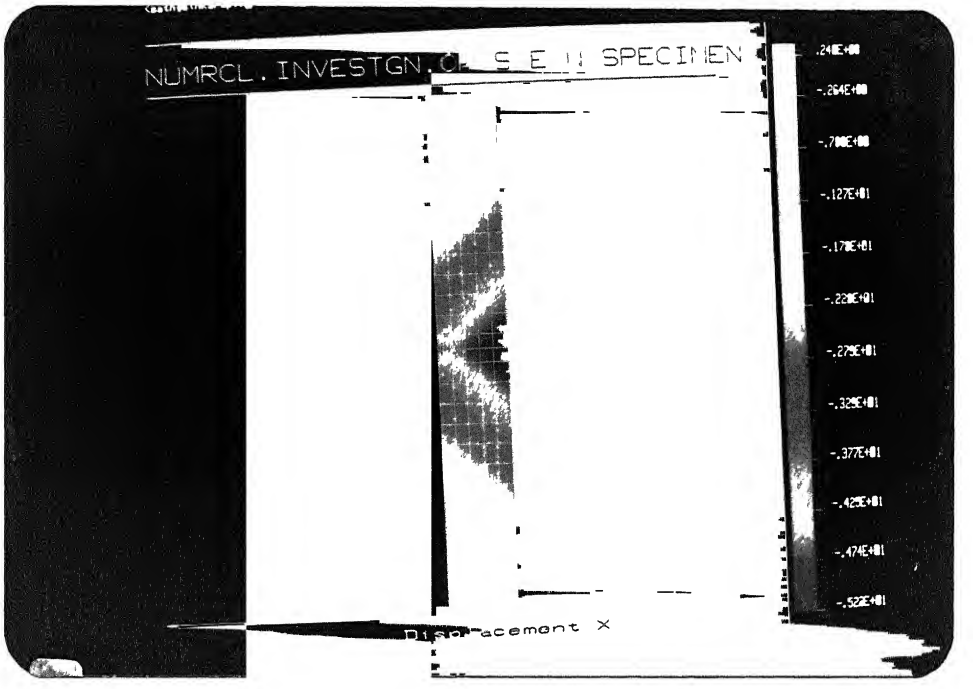

FIG. 2.11

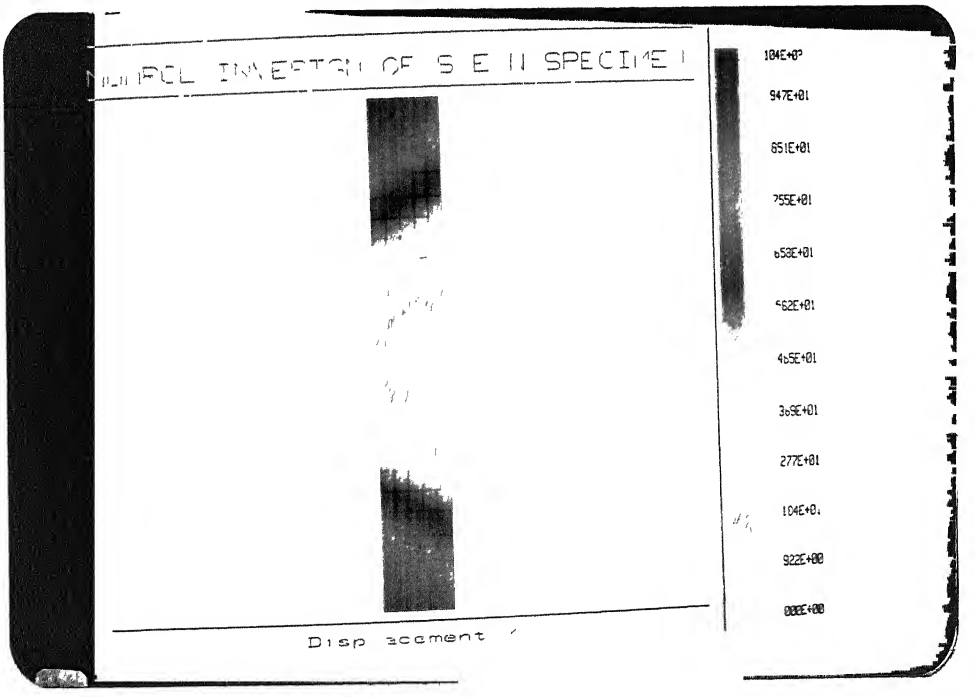

FIG. 2.10

2.9 Closure

In this chapter, Finite Element Formulation of Plane elasticity problem subjected to Body force, Surface force and Thermal loading has been discussed. Also modelling a crack, with 8-noded isoparametric quadrilateral element is discussed It is seen that a large number of elements are required to model a crack-tip In the case of a radial crack problem, if one solves a problem as a whole, the number of elements will phenomenally increase as the number of cracks increases. However, if one takes into account the symmetry of the problem, the amount of computation can be reduced. The exact requirement of incore memory and CPU time largely depends upon the solution procedure Next chapter discusses Potter's solution algorithm which uses minimum amount of incore memory for solving a cyclically symmetric problem.

CHAPTER 3

SOLUTION ALGORITHM FOR SOLVING A CYCLICALLY SYMMETRIC PROBLEM

3.1 Introduction :

Annular disk without crack can be easily analysed as an axisymmetric problem But as soon as cracks are formed the structure looses its axisymmetric nature. Modelling of a crack involves the use of a large number of small elements near the crack tip. As the number of cracks increases, analysing the problem as a whole becomes prohibitive and one would require large computer resources to solve the problem However, if the cracks are periodic and of equal length, then this periodicity can be utilised in solving the problem The assumption of periodic cracks of equal lengths has been used by all earlier investigators [3-6] and this assumption has been experimentally verified by Shukla [7] for the case of internal pressure loading However, extending the same logic one can assume that cracks occur with certain periodicity in rotating discs too. In the case of Clutch plates in an Automobile, failure has been observed with three radial cracks emanating from inner boundary.

3.2 Solution Algorithms for a Cyclically Symmetric Problem .

A problem is cyclically symmetric when geometry of the structure, material properties, loading and boundary conditions are also cyclically symmetric. Since, the cracks occur with certain periodicity, the problem of an annular disc with radial cracks can be idealised as a cyclically symmetric problem

In the case of static analysis, the displacement vector of each sector are identical and it is enough if one analysed only one repeating sector of the whole structure. In order to impose the condition that the structure is cyclically symmetric, it is desirable that the global stiffness matrix is referred to the global polar co-ordinates.

3.3 Transformation from Global Cartesian to Global Polar :

For a cyclically symmetric problem, to apply the condition that the displacement vector of the first and last partition is same, it becomes necessary to convert the problem form global cartesian co-ordinate system to global polar co-ordinate system.

For any node point shown in Fig. (3.1) the transformation is defined as

$$\begin{Bmatrix} x_i \\ y_i \end{Bmatrix} = [T_i] \begin{Bmatrix} r_i \\ \theta_i \end{Bmatrix} \quad \text{Where } T_i = \begin{bmatrix} \cos\phi_i & -\sin\phi_i \\ \sin\phi_i & \cos\phi_i \end{bmatrix} \quad \text{---(3 1)}$$

$$\text{or} \begin{Bmatrix} r_i \\ \theta_i \end{Bmatrix} = [T_i]^T \begin{Bmatrix} x \\ y \end{Bmatrix} \quad \text{and} \quad \phi_i = \tan^{-1}(Y_i/x_i)$$

Therefore, for an element, co-ordinate transformation is defined as,

$$\{U\} = [T]\{U\}_p \qquad (3.2)$$
$$\{F\} = [T]\{F\}_p$$

where the subscript 'p' refers to the polar co-ordinates and the Matrix [T] has on its diagonal the submatrices $[T_i]$ depending on the co-ordinates of each node Pre-multiplying the expression (3 15) by $[T]^T$ and using the Eq (3.2), we get

$$[K]_p\{U\}_p = \{F\}_p \qquad \text{...(3.3)}$$

where

$$[K]_p = [T]^T[K]\,[T] \qquad (3.4)$$

Eq.(3.3) can be solved by many techniques. One such efficient method viz., Potter's method which has been used to solve the equation is explained below.

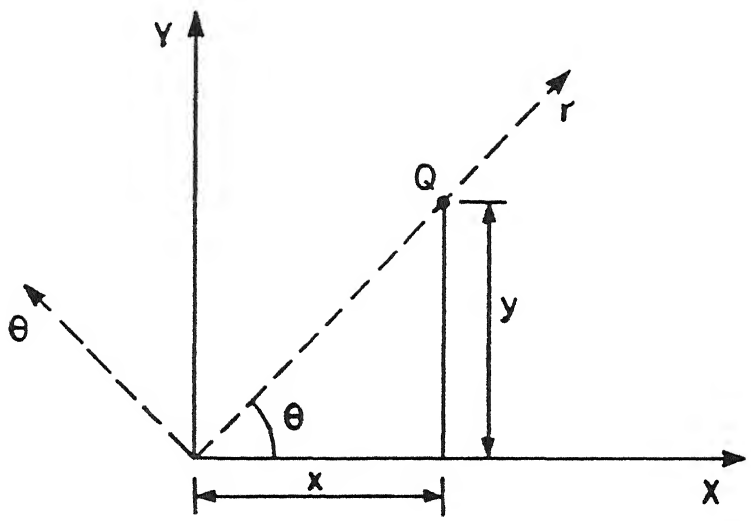

FIG.3 1 Transformation from Cartesian to Polar Co-ordinate

3.4 Potter's Method [27]:

This is a method of substructuring The basic approach is to split the problem into a number of small problems The concept of partitioning helps in understanding the method.

The stiffness equations for a typical substructure with extra partition Fig.(3 2) is,

$$[K]\{U\} = \{F\} \qquad (3.8)$$

The linear problem such as shown in Fig (3 3) will have global stiffness matrix in banded form This problem can be divided into four substructures I, II, III & IV are the dividing lines of the substructures & are known as partitions. Each partition is identified with the number of nodes it contains

Partition I contains node no. from 1 to 4 partition II, contains node no from 5 to 8 so on.

Partition is nothing but a convenient way of representing the global stiffness matrix. Effect of partitioning on global stiffness matrix is shown in Fig. (3.4). Matrix B_i, A_i and C_i are the submatrices and their meaning is as follows.

$[B_i]$ - It represents the effect of nodes of i^{th} partition on itself.

$[A_i]$ - It represent the effect of nodes of $(i+1)^{th}$ partition on nodes of i^{th} partition

$[C_i]$ - It represent the effect of nodes of $(i-1)^{th}$ partition on nodes of i^{th} partition

Equation (3 8) can now be represented as,

$$\begin{bmatrix} B_1 & A_1 & & \\ C_2 & B_2 & A_2 & \\ & C_3 & B_3 & A_3 \\ & & C_4 & B_4 \end{bmatrix} \begin{bmatrix} Z_1 \\ Z_2 \\ Z_3 \\ Z_4 \end{bmatrix} = \begin{bmatrix} G_1 \\ G_2 \\ G_3 \\ G_4 \end{bmatrix} \qquad (3\ 9)$$

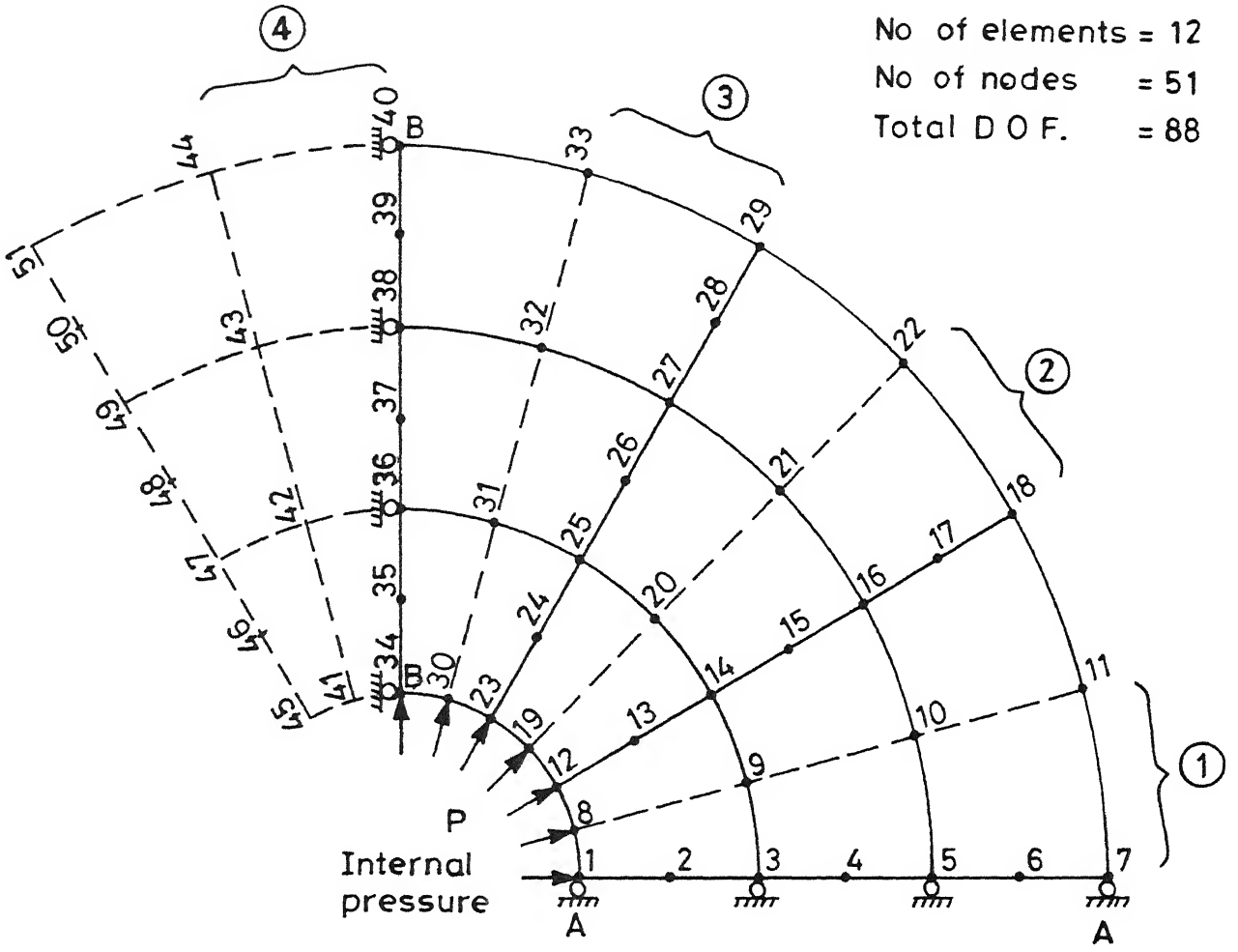

Fig 3 2 Typical substructure of a disc with extra partition for Potter's method

Partition No	First Node	Last Node	First Element	Last Element
1	1	11	1	3
2	12	22	1	6
3	23	33	4	9
4	34	44	7	12

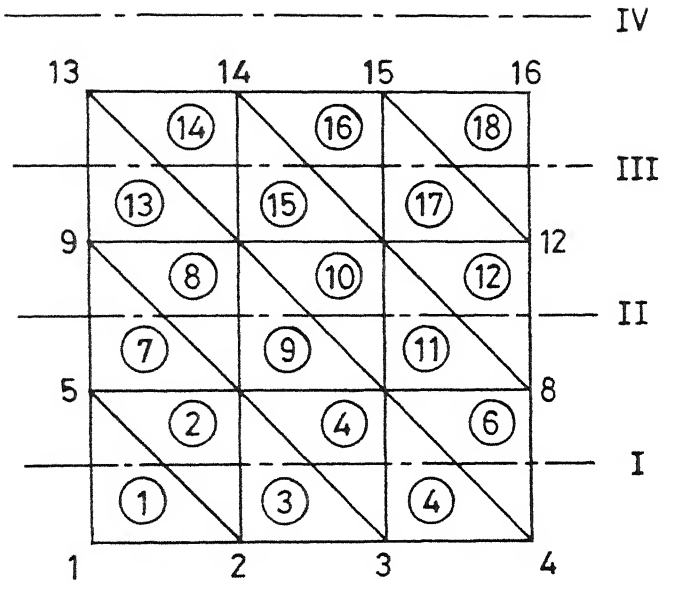

Fig 3 3 Partitioning of a finite element scheme

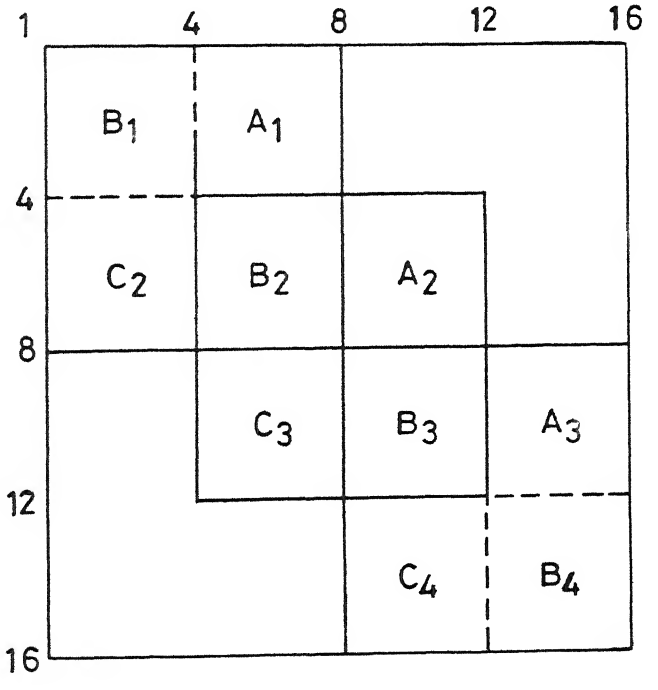

Fig 3 4 Typical global stiffness matrix of linear structure.

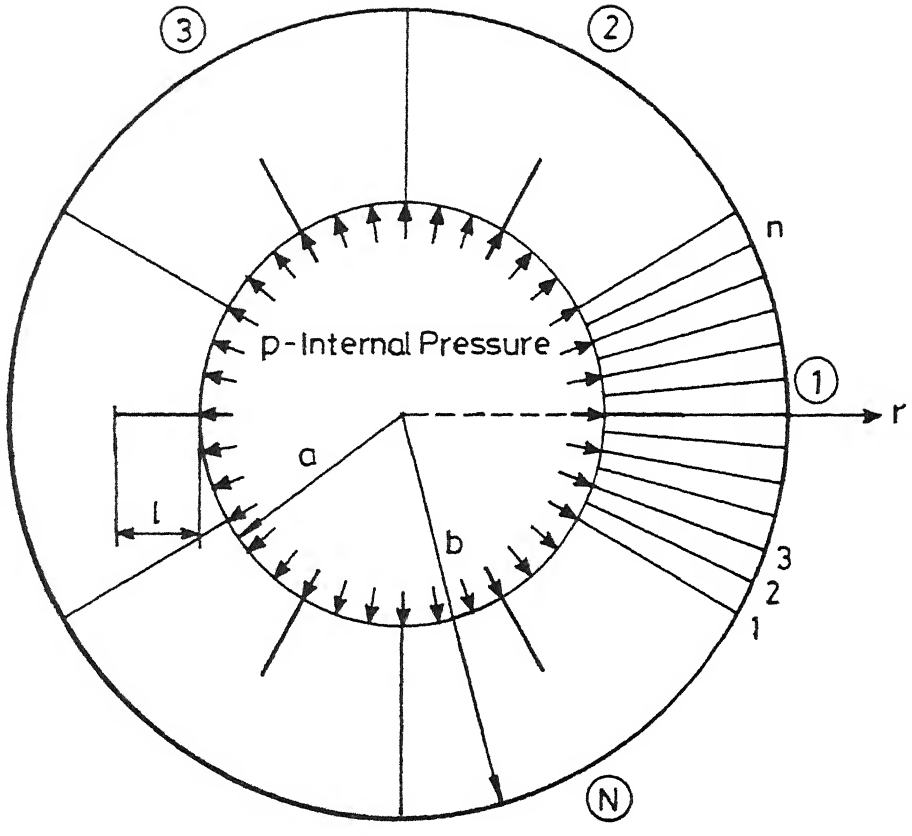

① ② ③ ---- Ⓝ Sector nos

1 2 3 ----- n Partition nos.

Fig. 3.5 A rotationally periodic structure.

Where, $\{Z_i\}$ is the displacement vector of i^{th} partition
$\{G_i\}$ is the force vector of i^{th} partition

Potter's Method does not calculate displacement of nodes individually, but instead calculates displacement vector for each partition (i.e) Z_i's This means that for example when it obtains the displacement vector of partition I, displacement of node 1 to 4 are obtained simultaneously.

Potter's Method is an out of core solution technique At a time it requires only submatrices of the i^{th} partition in the core memory of the computer All other matrices are stored on secondary storage devices such as taper, disks This makes optimum use of the computer in core memory

3.4.1 Global Stiffness Matrix and Sector Stiffness Matrix for A Cyclically Symmetric Structure:

In a Cyclically symmetric structure, a substructure can be identified as the one which repeats itself periodecally.

Consider a symmetric structure as shown in Fig (3 5) It has N substructures and each is divided into n partitions, thus the total number of partitions are m (=Nxn) Unlike in Fig (3.3), here the last partition nemely the m^{th} partition and the first partition are connected. Hence, by the definition of submatrices [A], [B] and [C], in the present case matrices C_1 and A_m exist. Thus the global stiffness matrix takes the form,

$$\begin{bmatrix} B_1 & A_1 & \emptyset & & C_1 \\ C_2 & B_2 & A_2 & & \\ & & & & \\ A_m & \emptyset & & C_m & B_m \end{bmatrix} \qquad (3.10)$$

Partition 1 & (n+1) constitutes as sector boundaries. Since the structure is cyclically symmetric, in the static case the displacement vector of each sector is same i.e.,

$$\{Z_{n+1}\} = \{Z_1\}, \quad \{Z_{n+2}) = \{Z_2\} \quad ----$$
$$\{Z_{n+i}\} = \{Z_i\}, \quad \{Z_{2n}\} = \{Z_n\} \quad ---- \quad (3.11)$$

Using the above condition the overall problem can be reduced to only one sector and the stiffness matrix takes the form :

$$\begin{bmatrix} B_1 & A_1 & & & C_1 \\ C_2 & B_2 & A_2 & & \\ & & & & \\ A_m & & & C_n & B_n \end{bmatrix} \quad . \quad (3.1Ø)$$

Due to finite element formulation of the problem,

$[C_1] = [A_n]^T$ and $[C_{i+1}] = [A_i]^T$ for i = 1,2, .. , n-1

3.4.2 Evaluation of Displacement vectors:

The static equilibrium at each station can be represented as follows .

For the first station,

$$[C_1]\{Z_n\} + [B_1]\{Z_1\} + [A_1]\{Z_2\} = [G_1] \quad (3.14)$$

Similarly for i^{th} station,

$$[C_i]\{Z_{i-1}\} + [B_i]\{Z_i\} + [A_i]\{Z_{i+1}\} = [G_i] \quad (3.15)$$

For the n^{th} station, A_n the coupling stiffness matrix with the first station of the next sector The above equation can be modified as,

$$\{Z_1\} = -[P_1]\{Z_2\} + [q_1] + [Q_1]\{Z_n\} \quad (3.16)$$

and

$$\{Z_i\} = -[P_i]\{Z_{i+1}\} + [q_i] + [Q_i]\{Z_n\} \quad (3.16\text{-}A)$$

where,

$$[P_1] = [B_1^{-1}][A_1]$$
$$[q_1] = [B_1^{-1}]\{G_1\}$$
$$[Q_1] = [B_1^{-1}][C_1]$$
$$[P_i] = ([B_i] - [C_i][_{i-1}])^{-1}\,[A_i]$$
$$[q_i] = ([B_i] - [C_i][_{i-1}])^{-1}\,(\{G_i\} - [C_i]\{q_{i-1}\})$$
$$[Q_i] = -([B_i] - [C_i][_{i-1}])^{-1}\,([C_i][Q_{i-1}]) \quad i = 2,3, \text{--}n \quad (3.18)$$

Considering the equilibrium at the n^{th} station,

$$[C_n]\{Z_{n-1}\} + [B_n]\{Z_n\} + [A_n]\{Z_{n+1}\} = [G_n] \quad (3.19)$$

Because of Cyclic symmetry $\{Z_{n+1}\} = [Z_1]$

Hence,

$$[C_n]\{Z_{n-1}\} + [B_n]\{Z_n\} + [A_n]\{Z_1\} = [G_n] \quad (3.2Ø)$$

Substituting for $\{Z_1\}$ from Eqn (3.16) gives,

$$[C_n]\{Z_{n-1}\} + [B_n]\{Z_n\} + [A_n]([-P_1]\{Z_2\} + \{q_1\} + [Q_1]\{Z_n\}) = [G_n] \quad (3.21)$$

i e

$$[R_1]\{Z_2\} + [S_1]\{Z_n\} + [C_n]\{Z_{n-1}\} = [u_1] \quad (3.22)$$

where, $[R_1] = [-A_n][P_1]$

$[S_1] = [B_n] + [A_n][Q_1]$

$[u_1] = [G_n] - [A_n][q_1]$

$\{Z_3\}$, ---$\{Z_{n-2}\}$ gives,

$$[R_i]\{Z_{i+1}\} + [S_i]\{Z_n\} + [C_n]\{Z_{n-1}\} = [u_i] \quad (3.23)$$

Here, $[R_i] = [-R_{i-1}][P_i]$

$[S_i] = [S_{i-1}] + [R_{i-1}][Q_i]$

$[u_i] = [u_{i-1}] - [R_{i-1}][q_i]$ i= 2,3 ---n-2,

Rearranging the $(n-2)_{nd}$ equation yields,

$$([R_{n-2}] + [C_n]\{Z_{n-1}\} + ([S_{n-2}]\{Z_n\} = \{u_{n-2}\} \quad (3.24)$$

Substituting for $\{Z_{n-1}\}$ from Eqn (3 1Ø) gives,

$$[([R_{n-2}] + [C_n])([Q_{n-1}] - [P_{n-1}]) + [S_{n-2}]]\{Z_n\} = [\{u_{n-2}\} - ([R_{n-2}] + [C_n])\{q_{n-1}\} \quad (3.25)$$

After evaluating $\{Z_n\}$ a series of backward substitutions in Eqs (3 16) & (3.17) will provide all the unknown displacements $\{Z_{n-1}\}$, $\{Z_{n-2}\}$, ----- $\{Z_1\}$

3.5 Closure :

In this chapter, Potter's solution algorithm has been discussed to solve a problem which has cyclic symmetry. In the next two chapters, the radial crack problems subjected to centrifugal and thermal loading have been extensively analysed using the software developed in this chapter.

CHAPTER 4

EVALUATION OF S.I.F. FOR ROTATING ANNULAR DISC WITH RADIAL CRACKS

4.1 Introduction :

In this chapter, the results of the analysis performed on a rotating annular disc with radial cracks using the software discussed in the previous chapter is presented S.I.F s have been calculated as a function of crack length, b/a ratio and number of cracks. First S.I.F s as function of number of cracks (n) are calculated for three crack length ratios with {l/(b-a)} as parameters Such graphs are obtained for two different b/a ratios Next, S I F s as a function of crack length are calculated for three b/a ratios as parameters and such graphs are obtained for two different number of cracks. These calculations have been done for both inner and outer cracks.

4.2 Evaluation of Element Body Force Vector :

In the previous chapter the element body force vector has been derived as;

$$\{f_b\} = \int\int [N]^T \{F\}\, t\, dxdy \qquad \ldots(4.3)$$

The vector {F} can be expressed in terms of nodal values as,

$$\{F\} = \begin{Bmatrix} F_x \\ F_y \end{Bmatrix}$$

$$= \begin{bmatrix} N_1 & \emptyset & N_2 & \emptyset & \ldots & N_8 & \emptyset \\ \emptyset & N_1 & \emptyset & N_2 & \ldots.. & \emptyset & N_8 \end{bmatrix} \begin{Bmatrix} F_{x1} \\ F_{y1} \\ \\ . \\ . \\ F_{x8} \\ F_{y8} \end{Bmatrix} \qquad \ldots.(4.2)$$

$$= [N]\, \{F_b\}^e$$

Thus,

$$\{f_b\}^e = \int\int [N]^T [N]\, t\, dxdy\, \{F_b\}^e \qquad \ldots.(4.3)$$

Now, the centrifugal force at a point in polar co-ordinates is given by,

$$F_r = r_i w^2 \qquad \ldots.(4.4)$$

where,

$$= \text{density of the material,}$$

$$w = \text{angulr speed of rotation and}$$

$$r_i = \text{radius at node i}$$

Transforming into cartesian co-ordinates, the nodal forces are given by,

$$F_{x_i} = F_{r_i} \cos\theta_i$$

$$F_{y_i} = F_{r_i} \sin\theta_i$$

$$\text{where } \theta_i = \tan^{-1}(y_i/x_i) \qquad \ldots.(4.5)$$

This integral (Eq (4 3)) when evaluated by Gauss-quadrature technique yields the consistent loads at each node as shown in Fig.(4.1). Looking at the Fig.(4.1) , one is surprised to see that the nodal forces are unequal and the corner nodal forces are negative However, the mid-side nodal forces are positive and in the direction of body force. The apparent ambiguity is due to consistent force formulation. A similar effect is explained by Robert D.Cook [28] when plane 8-noded quadratic element is chosen. Further, he has shown that the nodal forces are equal and in the same direction as of body force when the plane 4-noded linear element is chosen.

4.3 Preparation of Input Data :

As large amount of input data is required to solve the problem, it is difficult to prepare the complete input file manually. Instead programs have been prepared to aid in preparing the data. The procedure adopted is explained behind.

To prepare input file for a problem, it is divided into 3 parts as shown in Fig.(4 2).

The program basically prepares co-ordinates of each node and nodal connectivity of the eight noded isoparametric elements for a sector of an uncracked disc The input data for the program is number of radial lines, number of divisions in the radial lines, angles at which radial lines appear, radial distance of the radial divisions and the node number at which first node will start. This program is sufficient to generate input data for part 1 and part 3 mentioned above

For part 2 the same program is used initially to calculate nodal co-ordinates and nodal connectivity as though it has no crack tip. Later these output become the input for another program viz , 'inn f'/ 'out f' depending on whether it is an inner crack problem or outer crack one, which introduces the Quarter Point (Q-P) elements at the crack tip

Thus, after getting the modified output file from 'inn.f'/ 'out f' for part 2, it is added with the output files of part 1 and part 3 suitably to generate the complete input file.

4.4 Numerical Results :

In order to obtain accurate results, close partitions are formed near the crack line and it becomes less dense as it goes away from the crack line as shown in Fig (4.3) and Fig.(4 4) As the number of cracks increases the sector angle becomes smaller and smaller. Thus contrary to the total size of the problem the CPU time and memory decreases as number of cracks increases. This is a tremendous advantage as fracture mechanics problem requires large number of elements in the vicinity of the crack tip. The S.I.F. is calculated using CTOD method. In all the cases, θ displacement is suppressed on sector boundaries. It is justifiable because of symmetry.

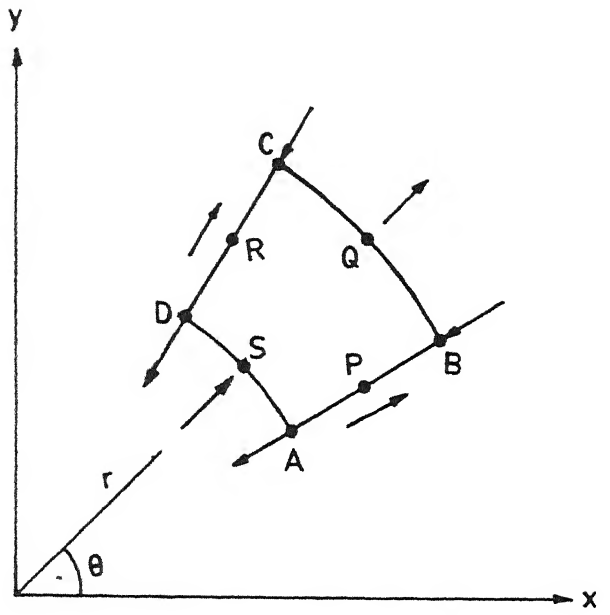

FIG 4 1 Nodal load distribution obtained by F E M. for Body force

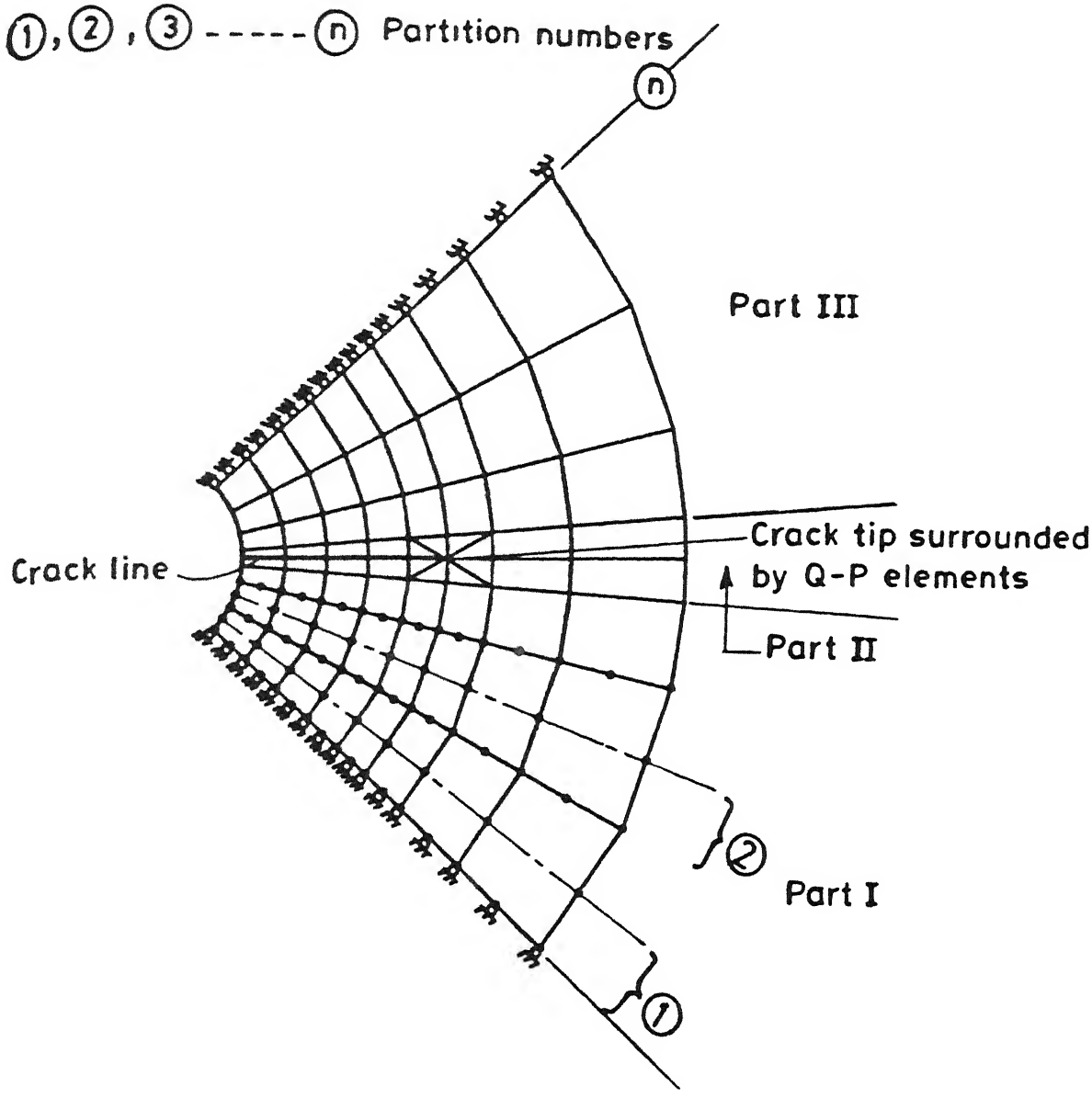

FIG 4 2 Finite Element Mesh showing Partitions

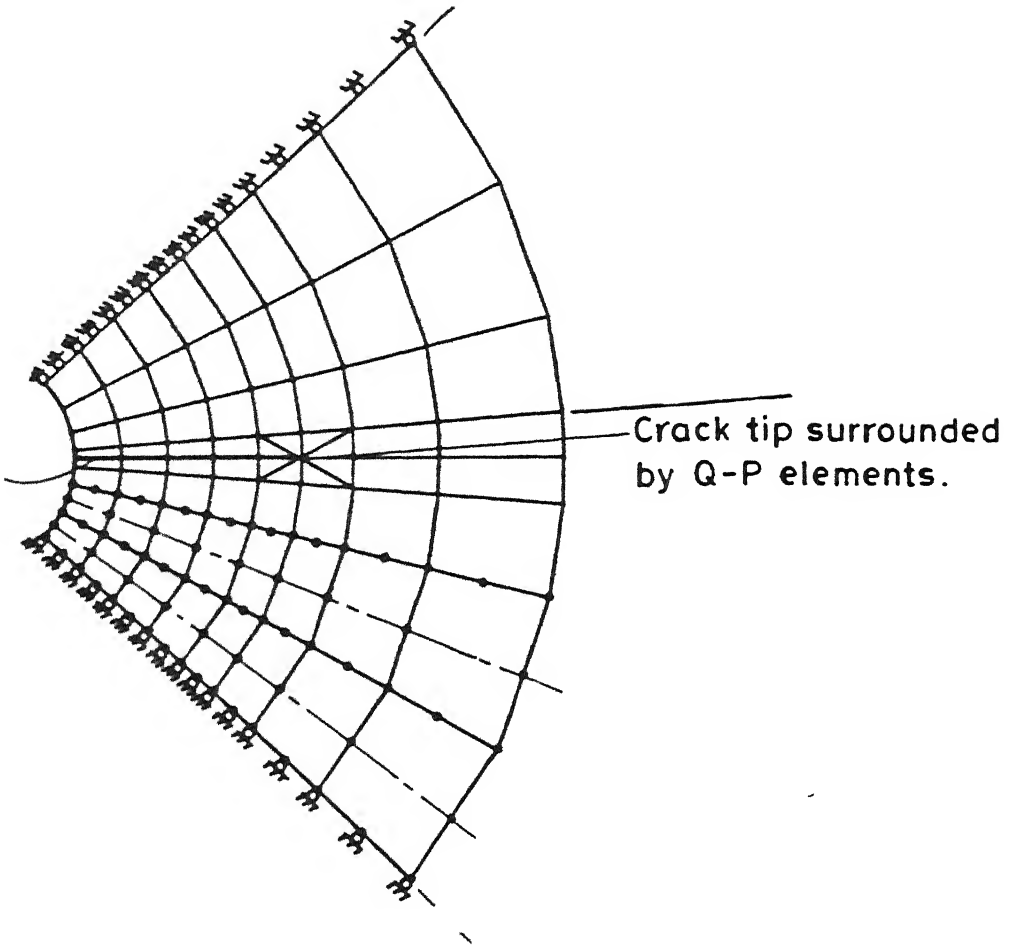

FIG 4 3 Finite Element Mesh for a sector with one Radial crack originating from Inner boundary

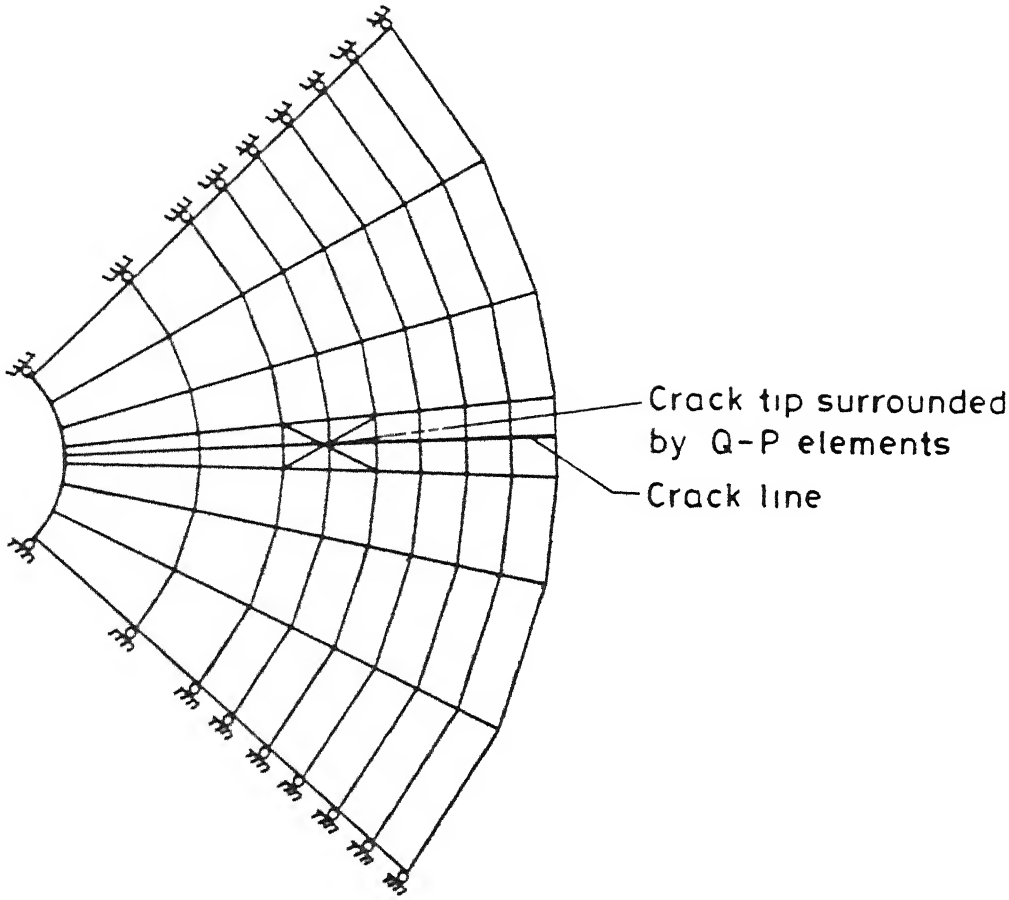

FIG.4.4 Finite Element Mesh for a sector with one Radial crack originating from Outer boundary

4.4.1 Periodic Radial cracks originating from inner boundary :

First, S.I.F.s as a function of number of cracks (n)=3,4,6,12,20,24 & 36 are calculated for three crack length ratios (l/b-a) namely Ø.1,Ø.5 & Ø.7 and each for two different b/a ratios viz. 2 & 1Ø. Next, S.I.F.s as a function of crack length ratios (l/b-a) from Ø.1 to Ø.8 in steps of Ø.1 are calculated for three b/a ratios namely 2,3 & 1Ø and each for two different number of cracks viz. 8 & 4. The results are non-dimensionalised by dividing it by $K_o = ((3+v)/8)*(\int w^2(b^2-a^2))$. These results are shown graphically from Figs.(4.5-4.12).

It is observed from the graphs that,

i) S.I.F. decreases as the number of cracks increases for constant crack length and b/a ratio.

ii) S.I.F. increases as the crack length increases for the same number of cracks and b/a ratio.

iii) S.I.F. decreases as b/a increases keeping b constant for the same crack length ratio and number of cracks.

The first two observations are in line with common-sense, but the third observation is less obvious. In changing b/a ratios, the inner radius was reduced to increase the b/a ratio. Fig.(4.13) shows the variation of σ_θ and σ_r at the central radius of an annular disc (without crack) as a function of b/a ratio. In this case, the variation of b/a was achieved by keeping 'b' constant and 'a' was reduced. Fig.(4.14) shows a similar graph wherein 'a' was kept constant and 'b' was increased to get various b/a ratios. Since in an uncracked annular disc, σ_θ decreases when 'a' is reduced, the S.I.F. value also decreases. If b/a ratio was changed by increasing 'b' then, S.I.F. would have increased for increasing b/a ratios. This shows that the b/a ratio alone is not sufficient to represent the results in non-dimensional form.

4.4.2 Periodic Radial cracks originating from Outer boundary :

S I F s are calculated similarly for all the parameters as that of inner cracks and the results have been shown graphically from Figs (4.15-4.22).

It is observed from the graphs that similar trend is present in outer cracks as that of inner cracks (Ref Sec 4 3 1) except that the magnitude of S I.F. is little greater for an inner crack as compared to an outer crack of the same dimensions.

4.4.3. Display of output data :

In order to validate the correctness of the solution algorithm, various contours such as $(\sigma_1-\sigma_2)$, $(\sigma_1+\sigma_2)$, (σ_r), (σ_θ), (u_r), (u_θ) and Deformed mesh are drawn using the Post-processor developed These are shown in Figs.(4.23-4.36). The symmetry of these indicates qualitatively that the solution algorithm is correct. Figs.(4.37 & 4.38) show the Mode-I isochromatics (contours of $\sigma_1-\sigma_2$) observed in a Photo-elastic experiment [28] for annular discs subjected to internal pressure with cracks emanating from inner and outer boundaries. Though in the case of rotating discs, the loading pattern is different, only Mode-I exists at the crack-tip due to centrifugal forces The contours of $(\sigma_1-\sigma_2)$ for both inner and outer cracks are qualitatively similar to Figs.(4.37-4.38). This completely validates the correctness of the algorithm used.

4.4.4 Plastic zone at the crack-tip :

In this chapter, only Linear Elastic Fracture Mechanics (LEFM) approach is used for evaluating S I F. In actual engineering materials, plastic-zone invariably exits at the crack-tip and if the zone is small compared to the crack length then, LEFM approach is valid Plastic zone is evaluated by using the Von-Misces yield criterion as given below;

$$\sigma_1^2+\sigma_2^2-\sigma_1\sigma_2 = \sigma_y^2$$

In the FEM modelling, disc was considered to be of Aluminium of the values of E = 70 GPa and σ_{yield} = 140 MPa The plastic zone for various RPM are obtained for both inner and outer cracks. From the Figs.(4 39-4 40), it is clear that the plastic zones are very small and LEFM approximation is valid

4.5 Closure :

It is successfully demonstrated that the concept of cyclic symmetry is very helpful in determining the S I.F in the case of a rotating disc with radial cracks. In the next chapter, evaluation of S.I F in an annular disc subjected to thermal loading is discussed.

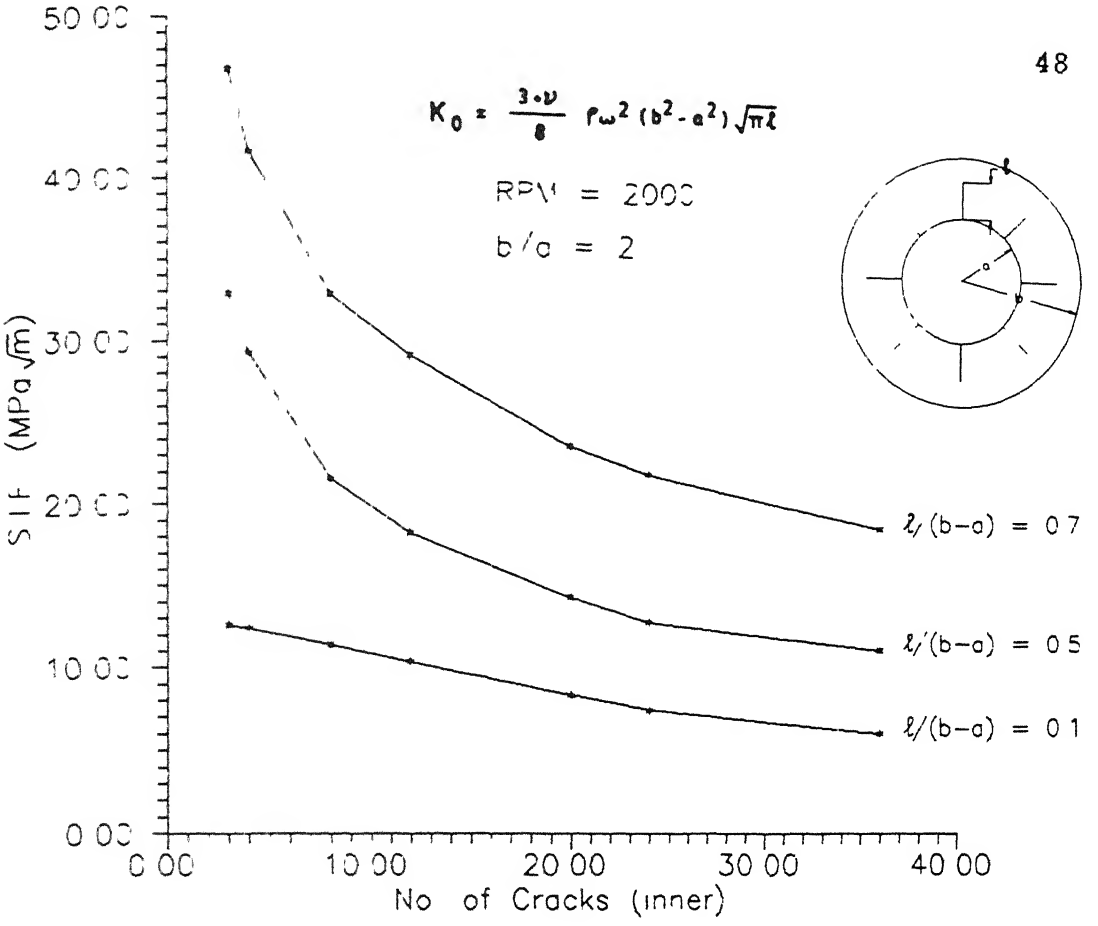

FIG.4.5 Curves of S I.F's as a function of Number of Inner cracks with 1/(b-a) as parameter for b/a = 2

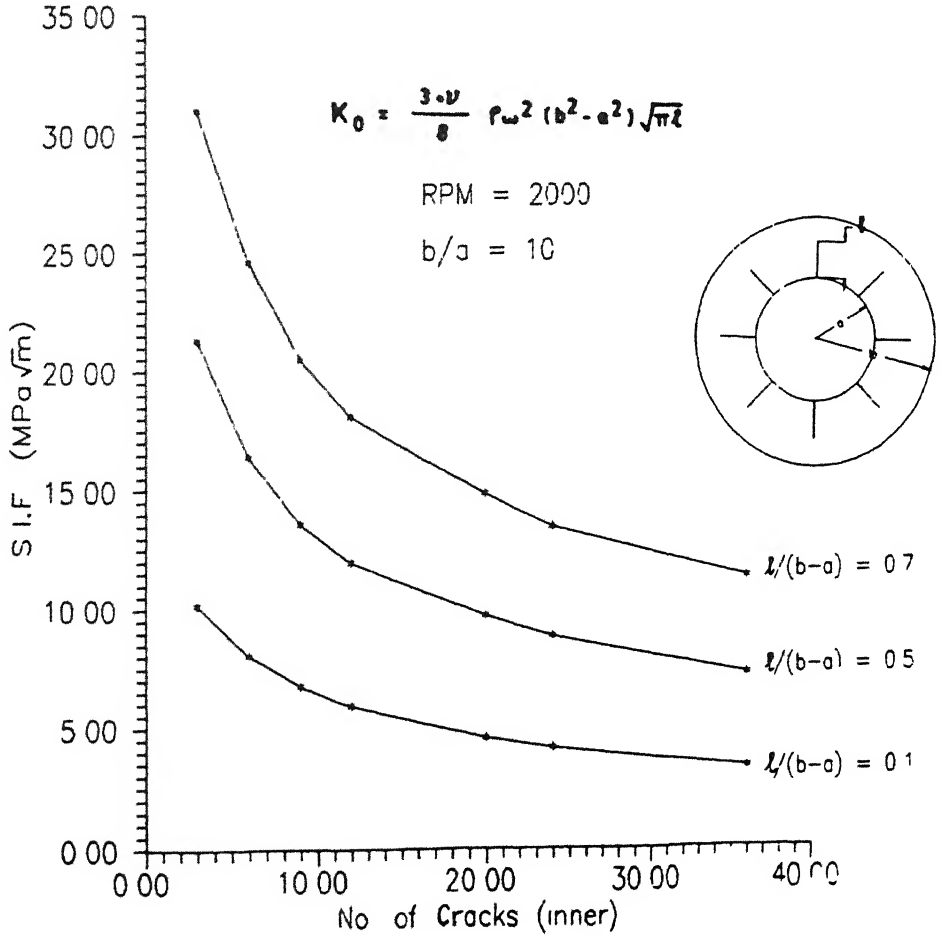

FIG.4.6 Curves of S.I.F's as a function of Number of Inner cracks with 1/(b-a) as parameter for b/a = 10

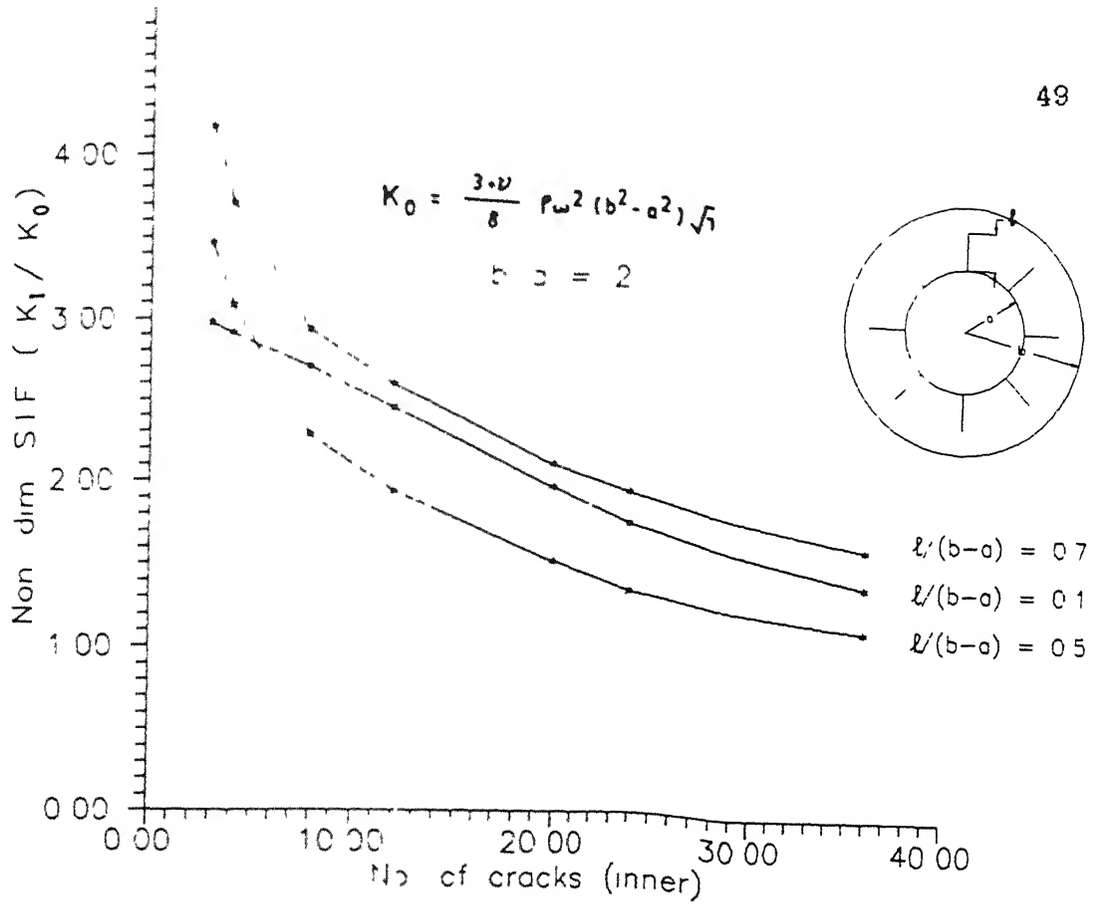

FIG 4 7 Curves of Non-dimensionalised S.I F's as a function of Number of Inner cracks with l/(b-a) as parameter for b/a = 2

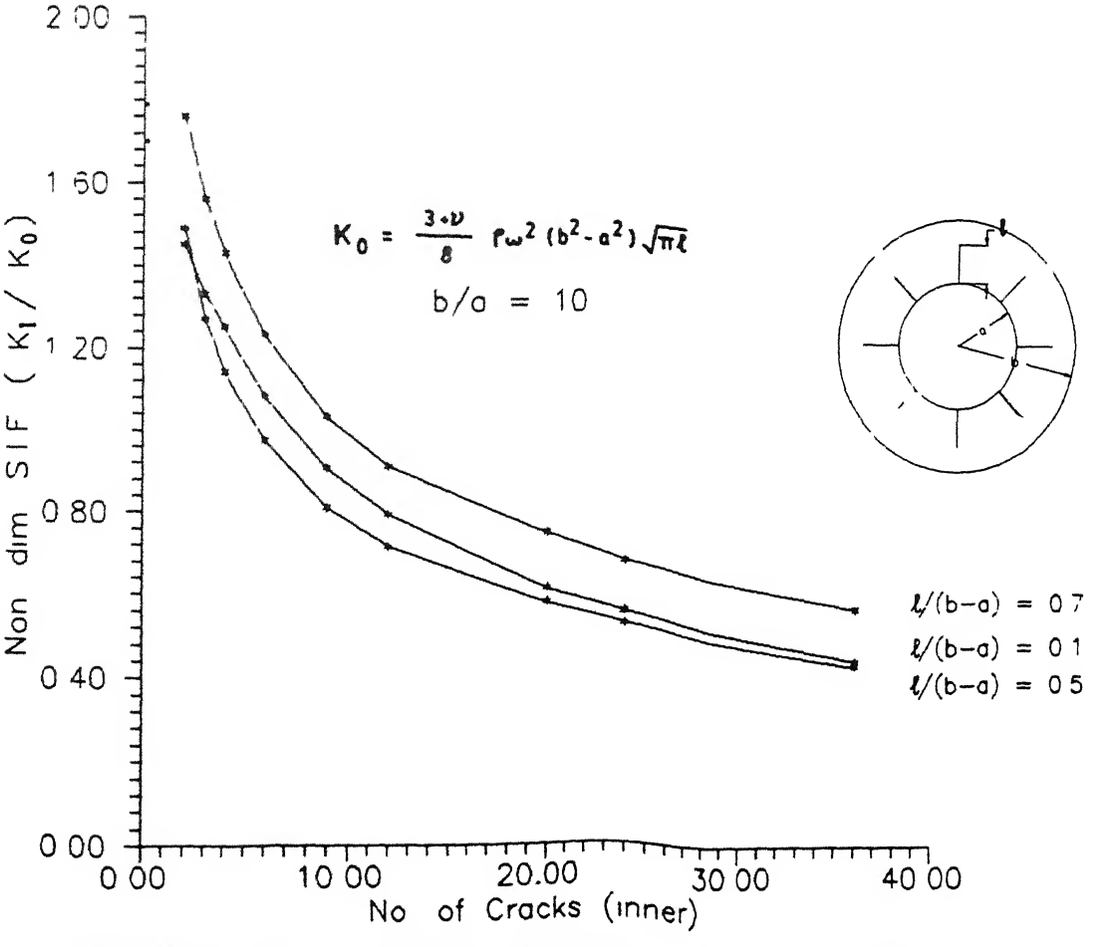

FIG.4.8 Curves of Non-dimensionalised S.I.F's as a function of Number of Inner cracks with l/(b-a) as parameter for b/a = 1Ø

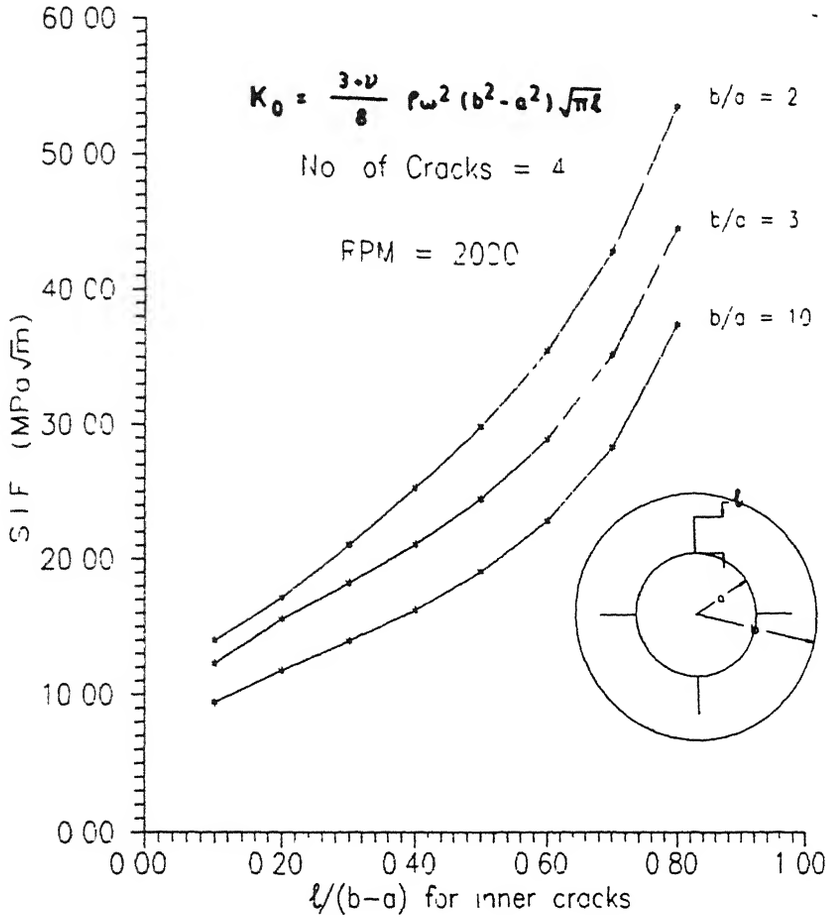

FIG.4 9 Curves of S.I.F 's as a function of 1/(b-a) with b/a as parameter for 4 Inner cracks

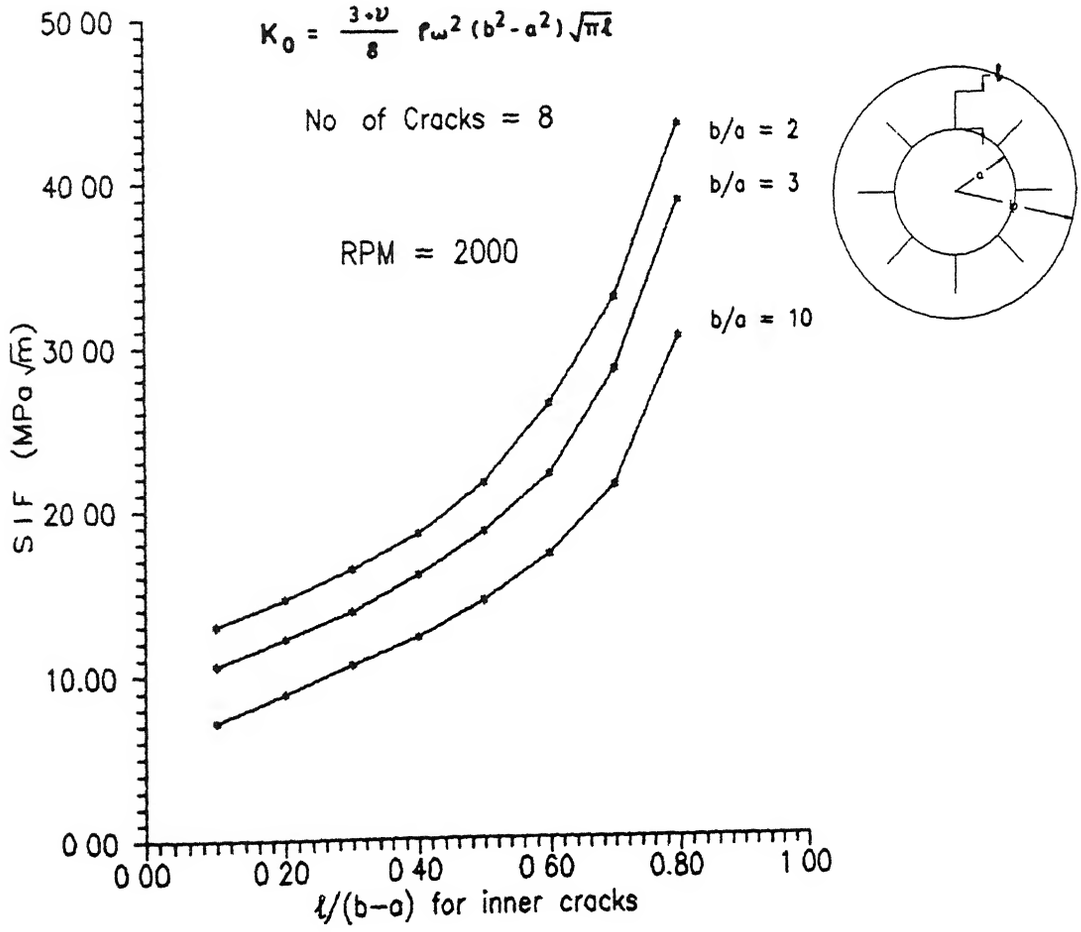

FIG 4.1Ø Curves of S.I.F.'s as a function of 1/(b-a) with b/a as parameter for 8 Inner cracks

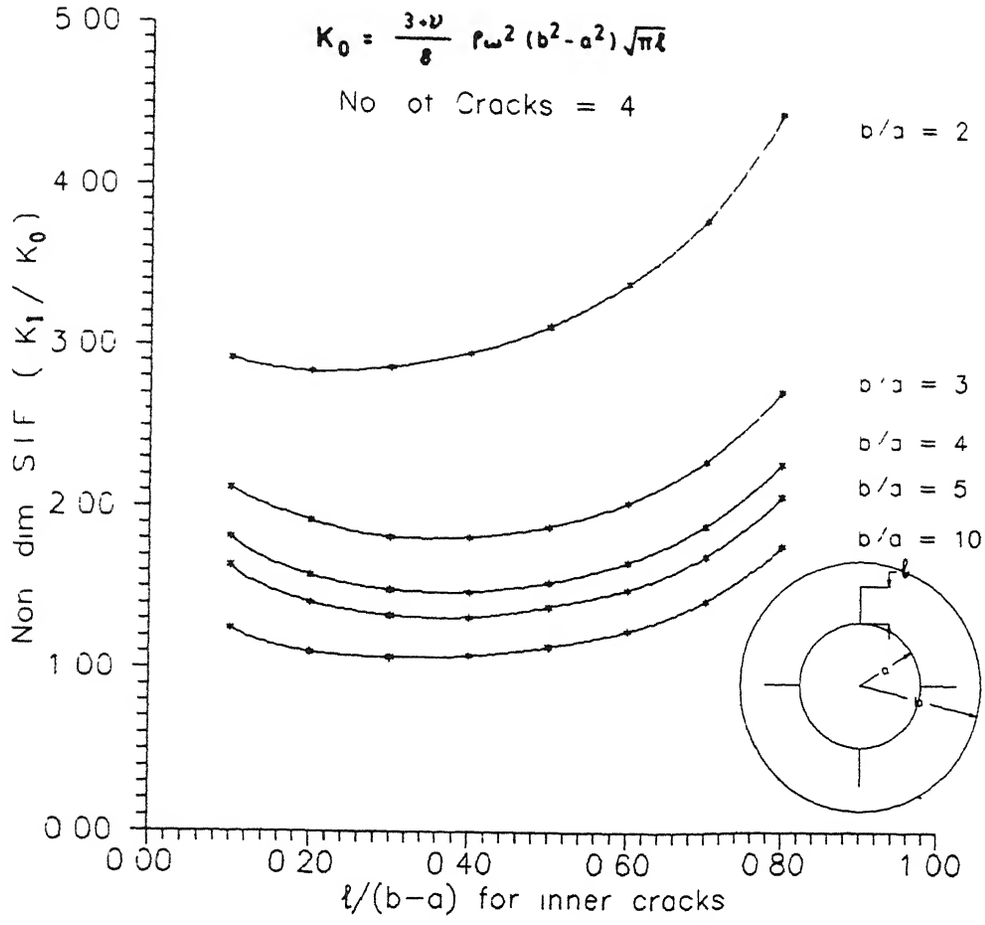

FIG 4 11 Curves of Non-dimensionalised S.I F 's as a function of l/(b-a) with b/a as parameter for 4 Inner cracks

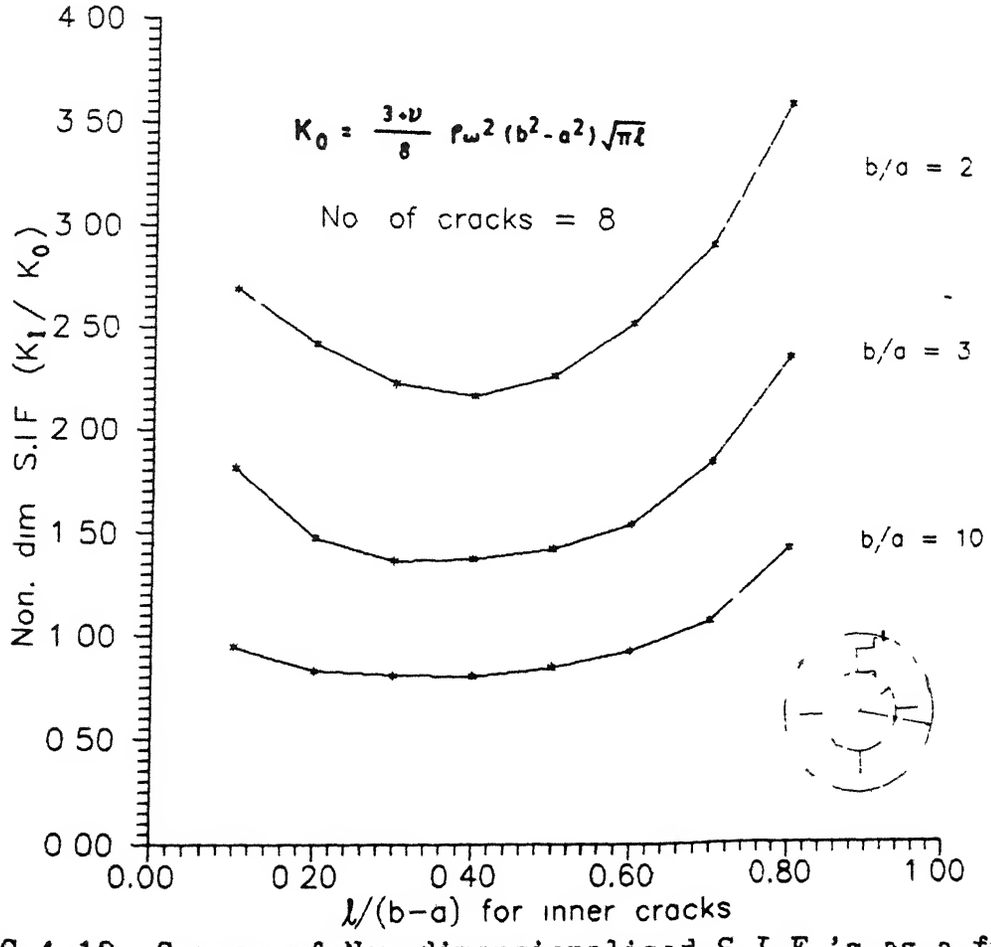

FIG.4.12 Curves of Non-dimensionalised S.I.F.'s as a function of l/(b-a) with b/a as parameter for 8 Inner cracks

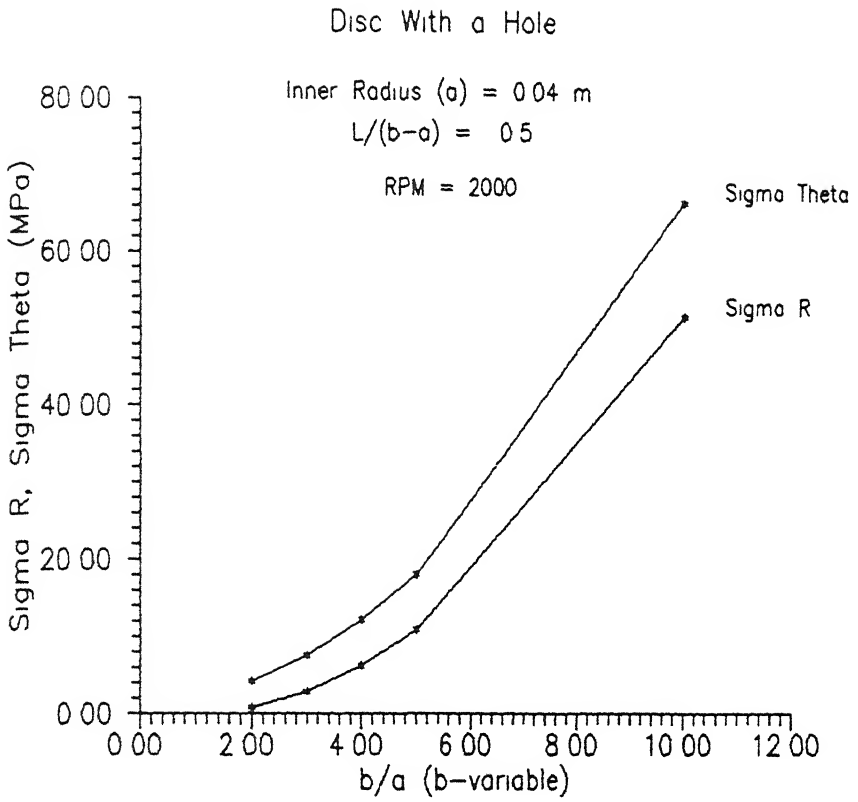

FIG 4 13 Stresses at the Central radius of a Rotating Annular disc for various values of b/a ('b' increases and 'a' is constant)

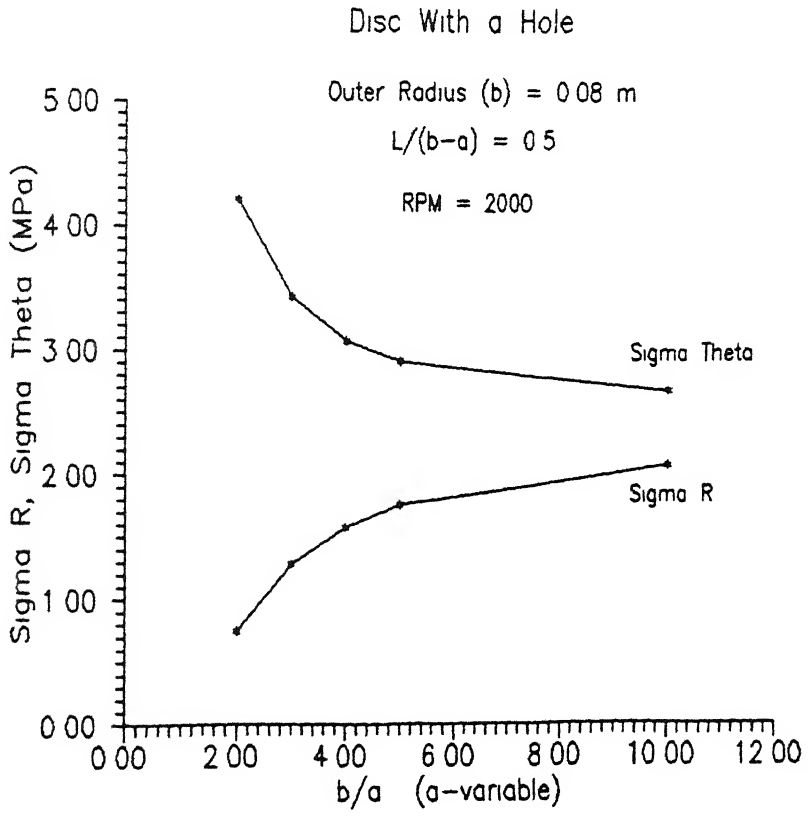

FIG 4.14 Stresses at the Central radius of a Rotating Annular disc for various values of b/a ('a' decreases and 'b' is constant)

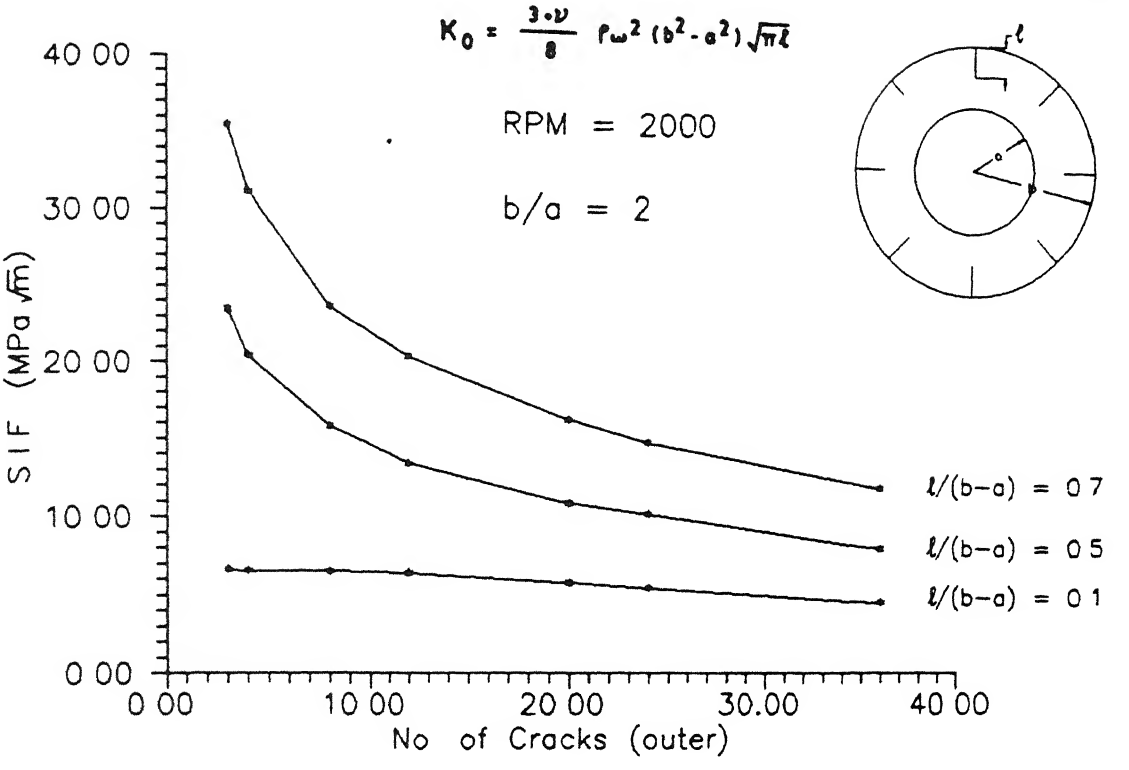

FIG 4 15 Curves of S I F's as a function of Number of Outer cracks with l/(b-a) as parameter for b/a = 2

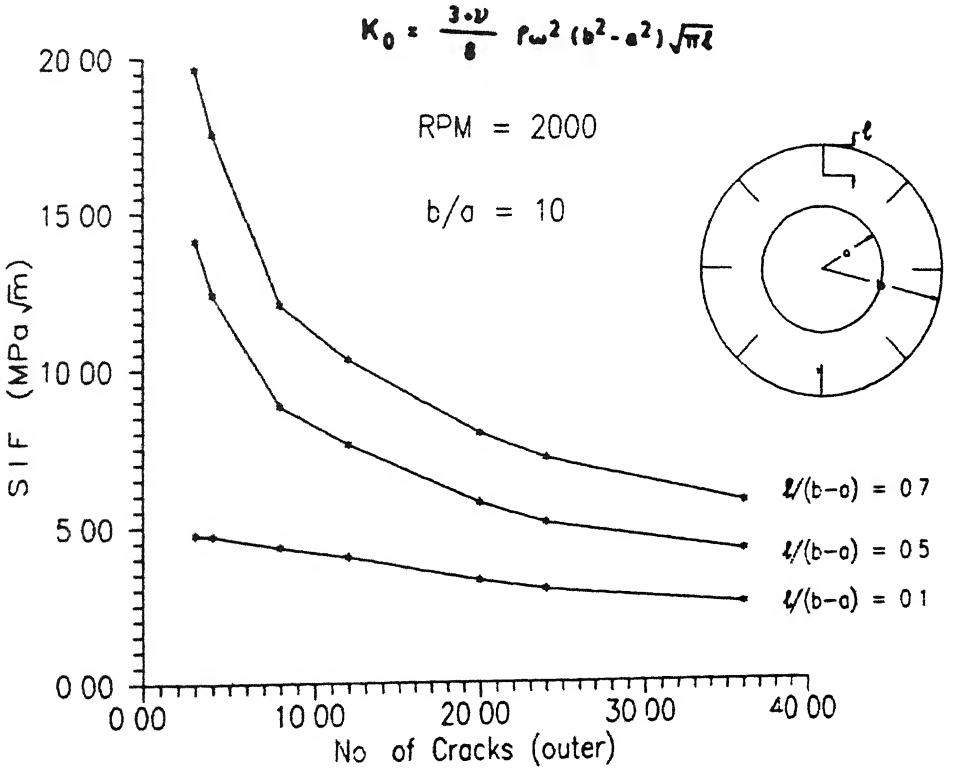

FIG.4.16 Curves of S.I.F's as a function of Number of Outer with l/(b-a) as parameter for b/a = 10

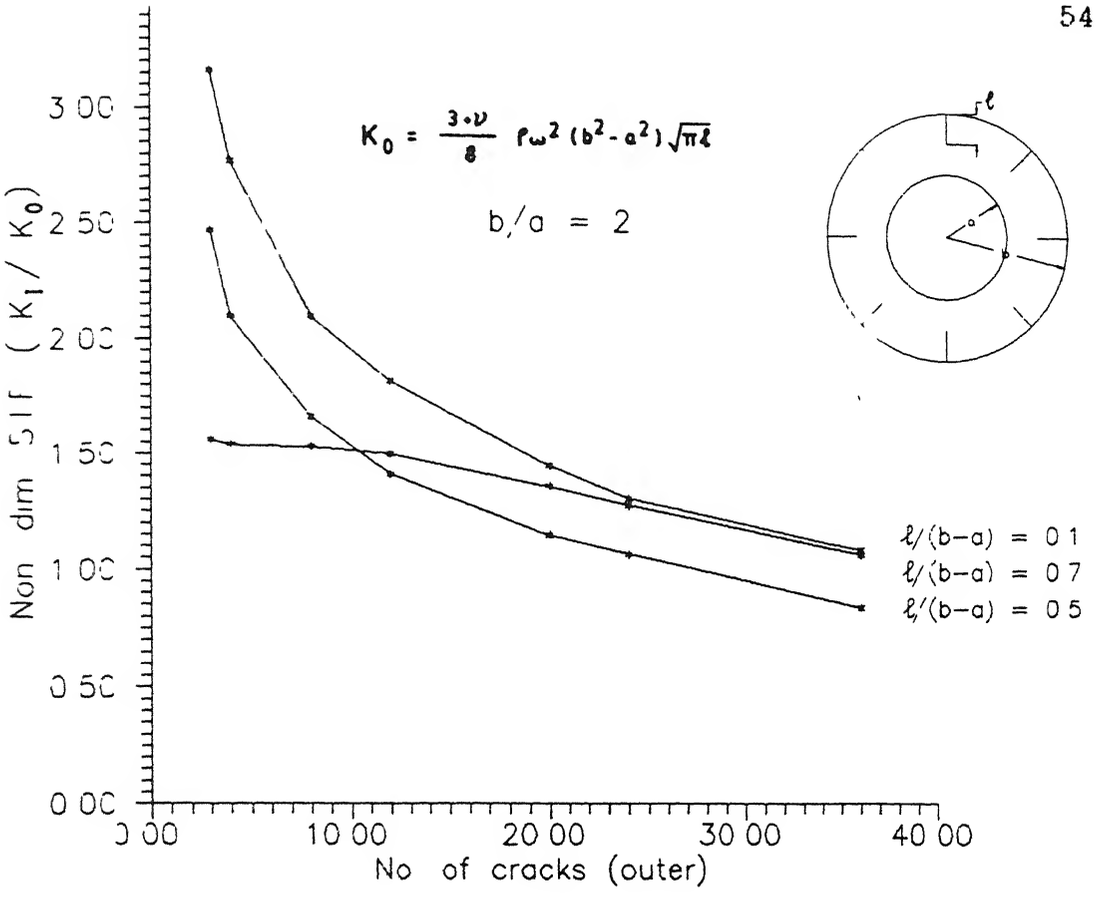

FIG.4 17 Curves of Non-dimensionalised S I F's as a function of Number of Outer cracks with l/(b-a) as parameter for b/a = 2

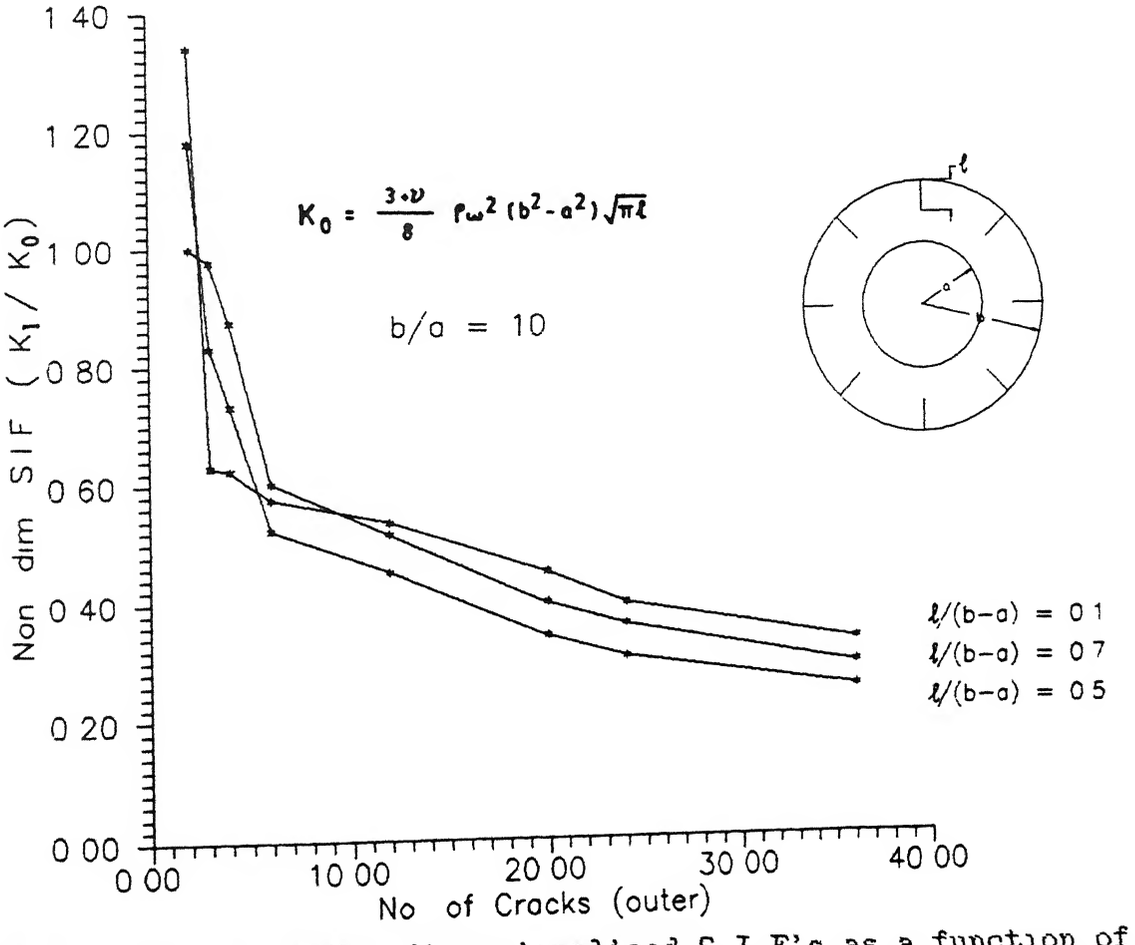

FIG 4.18 Curves of Non-dimensionalised S I.F's as a function of Number of Outer cracks with l/(b-a) as parameter for

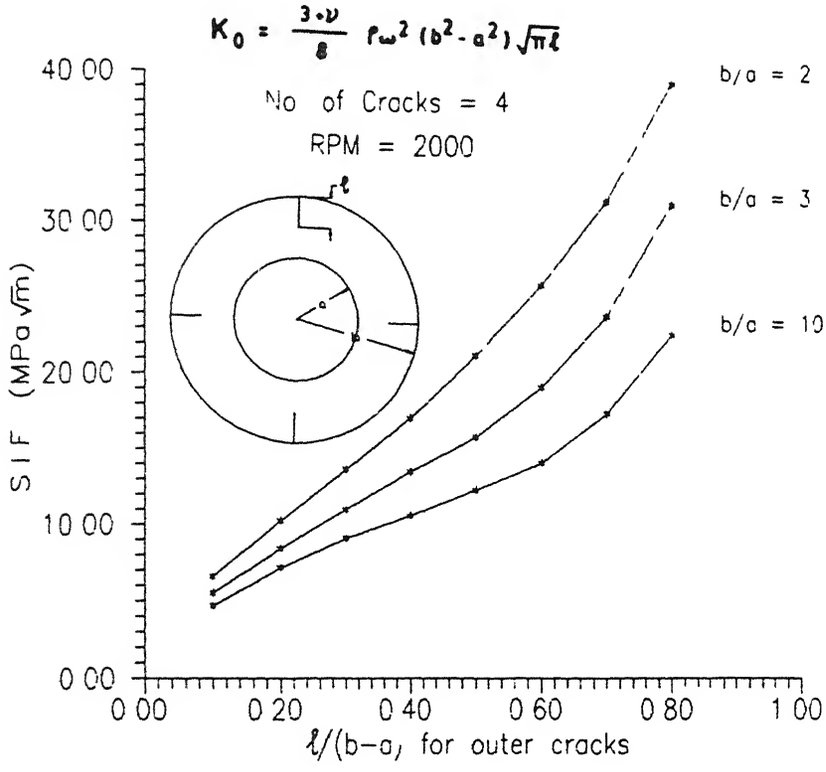

FIG.4 19 Curves of S.I.F.'s as a function of 1/(b-a) with b/a as parameter for 4 Outer cracks

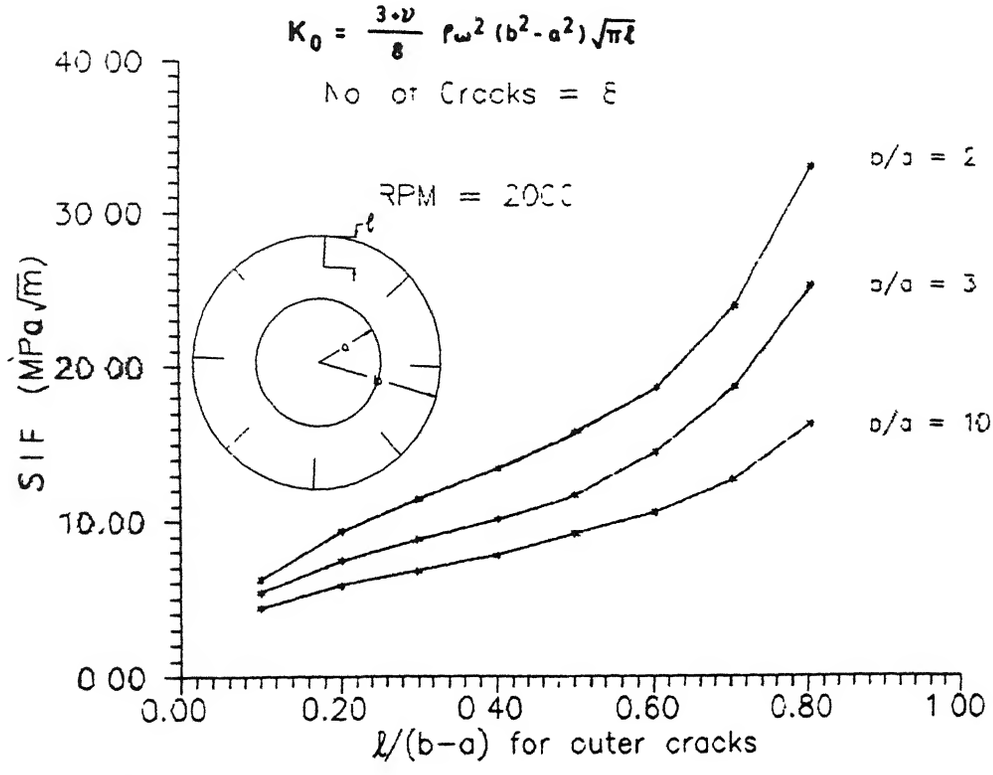

FIG.4.2Ø Curves of S.I.F.'s as a function of 1/(b-a) with b/a as parameter for 8 Outer cracks

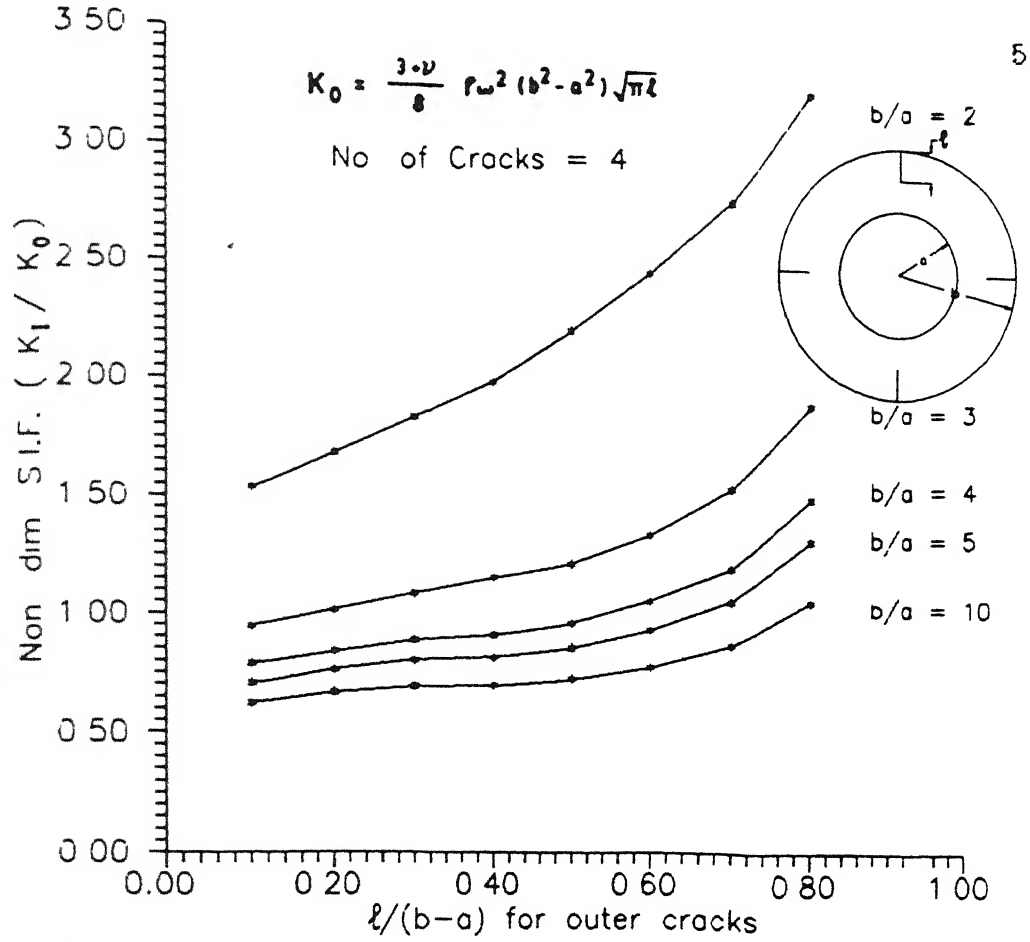

FIG.4 21 Curves of Non-dimensionalised S I.F 's as a function of 1/(b-a) with b/a as parameter for 4 Outer cracks

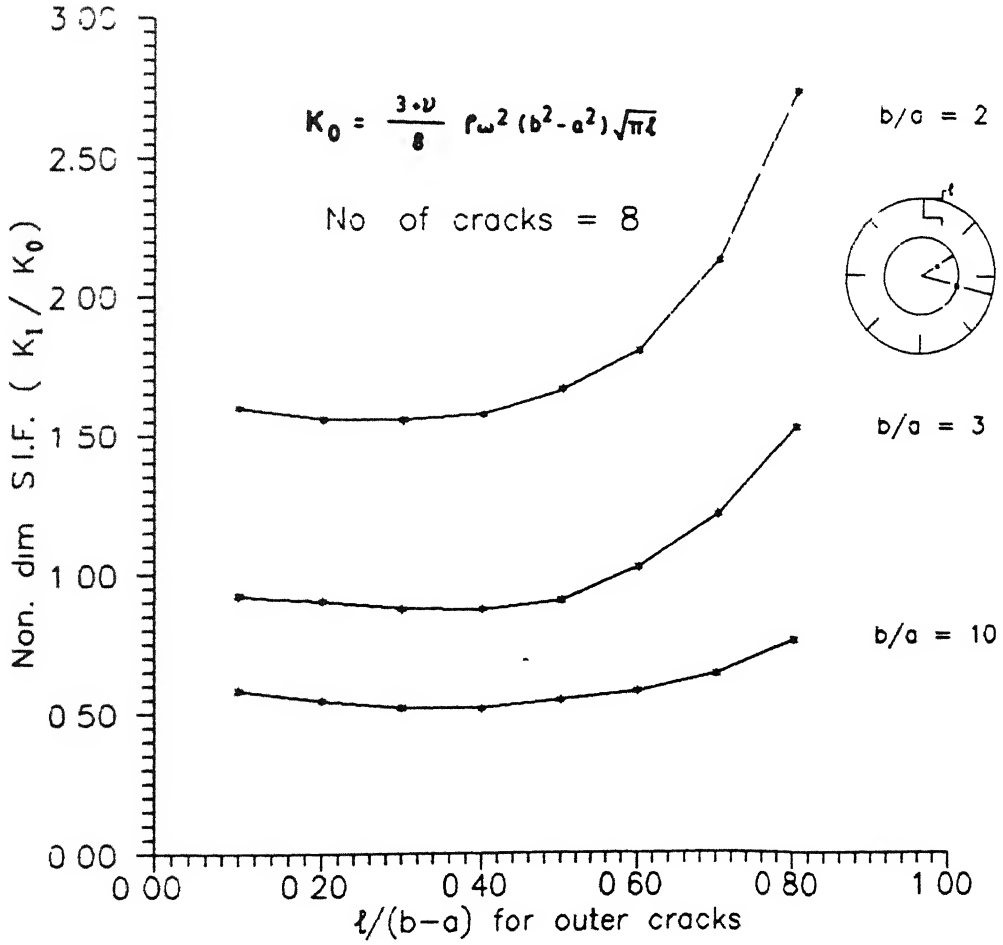

FIG.4.22 Curves of Non-dimensionalised S.I.F.'s as a function of 1/(b-a) with b/a as parameter for 8 Outer cracks

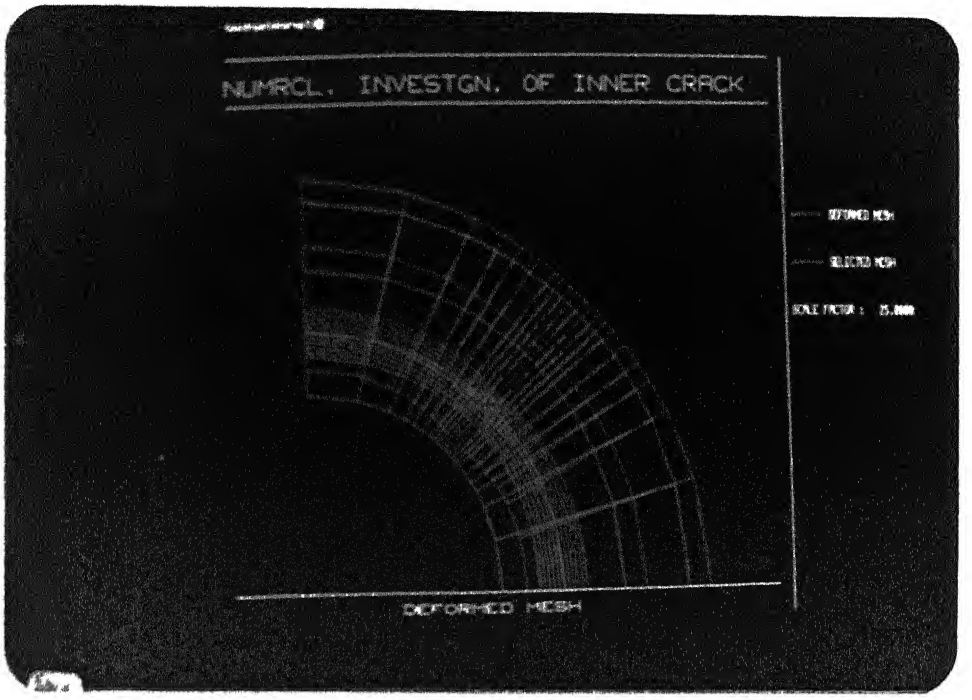

FIG. 4 23

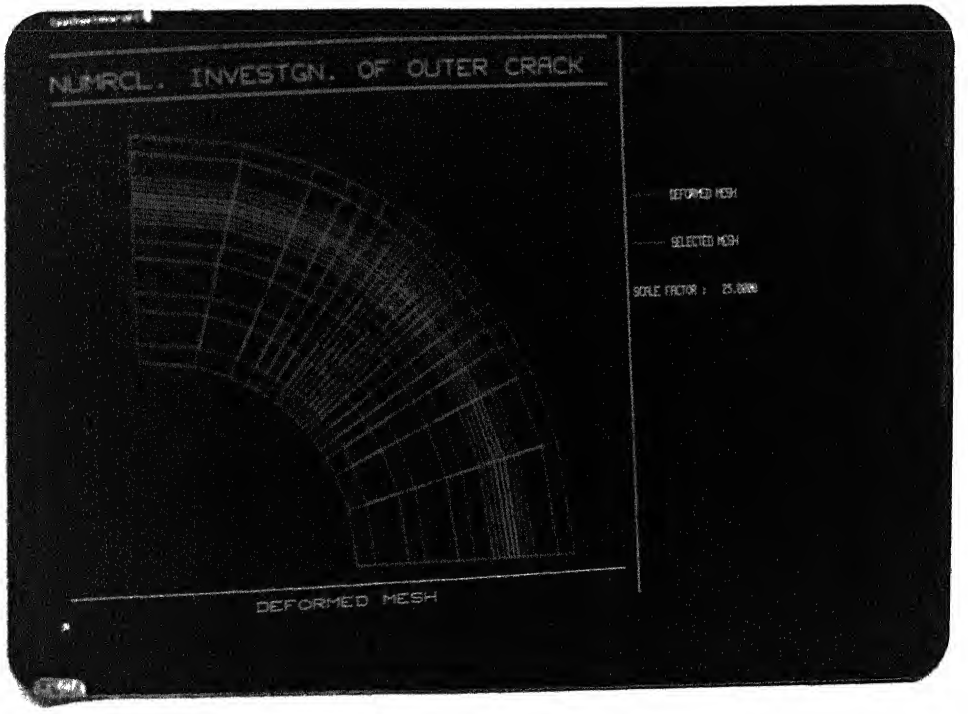

FIG. 4.24

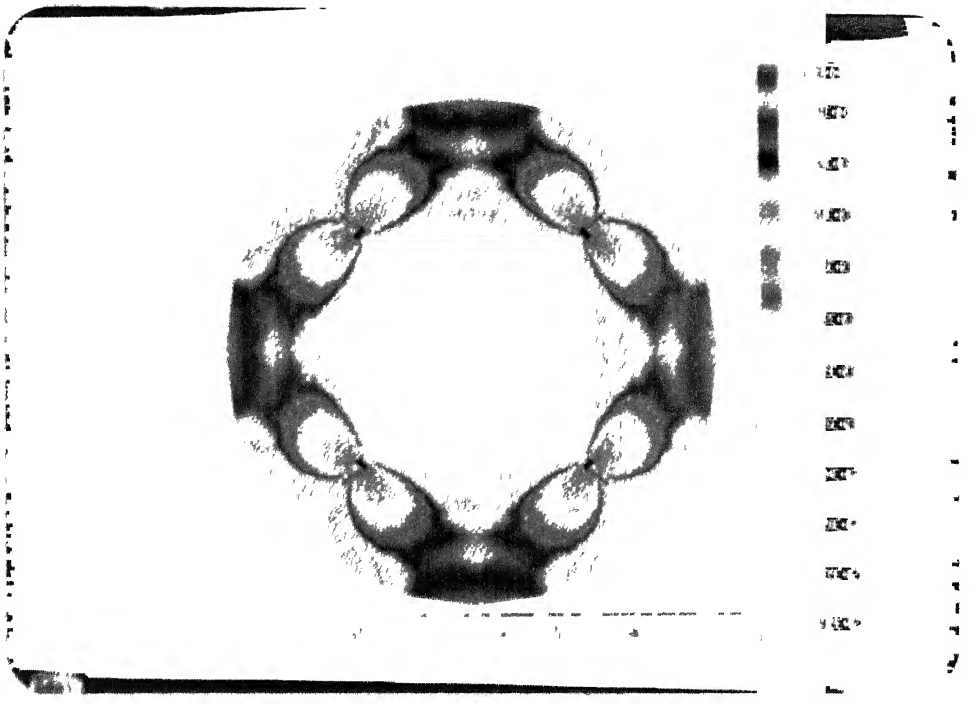

FIG 4 25

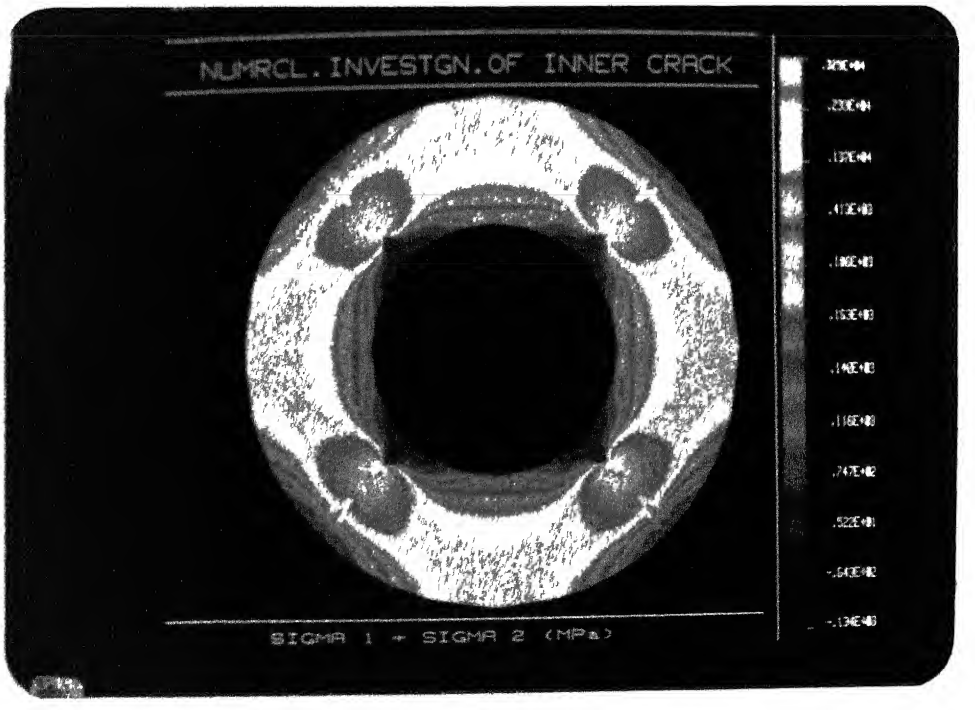

FIG. 4.26

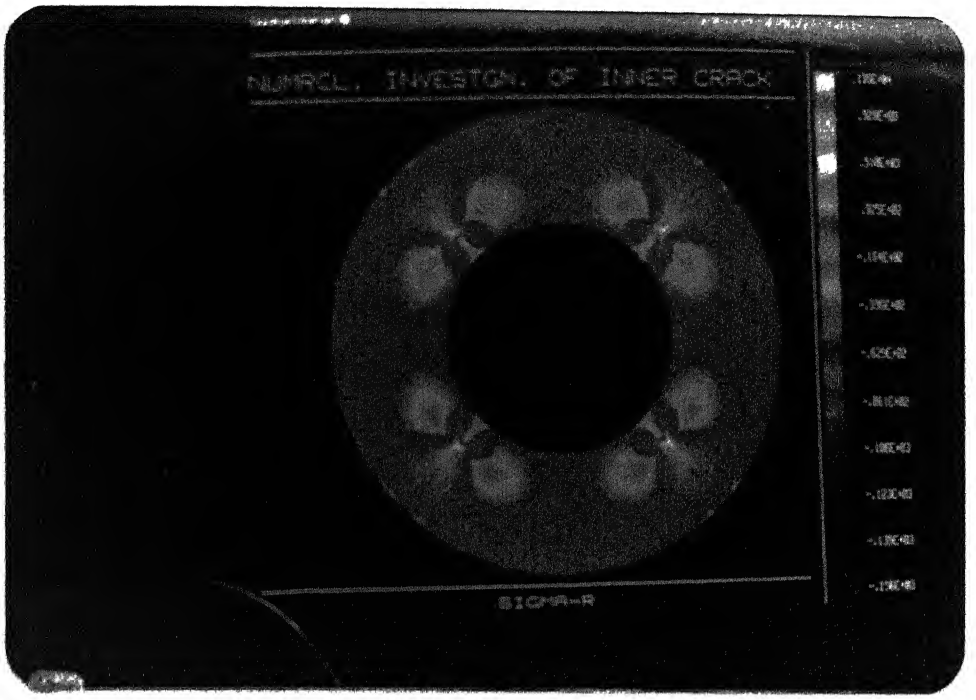

FIG 4.27

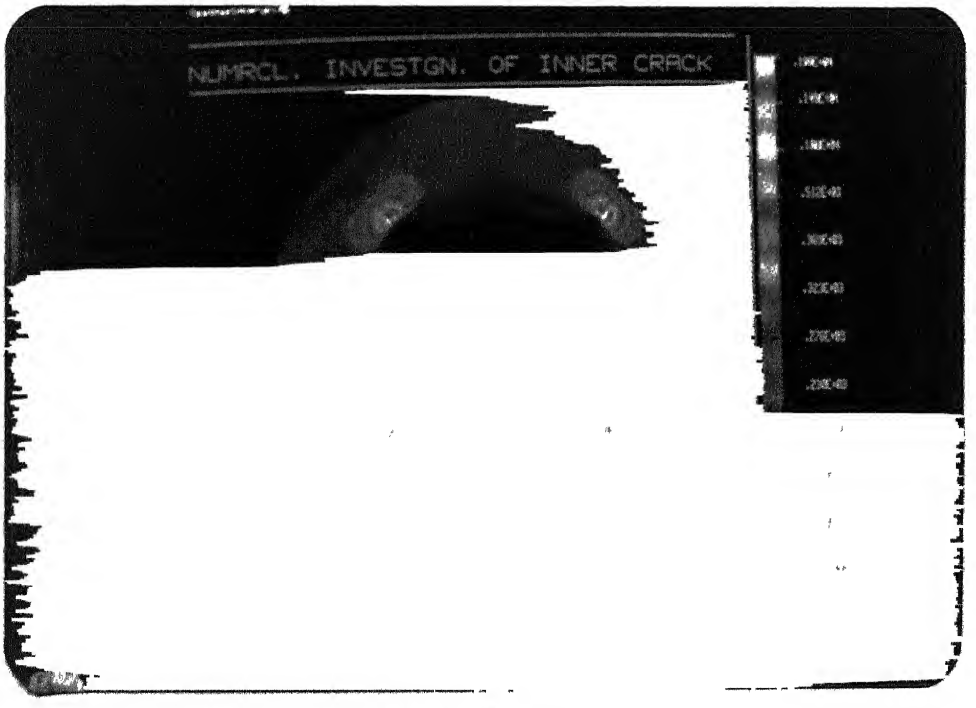

FIG. 4.28

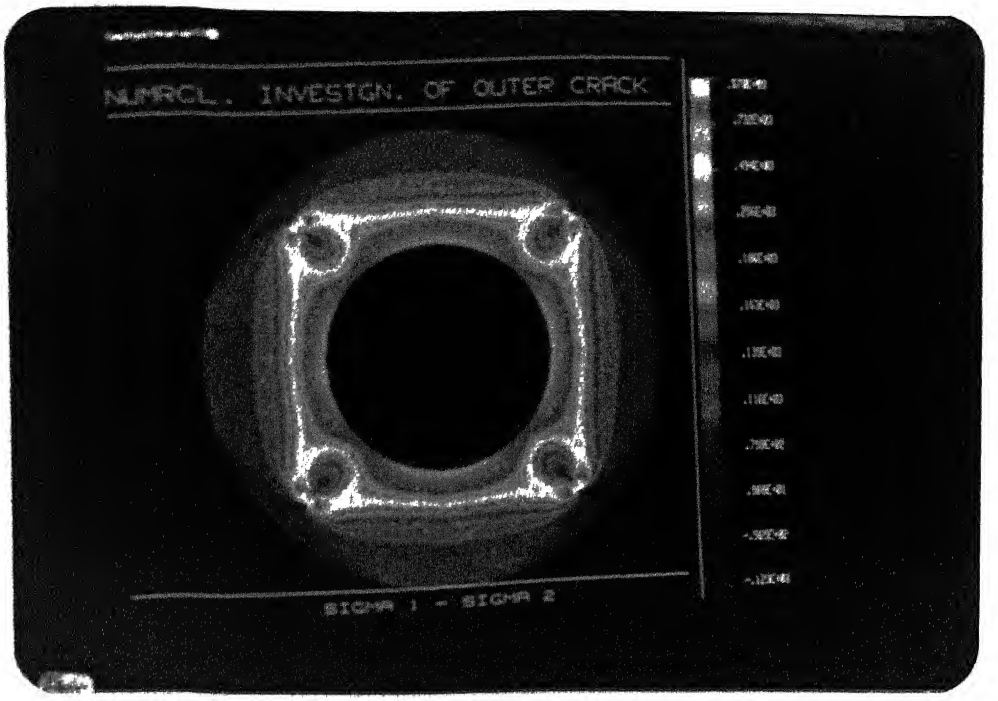

FIG. 4.29

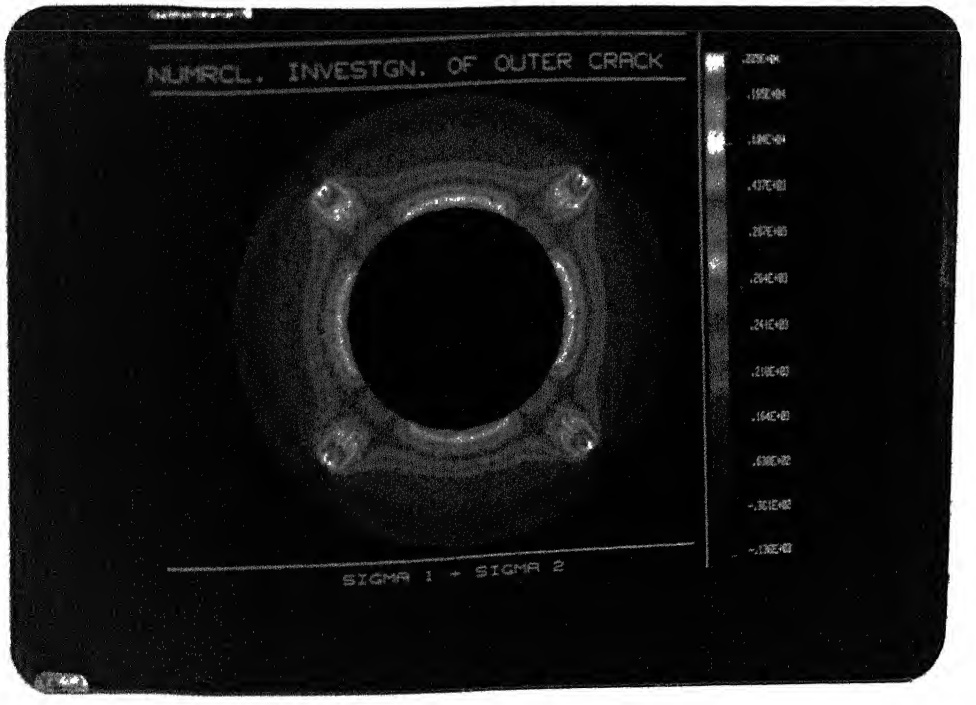

FIG. 4.30

FIG 4.31

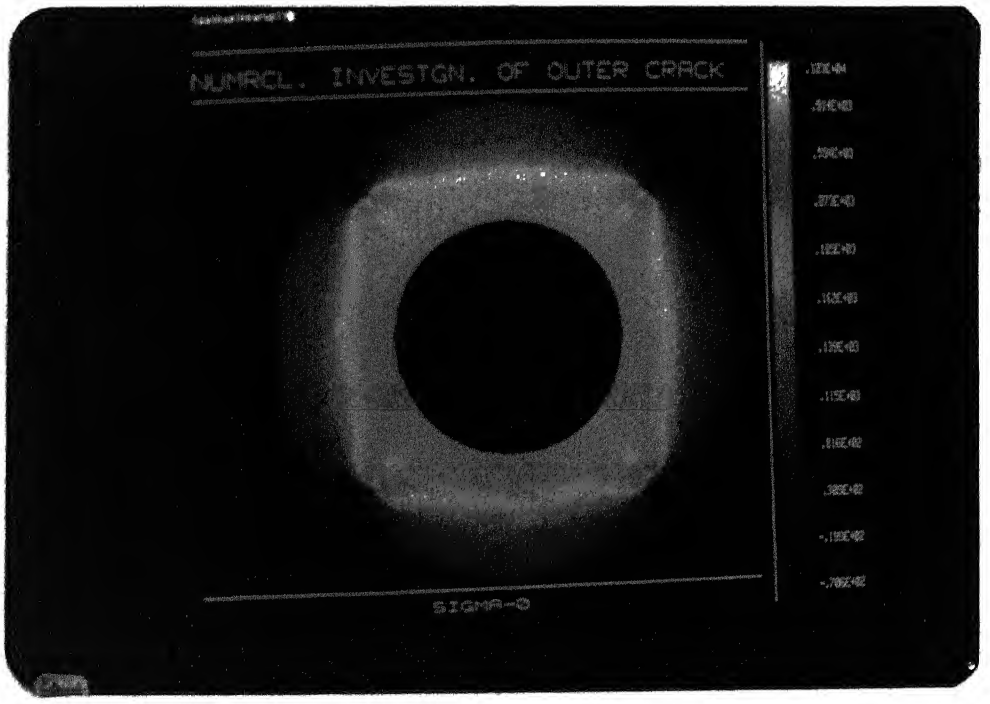

FIG. 4.32

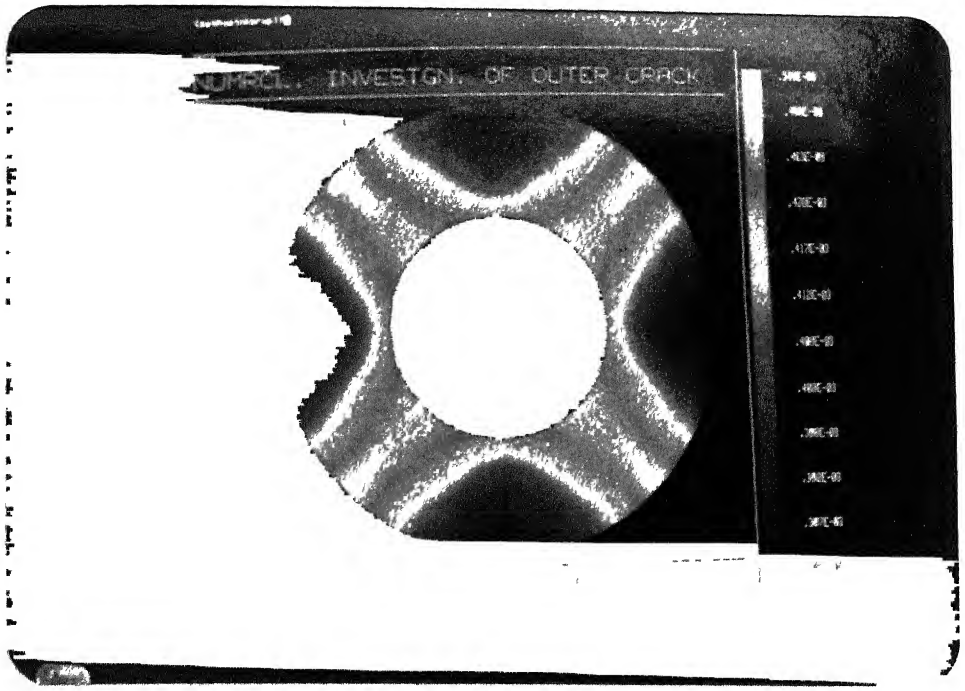

FIG. 4.33

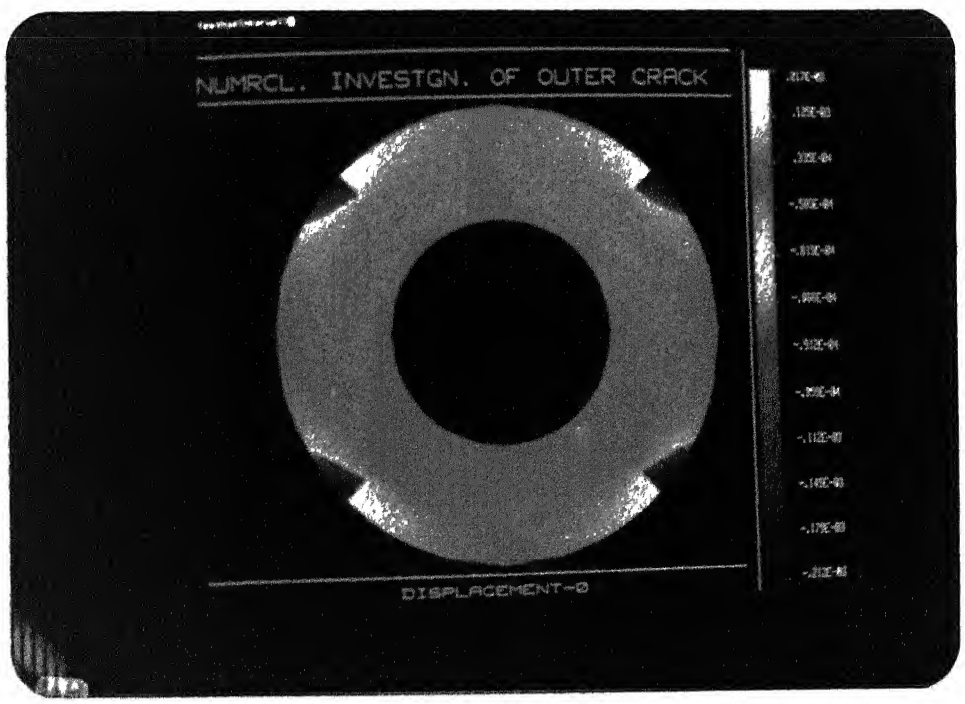

FIG. 4.34

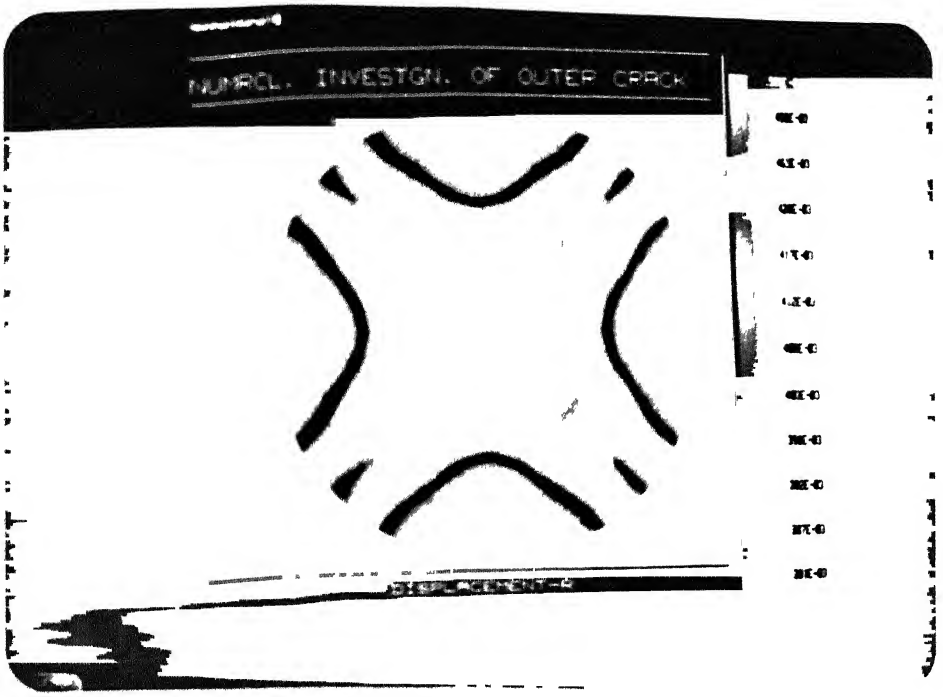

FIG. 4 35

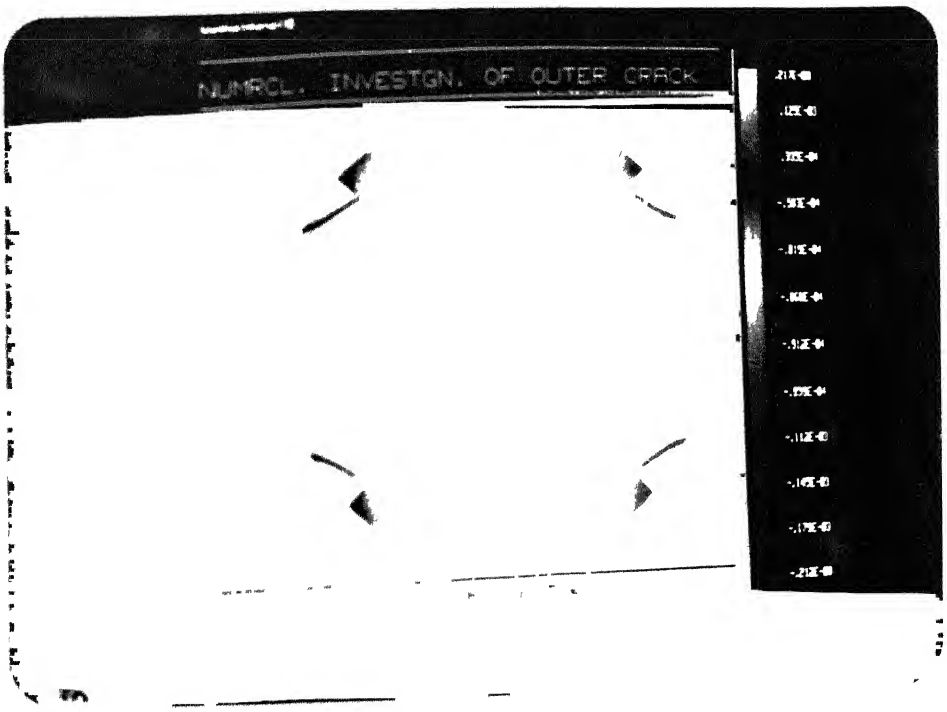

FIG. 4.36

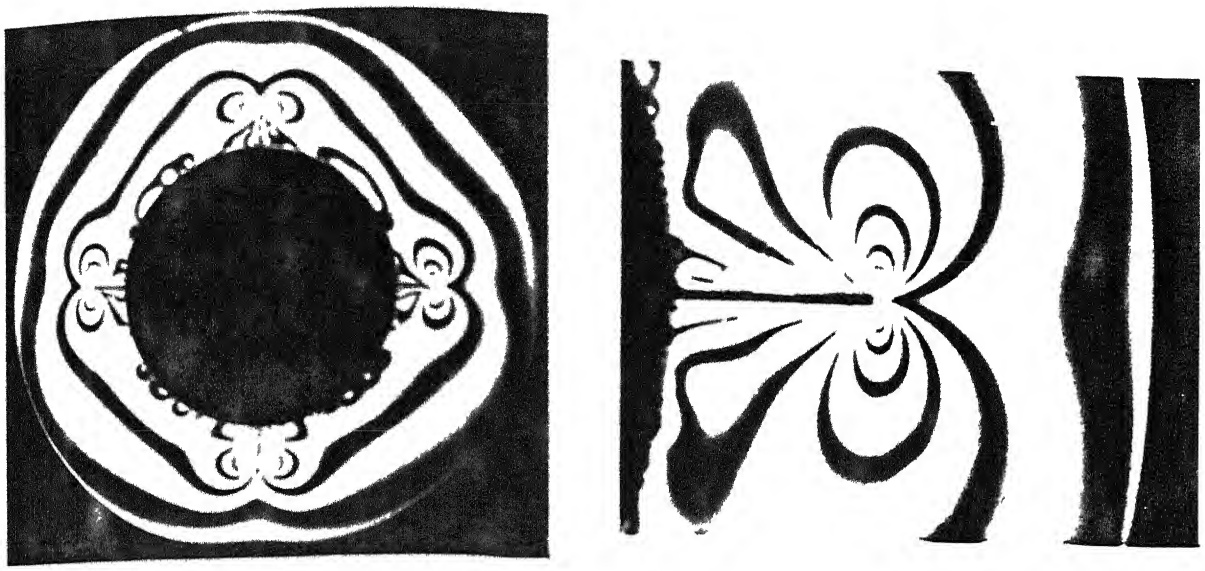

FIG 4.37 [illegible] obtained experimentally in an Annular [illegible] with 4 Inner cracks subjected to Internal [illegible] [28]

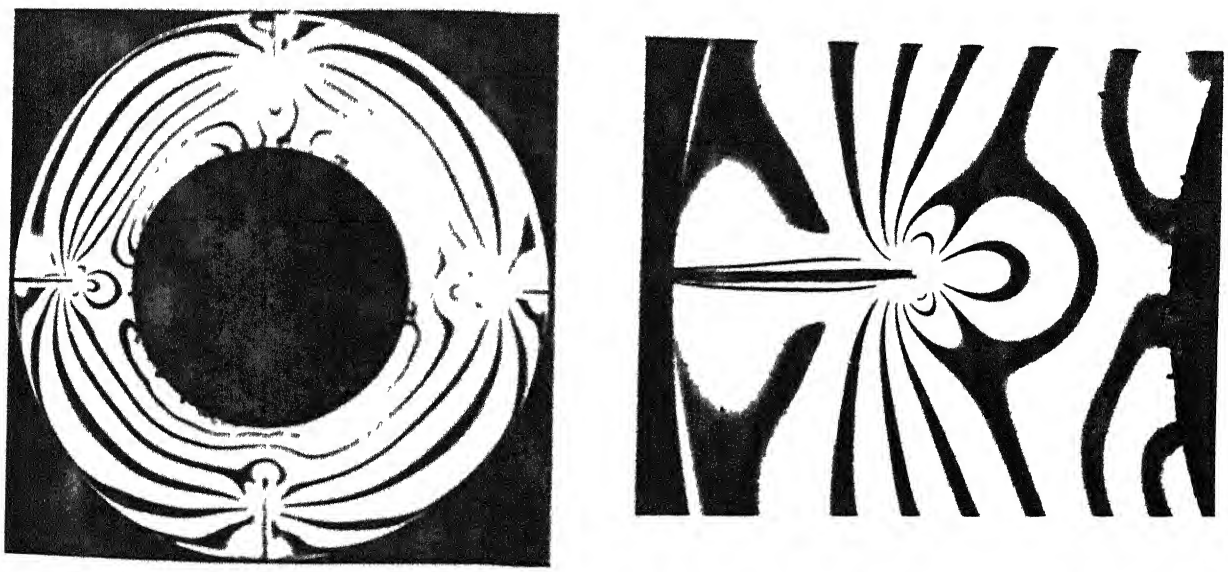

FIG.4.38 $(\sigma_1-\sigma_2)$ contours obtained experimentally in an Annular disc with 4 Outer cracks subjected to Internal pressure [28]

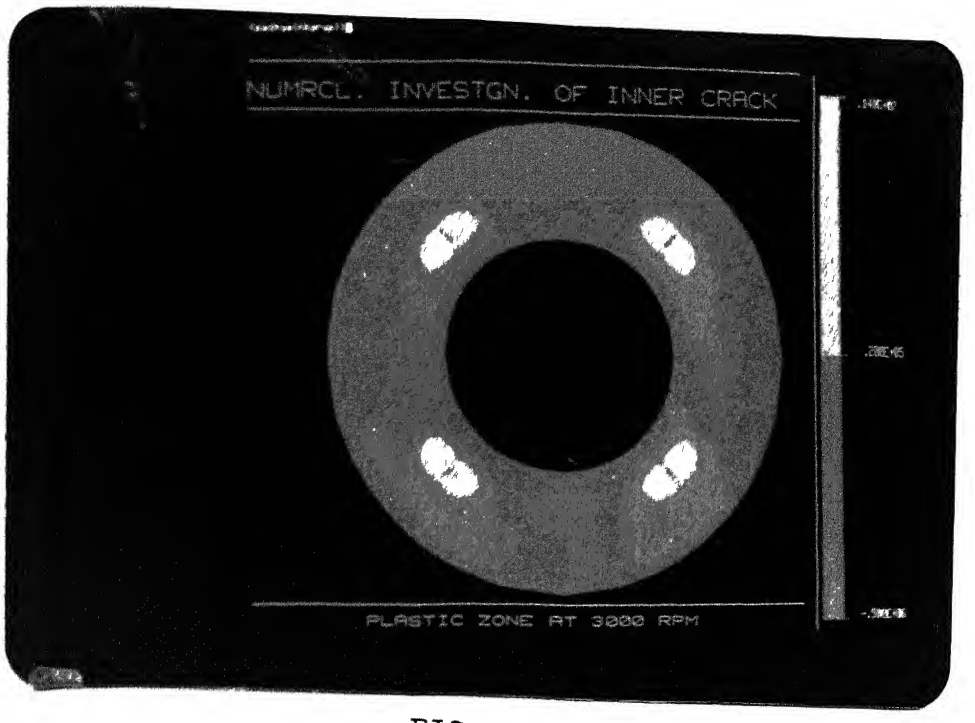

FIG 4.39

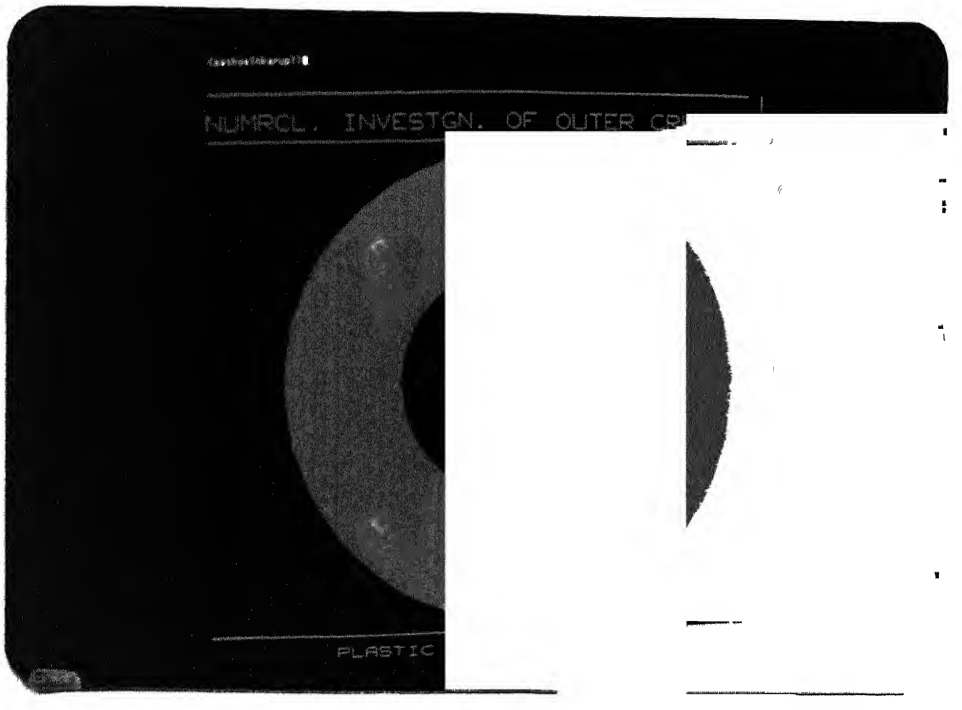

FIG. 4 40

CHAPTER 5

EVALUATION OF S.I.F. OF AN ANNULAR DISC SUBJECTED TO THERMAL STRESS

5.1 Introduction :

In this chapter, evaluation of S.I.F. in an annular disc subjected to thermal loading is discussed. It has been observed that the Clutch plate in an Automobile fail due to cracks emanating from inner boundary. An attempt has therefore been made to find the temperature distribution in a clutch plate enabling to calculate the S.I.F. of cracks in such plate.

5.2 Evaluation of Element Thermal Force Vector :

In Chapter 2, the element Thermal force vector has been derived as;

$$\{f_t\} = \iint [B]^T [D]\{\epsilon_o\}\, t \; dxdy \qquad \ldots(5.1)$$

But $\{\epsilon_o\} \alpha \{T\}$

Thus, if the Temperature distribution (T) in a disc is known, the stresses due to thermal loading can be evaluated by FEM.

5.3 Numerical Results :

A sample clutch plate of certain dimensions is taken and its Transient Temperature distribution is obtained by combination of FEM and Finite Difference Methods (FDM). The solution procedure is attached in Appendix 'B'. The Temperature

distribution so obtained is shown in Figs.(5.1-5.3). $(\sigma_1-\sigma_2)$ and σ_1 values have also been calculated for such plate and these contours are shown in Figs.(5.4-5.5). σ_1 being maximum at the inner boundary possibly explains the cause for cracks emanating from the inner boundary in clutch plates.

If such a clutch plate has 4 cracks from inner bounday, then its S.I.F. has been evaluated using the software developed by Cyclic Symmetry concept. The results have been obtained considering different temperature distributions such as T = r, T = r^2, T = 1/r, T = log r, T = log r + 500 and the actual distribution as obtained above. The results have been tabulated in Tab.(5.1). The $(\sigma_1-\sigma_2)$ contour developed for logarithmic distribution is shown in Fig.(5.6). The $(\sigma_1-\sigma_2)$ contour compare well with the isochromatics corresponding to Mode-I type of loading. This qualitatively indicates the correctness of the implementation.

5.4 Closure :

It has been shown that the concept of cyclic symmetry can be used effectively to determine the S.I.F. in the case of an annular disc subjected to Thermal loading. Next chapter deals with the Experimental Methods to determine the S.I.F.'s.

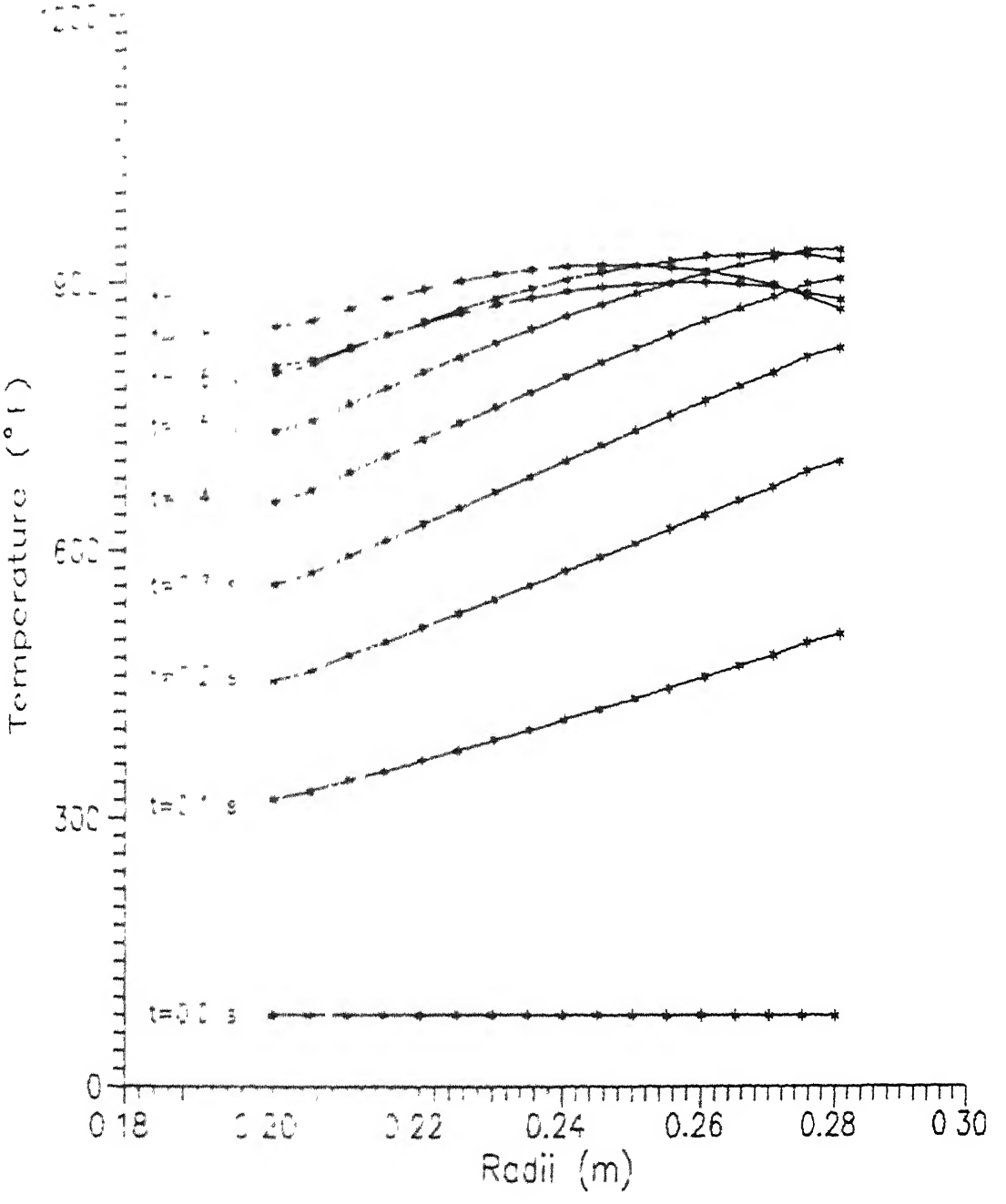

FIG.5.1 Transient Temperature distribution in a Clutch plate at the Surface as a function of Radius

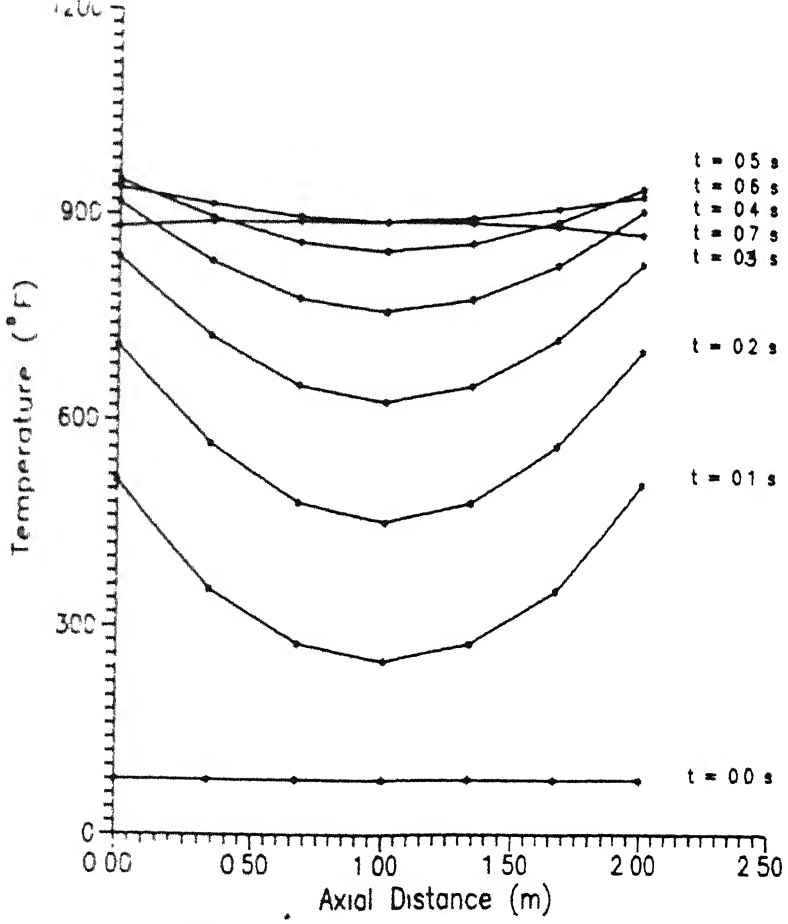

FIG.5.2 Transient Temperature distribution in a Clutch plate at the Outer Radius as a function of Distance in Axial direction

FIG.5 3 Temperature Distribution in a Clutch plate at the Surface as a function of Radius at

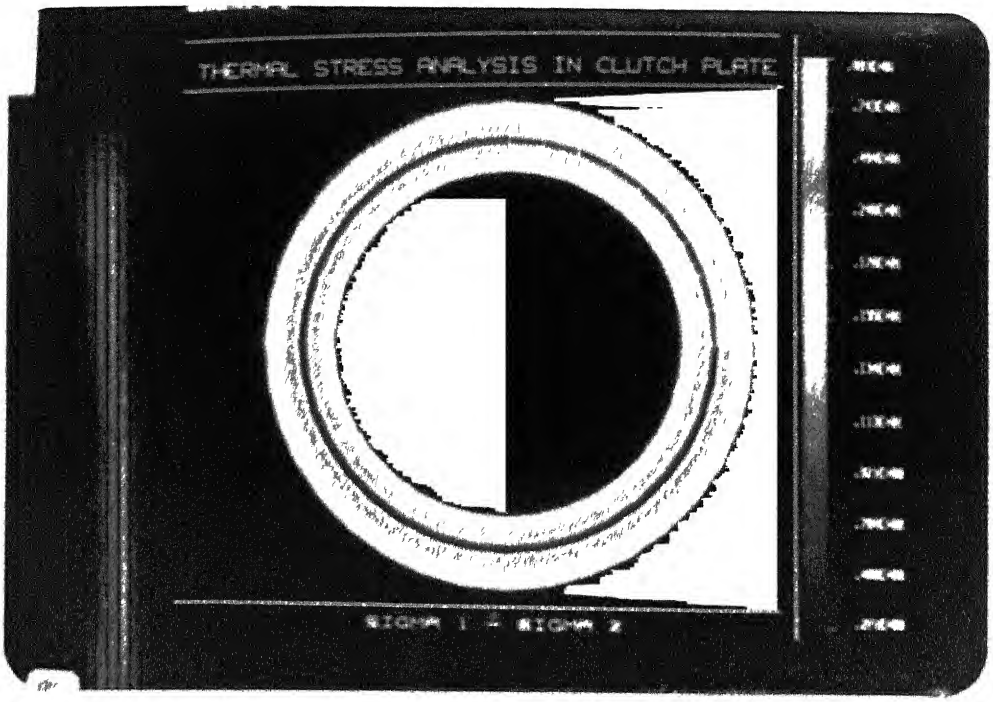
THERMAL STRESS ANALYSIS IN CLUTCH PLATE

FIG. 5.4

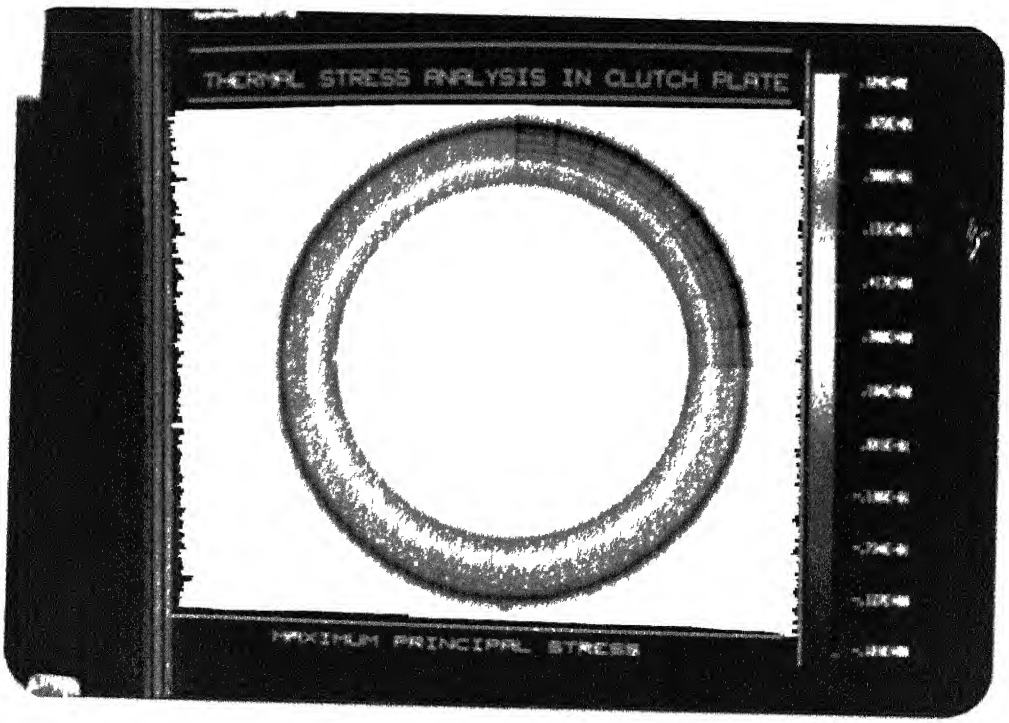
THERMAL STRESS ANALYSIS IN CLUTCH PLATE
MAXIMUM PRINCIPAL STRESS

FIG. 5.5

S No	Distribution	S I F (MPa$\sqrt{m}$)
1	T = r	0.129×10^{-3}
2	T = r^2	0.626×10^{-3}
3	T = 1/r	0.224×10^{-3}
4	T = log r	$0 536 \times 10^{-3}$
5	T = log r + 500	0.669×10^{-3}
6	as obtained in the analysis	0.420×10^{-3}

Table 5 1 S.I F's for a Clutch Plate with 4 Inner Cracks Subjected to Various Thermal Loadings.

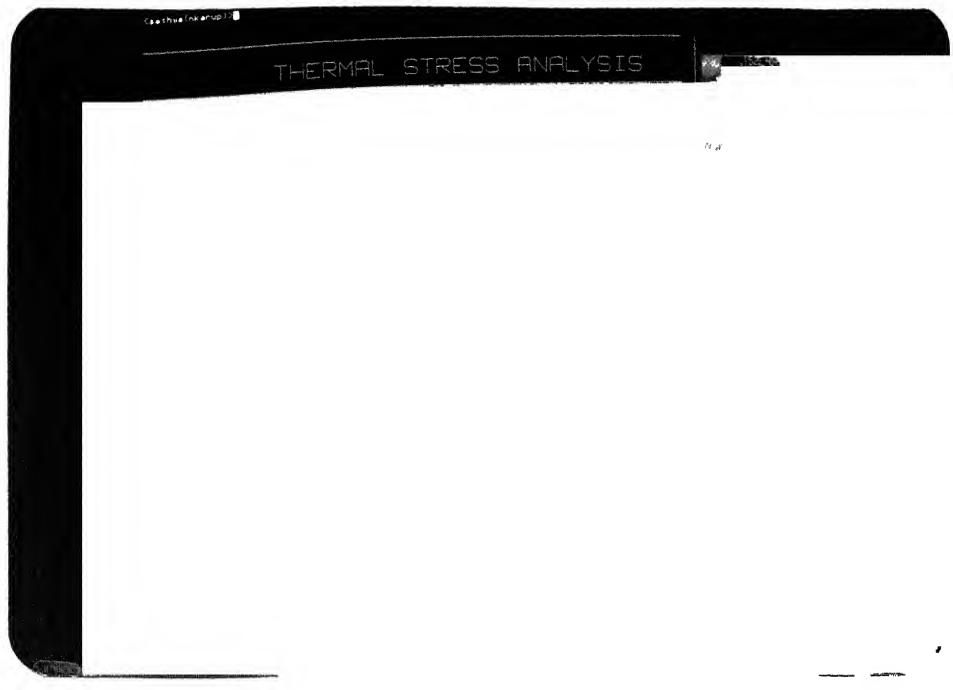

FIG 5.6

CHAPTER 6

EXPERIMENTAL DETERMINATION OF STRESS INTENSITY FACTORS

6.1 Introduction :

In the previous chapters, the use of Finite Element Method in the determination of S I F for the radial crack problem subjected to various loading conditions (body force and thermal loading) was discussed Chauhan [28] has evaluated the S.I F. using Transmission Photo-elasticity for the case of internal pressure loading He has confirmed that as the number of cracks increases, the S.I F. decreases.

For the case of annular disc with large number of radial cracks subjected to centrifugal loading, no corresponding experimental results are reported in the literature. In this chapter, the preliminary studies conducted to evaluate S.I F. using Strain gauges and Photoelastic coatings are discussed.

6.2 Determination of S.I.F through Strain gauges :

6.2.1 Strain field at the tip of a crack:

It is shown in Ref [30] that a modified form of the Westergaard equations can be applied to describe the stress field associated with a single-ended crack in terms of two stress functions Z & Y by

$$\begin{aligned} \sigma_{xx} &= ReZ - yImZ' - yImY' + 2ReY \\ \sigma_{yy} &= ReZ + yImZ' + yImY' \\ \mu\tau_{xy} &= -yReZ' - yReY' - ImY \end{aligned} \qquad \ldots(6.1)$$

where

$$Z(z) = \sum_{n=\emptyset}^{N} A_n z^{n-\frac{1}{2}}$$

$$Y(z) = \sum_{m=\emptyset}^{M} B_m z^m, \quad z = x + iy, \quad z' = dZ/dz, \quad Y' = dY/dz$$

Substituting Eq (6.1) into the stress-strain relations gives,

$$E\epsilon_{xx} = (1 - v)\mathrm{Re}Z - (1 + v)\, y\mathrm{Im}Z' - (1 + v)\, y\mathrm{Im}Y' + 2\,\mathrm{Re}Y$$

$$E\epsilon_{yy} = (1 - v)\mathrm{Re}Z + (1 + v)\, y\mathrm{Im}Z' + (1 + v)\, y\mathrm{Im}Y' - 2v\mathrm{Re}Y$$

$$\mu v_{xy} = - y\mathrm{Re}Z' - y\mathrm{Re}Y' - \mathrm{Im}Y \qquad \ldots(6\ 2)$$

Of particular importance is the radial strain because this strain can be measured effectively at a large number of points in the field with commercially available strip gauges with 1Ø sensing elements on each strip. The radial strain is obtained from Eq.(6.2) by using the strain equation of transformation

$$\epsilon_{rr} = \epsilon_{xx}\cos^2\theta + \epsilon_{yy}\sin^2\theta + \tau_{xy}\sin\theta\cos\theta \qquad \ldots(6.3)$$

which can be reduced to the following by using Eq.(6.2) and its derivatives.

$$\begin{aligned} 2\mu\epsilon_{rr} = {} & A_o n^{-\frac{1}{2}} \left(k\cos\frac{\theta}{2} - \frac{1}{2}\sin\theta\,\sin\frac{3\theta}{2}\cos 2\theta \right. \\ & \left. + \sin^2\theta\cos\theta\cos\frac{3\theta}{2}\right) + B_o(k + \cos 2\theta) \\ & + A_1 r^{\frac{1}{2}}\cos\frac{\theta}{2}\left(k + \sin^2\frac{\theta}{2}\cos 2\theta - \sin^2\theta\cos\theta\right) \\ & + B_1 r\cos\theta\,(k + 1 - 6\sin^2\theta) + A_2 r^{3/2}\left(k\cos\frac{3\theta}{2}\right. \\ & \left. - \frac{3}{2}\sin\frac{\theta}{2}\cos 2\theta - 3\sin^2\theta\cos\theta\cos^2\theta\right) \\ & + 2B_2(r^2/(1+v))(1 - (3 + 2v)\sin^2\theta\cos^2\theta \\ & + v\sin^2\theta\,(1 + \sin^2\theta)) \qquad \ldots(6.4) \end{aligned}$$

where $k = (1-v)/(1+v)$

6.2.2 Least Square Method to Evaluate S.I.F. :

In order to evaluate the strain field one can use strip gauges and these could be pasted along various θ's

For 'n' strain gauge sensors, Eq (6 4) may be used to form a system of equations in the unknown coefficients A_o, A_1, A_2, B_o, B_1 and B_2

$$2\mu\epsilon_{rr} = A_o\, r_1^{-\frac{1}{2}} z_{o1} + B_o\, r_1^{0} h_{o1} + A_1\, r_1^{\frac{1}{2}} z_{11} + B_1\, r_1^{1} h_{11} + A_2\, r_1^{3/2} z_{21} + B_2\, r_1^{2} h_{21}$$

$$\vdots$$

$$2\mu\epsilon_{rr_n} = A_o r_n^{-\frac{1}{2}} z_{on} + B_o r_n^{0} h_{on} + A_1 r_n^{\frac{1}{2}} z_{1n} + B_1 r_n^{1} h_{1n} + A_2 r_n^{3/2} z_{2n} + B_2 r_n^{2} h_{2n} \quad \ldots (6\ 5)$$

where g and h are functions of k and θ given in Eq (6 4)

Writing Eq.(6 5) in matrix form gives,

$$\{c\} = [D]\ \{AB\} \quad \ldots(6\ 6)$$

Since the total number of strain-gage readings exceed the number of unknown coefficients , i e., n > 6, Eq (6.6) represents an over-deterministic system of linear equations in the unknown coefficients. It is therefore necessary to statistically average the solution to make use of all the relevant data For this reason Eq (6 6) will be solved in the least-square sense For the least-squares solution of Eq (6.6), it is necessary to find a set coefficients {AB} which minimizes the vector {r} where

$$\{r\} = \{c\} - [D]\ \{AB\} \quad \ldots (6\ 7)$$

Ordinarily the solution to Eq (6 6) is obtained by forming the normal equations of the system,

$$[D]^T\ \{c\} = [D]^T\ [D]\ \{AB\} \quad \ldots(6.8)$$

which yield the least squares solution for the unknown coefficients

$$\{AB\} = ([D]^T [D])^{-1} [D]^T \{c\} \quad . \quad (6\ 9)$$

Note that {AB} is unique for a given set of n data points When using a power series such as those given by Eq (6 1),the formation of normal equations frequently gives rise to numerical instabilities when the number of terms in the series becomes large Previous experience with boundary collocation [31] indicates that these instabilities occur when more than 15 terms are used in the series expressions of Eq (6.1) Instabilities were not expected in this investigation since only six unknown coefficients were involved.

A second method for the least-squares solution of Eq.(6.6) which avoids the instabilities associated with the formation of the normal equations is the QR decomposition. In this procedure a sequence of Householder transformations are applied to matrix resulting in the partitioned product

$$[Q]D] = \begin{bmatrix} [R] \\ [o] \end{bmatrix} \quad . \ .(6.1\emptyset)$$

where matrix [Q] is orthogonal & matrix [R] is upper triangular If Eq (6.7) is multiplied by [Q],

$$[Q]\ \{r\} = [Q]\{c\} - [Q][D]\{AB\} \quad ...(6\ 11)$$

and if the product [Q] {c} is partioned as $[Q]\ \{c\} = \begin{bmatrix} \{f\} \\ \{g\} \end{bmatrix}$ ...(6.12)

it may be rewritten as

$$[Q]\ \{r\} = \begin{bmatrix} \{f\} - [R]\ \{AB\} \\ \{g\} \end{bmatrix} \quad . \ .(6\ 13)$$

The least-square solution to Eq (6 6) can then be found through standard elimination procedures on the determined system

$$[R]\ \{AB\} = \{f\} \qquad . \quad (6\ 14)$$

which minimizes the residual vector {r} Using the commercially available NAG subroutines, the least-squares solution to the linear system of Eq.(6.6) can be performed by QR decomposition

A software has been developed to solve such set of equations using QR decomposition [32].

6.2.3 Use of a Single Strain Gauge to evaluate S.I.F. :

In Eq (6 4), contribution of B_o parameter can be set to nil,

$$\text{if } (k+\cos 2\theta) = \emptyset$$

$$\text{i e} \quad \cos 2\theta = -k = -\frac{(1 - \nu)}{(1 + \nu)} \qquad ..(6.15a)$$

$$\text{also,} \quad K_I = \sqrt{8/3\ \pi r}\ E\epsilon_{rr} \qquad . \quad (6\ 16)$$

Thus K_I can be determined by measuring the strain at a point close to the crack-tip on a radial line whose inclination is defined in terms of Poisson's ratio of the material via Eq (6 15a), with another condition that the gauge must be placed at a position where radial co-ordinate $r > \emptyset.5 * t$ where t is the thickness of the specimen [33].

In case the orientation of the strain gauge (α) as shown in Fig.(6.1) is not the same as θ , the inclination , then the governing equation for its placement becomes as

$$\tan \theta/2 = -\cot 2\alpha \qquad ...(6.15b)$$

For Aluminium, taking $\nu = \emptyset\ 3$, θ is found to be equal to $6\emptyset°$.

An experiment was conducted to verify this procedure to find stress intensity factor using one strain gauge using SEN specimen which is explained as below :

6.2.4 Experimental Details :

Three specimens of size 310 * 35 * 3 2 mm were made of Aluminium and cracks were cut with a/w ratio equal to Ø 1, Ø 2, Ø 3 respectively on the edges using Ø.25 mm milling cutter.

One strain gauge each was pasted at r = 3mm & θ = 60° from the crack tip on both sides of the specimens of a/w equal to Ø 1 and Ø 2 and at r = 6mm & θ = 60° for the specimen of a/w equal to Ø 3. Close-up view of one such strain gauge pasted is as given in Fig.(6 2)

These strain gauges were connected in quarter bridge in the strain-indicator and the specimens were loaded in the MTS tensile testing machine with a grip length of 30 mm upto a maximum load of 5 kN in steps of Ø 5 kN and the strains developed as recorded in the indicator were noted The experimental set-up is shown in Fig.(6.3).

The strain readings noted are as tabulated in Tab (8 1). Also tabulated are the percentage errors in S I F using strain gauge as compared to the S I.F. evaluated by boundary collocation method

Although this method of strain-reading from single strain gauge pasted at a particular position and orientation requires the prior knowledge of the valid field and the plastic zone correction unlike the over-deterministic method, the results show that it could be be utilised to determine the Opening Mode Stress Intensity Factor (K_I) with accuracies sufficient for engineering applications

Experiments were also planned to be conducted on rotating discs to verify this method. But, as there was delay in getting the slip rings required for the experiments, they could not be conducted.

6.3 Determination of S.I.F. through Birefringent-coatings :

6.3.1 Introduction :

Birefringent-coating method, a branch of photo-elasticity is a whole field technique to study the stress distribution on the surface of a body. In this method, a thin layer of photoelastic plastic is bonded to the surface of the body under investigation. When load is applied to the body, the strains set up in it are transmitted to the photo elastic coating. The coating then becomes doubly refracting and a fringe pattern is visible when viewed in the field of polarised light This birefringence observed is directly proportional to the intensity of strain developed The data obtained by this technique is analogous to the data obtained from innumerable strain gauges of virtually zero gauge length A reflection type polariscope is used to observe the birefringence.

Consider a plane object with a thin coating as shown in Fig.(6.4) [34] subjected to loading which produces a plane state of stress It is assumed that the stresses do not vary through the thickness of the coating.

Let σ_{1p}, σ_{2p}, ϵ_{1p}, and ϵ_{2p} refer to the principal stresses and principal strains on the surface of the object and σ_{1c}, σ_{2c}, ϵ_{1c} & ϵ_{2c} correspond to the coating. If it is assumed that surface displacements are transmitted without distortion to the coating, then

$$\begin{aligned} \sigma_{3c} &= \sigma_{3p} = \emptyset \\ \epsilon_{1c} &= \epsilon_{1p} \\ \epsilon_{2c} &= \epsilon_{2p} \end{aligned} \qquad ..(6.17)$$

From stress-optic law, the difference of principal stresses $(\sigma_{1c} - \sigma_{2c})$ in the coating allowing for double passage of light is given by

$$(\sigma_{1c} - \sigma_{2c}) = \frac{F\sigma N}{2h_c} \qquad ..(6.18)$$

where N is the fringe order observed,
F is the materiala stress fringe value and
h is the thickness of the coating.

Using Eqs.(6.17) , it can be shown

$$(\sigma_{1p} - \sigma_{2p}) = \frac{E_p\ (1 + \nu_c)}{E_c\ (1 + \nu_p)} \quad \frac{NF\sigma}{2h_c} \qquad \ldots (6.19)$$

where E_p & ν_p are elastic modulus and poisson's ratio of the object and E_c & ν_c are elastic modulus and poisson's ratio of the coating

Also,

$$(\epsilon_{1p} - \epsilon_{2p}) = N\lambda/2h_cK \qquad \ldots (6.2Ø)$$

where K is the strain optic coefficient for the coating provided by the manufacturer and λ is the wavelength in nanometers of the light being used.

Thus, from Eqs.(6.19), it is seen that the difference in principal stresses or principal strains can be determined from the isochromatic fringe order in the birefringent coating. Also, the directions of the principal stresses or strains are obtained by the isoclinics

Isoclinic and Isochromatic are defined as follows .

1. **Isoclinic** : The locus of points where the directions of the principal stresses coincide with a particular orientation of polarizer analyser combination .

2. **Isochromatic** : It is the locus of points where the values of $(\sigma_1 - \sigma_2)$ are such as to cause a relative phase difference of $2m\pi$ when the background is dark and $(2m+1)\pi$,(m=Ø,1,2...) when the background is bright

6.3.2 Experiments conducted :

i) S.E.N. Specimen :

A specimen of size 31Ø * 35 * 3 mm of Aluminium was prepared and a crack of length 7 mm (a/w=Ø 2) was cut on one edge of the specimen using Ø.25 mm milling cutter A photoelastic coating of size 5Ø * 35 * 3 mm, of Type PS-1A (of Measurements Group Inc., U.S.A), of K factor .15 and thickness 3 mm was bonded onto the surface using PC-1 cement Note that a crack of the same size was also cut on the coating.

The specimen was loaded in a MTS tensile testing machine gradually. The photograph of the fringes seen through the reflection polariscope at a load of 5,ØØØ Newtons is shown as Figs.(6.5-6.6). The fringes represent the stress field near the crack tip. The fringes show a mixed-mode loading (Mode-I + Mode-II) and this is due to the fact that crack cut was not exactly perpendicular to the loading direction

ii) Rotating disc :

A disc of size 26Ø OD,3Ø ID, 3mm thickness was made of Aluminium Two internal cracks of length were cut diametrically opposite through Ø.25 mm milling cutter and photoelastic coatings were bonded onto the crack tips. The disc was clamped and driven by a 1/8 HP AC motor The disc was rotated at different speeds through a Variac connected in series.

The disc was viewed through reflection polariscope under stroboscopic illumination. The experimental set-up and the fringes seen at a speed of 3ØØØ RPM are shown as Figs.(6.7-6.8) However due to lack of time, this experiment could not be conducted in detail

6.4 Closure

It is seen that both Photo-elastic coating and Strain-gauge technique could be employed to find S I F. Though Photo-elastic coating is a whole-field technique, the centrifugal stresses are not sufficient to produce sufficient fringes on the coating Use of a singe strain gauge to find S.I.F. is a promising technique and with modern strain gauge instrumentation, it is possible to find even 1 micro-strain precisely. Hence, with the use of slip rings, one can expect to get better estimates of S.I.F. by strain-gauge technique in rotating discs

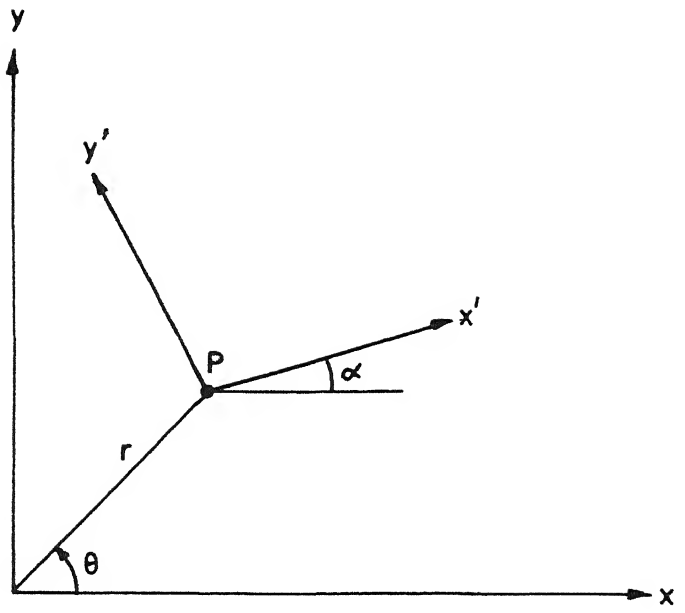

FIG.6 1 Orientation of Strain-gauge

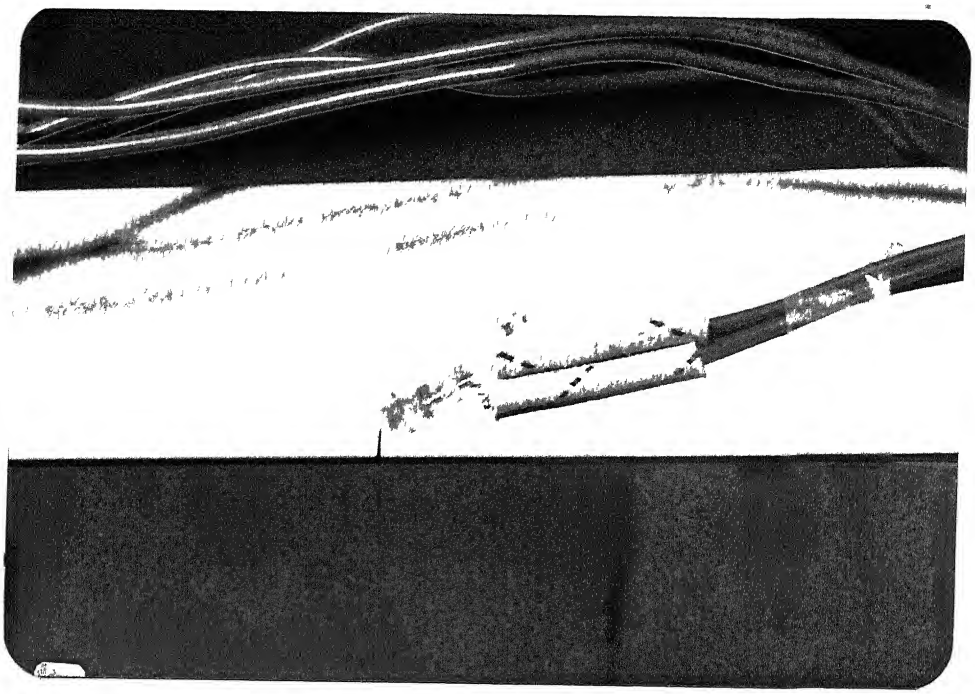

FIG 6 2 Close-up View of Strain-gauge pasted

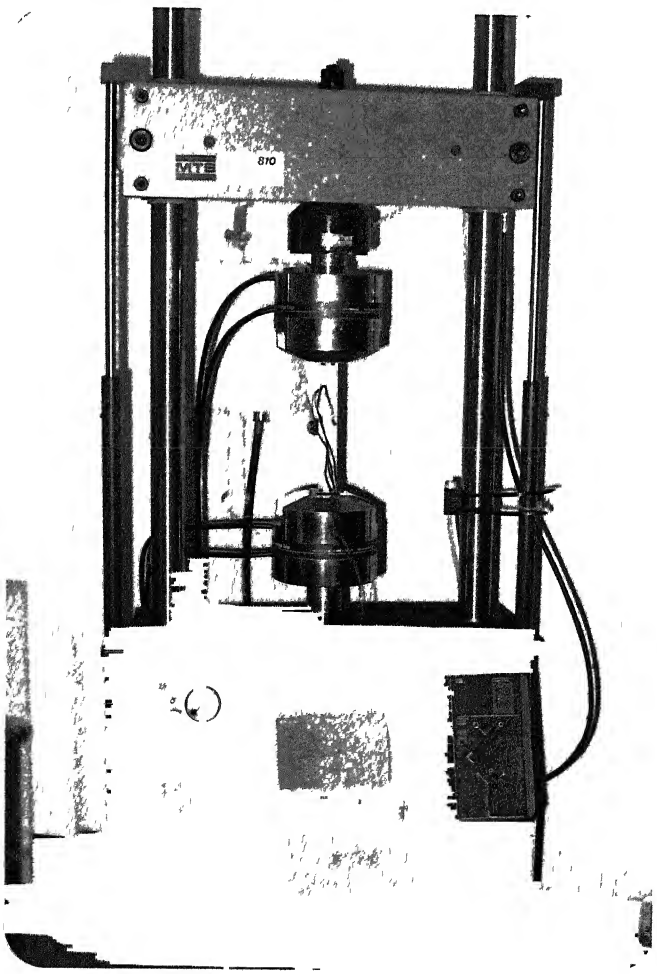

FIG. 6 3 Experimental Set-up for Strain Measurement

S. No	Load (N)	ϵ_A Micro	ϵ_B Micro	ϵ_{Avg} Micro	ϵ_t Micro	Error %
1	500	52	68	60	65	7 7
2	1000	107	134	120	130	7 7
3	1500	160	204	182	195	6 7
4	2000	212	270	241	259	6 9
5	2500	268	342	305	324	5 8
6	3000	320	414	367	388	5 4
7	3500	376	482	429	453	5 3
8	4000	428	552	490	518	5 4
9	4500	482	622	552	582	5 2
10	5000	540	692	616	647	4 8

Table 8.1· Strain Gage Readings in SEN Specimen
Strain Gage Length = 3 mm
Strain Gage Resistance = 120 Ω
Strain Gage Factor = 2.0

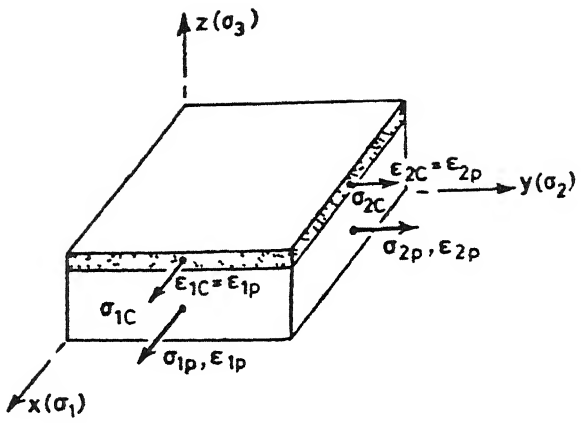

FIG.6.4 Stresses in Photo-elastic Coating

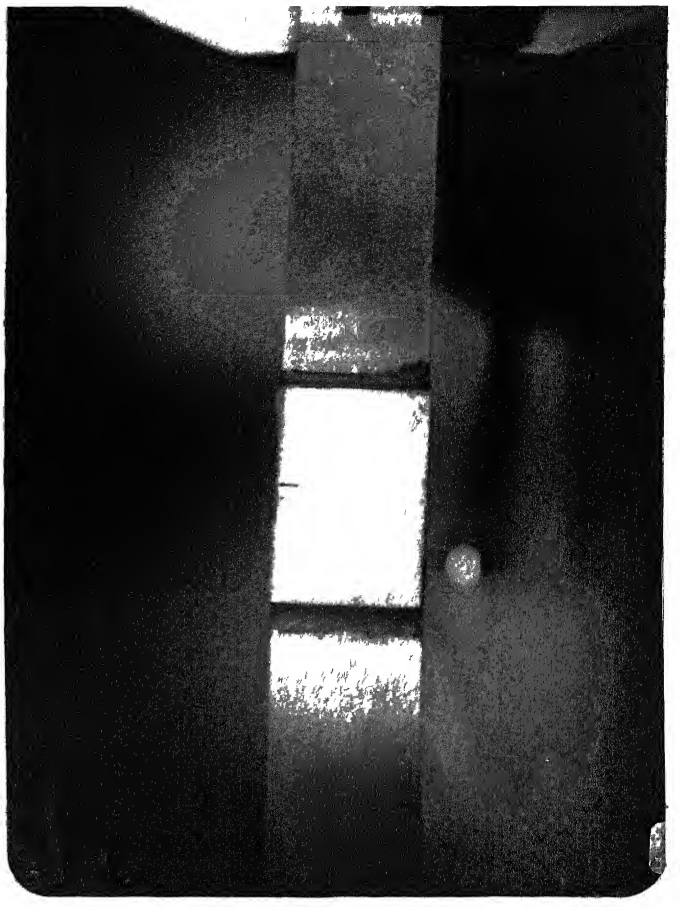

FIG 6 5 Fringes seen in Birefringent-Coating

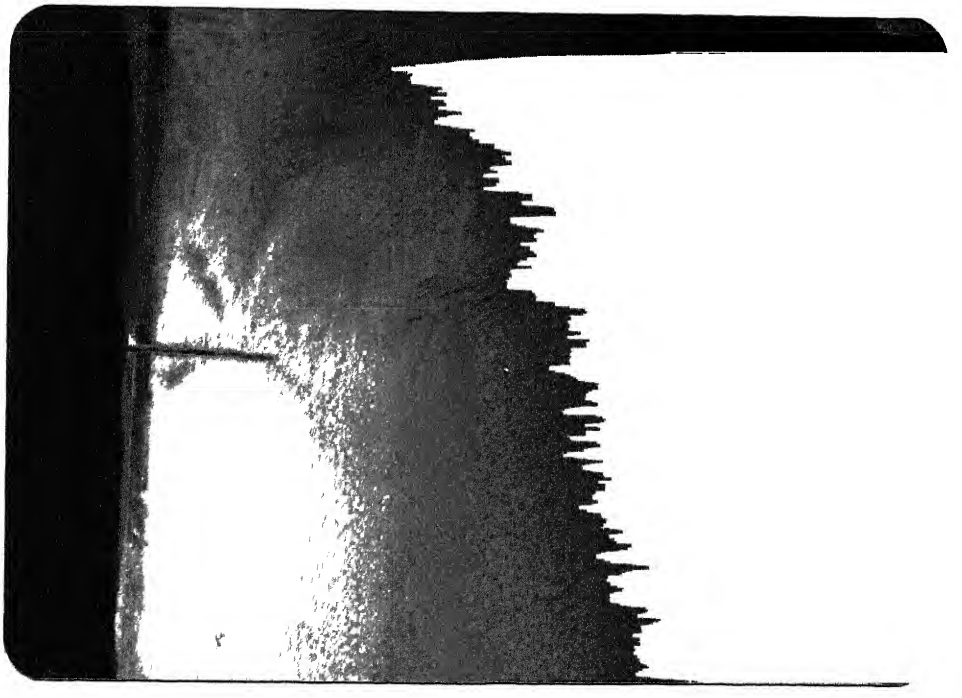

FIG. 6.6 Close-up View of Fringes seen in Birefringent-Coating

CHAPTER 7

CONCLUSIONS AND SUGGESTIONS FOR FUTURE WORK

It has been shown that cyclic symmetry concept could be used with success to determine S.I.F in the case of a rotating annular disc with periodic radial cracks Considerable amount of work has been done to determine S.I.F's as a function of crack lengths, number of cracks and b/a ratios for both, inner and outer cracks

It has been further shown that the concept of cyclic symmetry can be used also to determine the S I F in the case of an annular disc subjected to Thermal loading Transient temperature distribution in the case of a clutch plate has been found out using a combination of FEM and FDM.

Use of single strain gauge to find S.I.F is a promising technique with modern strain gauge instrumentation This has been verified finding S.I.F. of SEN specimen

Following are suggested for future work :

1 The program developed could be modified incorporating Centrifugal force , Axial loading and Boundary conditions such as to simulate the actual conditions in a clutch plate.

2 Strain-gauge technique could be utilised in finding S.I F in rotating discs using Slip rings

APPENDIX A

SHAPE FUNCTIONS OF 8-NODE ISOPARAMETRIC ELEMENT

$$N_1 = (1/4)\ (1-r)(1-s)(-r-s-1)$$

$$N_2 = (1/4)\ (1+r)(1-s)(r-s-1)$$

$$N_3 = (1/4)\ (1+r)(1+s)(r+s-1)$$

$$N_4 = (1/4)\ (1-r)(1+s)(-r+s-1)$$

$$N_5 = (1/2)\ (1-r^2)(1-s)$$

$$N_6 = (1/2)\ (1+r)(1-s^2)$$

$$N_7 = (1/2)\ (1-r^2)(1+s)$$

$$N_8 = (1/2)\ (1-r)(1-s^2)$$

APPENDIX - B

TEMPERATURE DISTRIBUTION IN A CLUTCH PLATE OF AN AUTOMOBILE

I) Introduction :

Clutch plate of an automobile is subjected to centrifugal and thermal stresses when it engages with the engine flywheel to transmit torque to the transmission shaft. If the temperature distribution in clutch plate is known, corresponding stresses can be calculated easily using the software discussed Z J Jania [29] derives an analytical expression for the transient temperature distribution in such plates assuming constant rate of wear of the rubbing surfaces. With this assumption, the rate of energy dissipation and hence the temperature distribution is only a function of time and it is constant along the radii. But, if the pressure due to the axial clamping force is assumed to be constant over the rubbing surfaces, the distribution becomes a function of radii also An attempt has therefore been made in this Appendix to find the Transient temperature distribution which occurs in such clutch plates assuming constant pressure by combination of FEM and FDM techniques as described below ·

II) Numerical Formulation :

Fig. 7.1 shows two clutch plates in contact under the action of an axial clamping force F Plate II is coated with frictional material and plate I is made of steel. Surfaces AD & BC where rubbing occurs can be thought of as plane sources of heat producing $q_o(t)$ kW per sq.mt. Temperature distribution in the Clutch plate I is governed by the Transient Fourier Conduction equation given below;

$$\frac{1}{r}\frac{\partial}{\partial r}\left(r\frac{\partial T}{\partial r}\right)+\frac{\partial^2 T}{\partial z^2}=\frac{Pc}{k}\frac{\partial T}{\partial t} \qquad \ldots(7.1)$$

where 'ρ' is Mass density, 'c' is Heat capacitance and 'k' is Thermal conductivity of the material This equation is solved along with the Boundary and Initial conditions Before discussing the Boundary conditions, it is first necessary to estimate the Rate of Heat generation ($q_o(t)$)

i) Rate of Heat generation :

A typical Power transmission can be idealised as shown in Fig 7.2 for the purpose of estimation of the rate of heat generation [29]. Here the Resistive load torque (T_R) is simulated by the brake For simplicity, all torques are assumed constant

When compliance of the system is neglected,

$$w_1(t) = \frac{T_1 - T_c}{I_1} t + r_1 \qquad (7.2)$$

$$w_2(t) = \frac{T_c - T_2}{I_2} t + r_2 \qquad ..(7.3)$$

where w(t) is angular velocity in rad/sec.,
T is torque in N-m,
I is Moment of Inertia in Newton-m-sec^2
r is initial velocity in rad/sec ,
t is time in sec.
and subscripts 1 and 2 pertain to the engine and load sides and 'c' refers to the clutch.

At the end of slip period (t_o),

$$w_1(t_o) = w_2(t_o)$$

$$\text{Therefore, } t_o = \frac{I_1 I_2 (r_1 - r_2)}{T_c (I_1 + I_2) - (I_2 T_1 + I_1 T_2)} \qquad ...(7.4)$$

It is assumed that the Pressure 'p' due to the axial clamping force is uniformly distributed over the plate area. Then the Clutch frictional torque (dT_c) over the elemental area $2\pi r dr$ is given by,

$$dT_c = \mu p r (2\pi r dr) \qquad ...(7\ 5)$$

where μ is the coefficient of friction

The rate at which heat is generated over the element area $2\pi rdr$ in the clutch during slipping is given by,

$$q_o(t) = \mu pr(w_1(t)-w_2(t)) \quad \ldots(7\ 6)$$

Thus, the rate of heat generation is directly proportional to the product of pressure and radial position Since the pressure is assumed to be constant, the rate of heat generation would be directly proportional to radial position of the plate.

The effect of lubricating oil is not considered in calculation of the rate of heat generation as it is difficult to keep track of change in lubrication from hydrodynamic to boundary type while the oil is squeezed out of the space between the plates as they close Depending on the type of lubricant, under boundary lubrication conditions, temperature can be 30 to 60 percent lower than in the case of dry friction.

ii) Boundary conditions :

At the rubbing interface AD & BC, the rate of heat generated is given by the Eqs (7 2-7 3 & 7.5-7.6). The ratios of heat flows into the plates I and II are not equal but depend on the thermal conductivity of the materials in contact If the thermal conductivities are k_1 and k_2, then the heat fluxes into the plates I and II are given by ,

$$q_1(t) = (k_2/k_1 + k_2)\ q_o\ (t) \quad \ldots(7\ 7)$$

$$q_2(t) = (k_1/k_1 + k_2)\ q_o\ (t)$$

Heat transfer from the clutch plates to the surroundings during slipping is assumed to be neglible Therefore, at the boundaries AB and CD,

$$q(t) = 0.$$

For axisymmetric problems only half the plate needs to be considered. Therefore the conditions are to be specified on the boundary EF also Here also it is assumed that $q(t) = 0$.

Then at boundaries BB,

$$q(t) = 0 \quad \ldots(7\ 8)$$

Eqs (7 7 & 7.8) are the boundary conditions necessary for the solution of Eq.(7.1).

iii) Initial Conditions :

In the beginning of engagement, the clutch temperature is the same as the ambient temperature T_o i e ,

$$\text{At time 't' = Ø, } T = T_o \qquad . \quad (7\ 9)$$

III) Solution Technique :

i) Galerkin Integral :

The first step in the Numerical solution of the Eq (7 1) is the formulation of the Galerkin integral This integral is obtained by multiplying the Eq.(7.1) with the weight function 'W' and integrating the product by parts over the whole domain. Thus the expression for the integral becomes,

$$I(T_1\ W) = \int_{\Omega} \left(pc\frac{\partial T}{\partial t} W + k \left(\frac{\partial T}{\partial r}\frac{\partial W}{\partial r} + \frac{\partial T}{\partial r}\frac{\partial W}{\partial z}\right)\right) 2\pi r dr dz$$

$$- \int_{\Gamma} q^* W\, 2\pi r\, ds \qquad \ldots 7\ 1Ø$$

where q^* is the prescribed heat flux on the boundary Γ. Here, W is required to satisfy homogeneous version of the essential boundary conditions.

ii) Finite Element Approximation :

In Galerkin Finite Element Method, the Temperature and the Weight function are approximated using same shape functions Thus over a typical element,

$$T = \{N\}^T \{T\}^e$$
$$W = \{N\}^T \{W\}^e \qquad \ldots (7\ 11)$$

where {N} is the Shape function vector and $\{T\}^e$ and $\{W\}^e$ contain the nodal values of T and W.

Substituting Eq 7.11 into Eq 7.1Ø, we get

$$I = \sum_{e=1}^{n_e} \{W\}^{eT} \{C\}^e \{\dot{T}\}^e + \{W\}^{eT} [K]^e \{T\}^e - \sum_{b=1}^{n_b} \{W\}^{bT} \{Q\}^b \quad (7\ 12)$$

where n_e = number of area elements,

n_b = number of line elements on the boundary Γ on which 'q' is specified and

$$[C]^e = \int\int \rho c [N]^T [N]\ 2\pi r dr dz \quad . \ 7.13$$

= Elemental Heat capacity matrix

$$[K]^e = \int\int k [B]^{eT} [B]\ 2\pi r dr dz \quad ...7.14$$

= Elemental Heat conductivity matrix

$$[Q]^b = \int q^* [N]^b\ 2\pi r dr db \quad .. 7.15$$

= Elemental Heat flux vector

Writing I in terms of Global Matrices,

$$I = \{W\}^T [C] \{\dot{T}\} + \{W\}^T [K] \{T\} - \{W\}^T \{Q\} \quad . .7.16$$

where [C],[K] & {Q} are obtained by assembling the appropriate elemental matrices Since $\{W\} \neq \{Ø\}$,

$$[C] \{\dot{T}\} + [K]^T \{T\} = \{Q\} \quad . .7.17$$

The time integration is done by Finite Difference Method as explained below

iii)Time Integration by Finite Difference Method :

The time integration of the Eq.(7.17) is done using a Finite Difference scheme We approximate the Time derivative {T} by the following difference formula;

$$\theta \{T\}_{i+1} + (1-\theta) \{T\}_i = \frac{\{T\}_{i+1} - \{T\}_i}{(\Delta t)_{i+1}} + O(\Delta t)^2_{i+1} \quad .(7.18)$$

where θ takes the values as Ø,1/2,2/3 or 1 depending on whether

it is Forward Difference, Crack-Nicolson, Galerkin, or Backward Difference scheme used Here, Backward difference scheme was used (θ=1)

Substituting Eq.7.18 into Eq.7 17,

$$[A]_{i+1} \{T\}_{i1} = \{B\}_{i,i+1} , \quad i = 0,1, \ldots \quad (7\ 19)$$

where,

$$[A]_{i+1} = [c] + (\Delta t)_{i+1}\ \theta\ [k] \quad \ldots (7.20)$$

$$\{B\}_{i,i+1} = \{[c] - (\Delta t)_{i+1}\ (1 - \theta)\ [k]\}\ \{T\}_i + (\Delta t)_{i+1}\ \{\ \theta\{Q\}_{i+1} + (1 - \theta)\ \{Q\}_i\ \} \quad \ldots (7.21)$$

This equation is solved from the first time step upto the required time. Time limit was chosen as 't' = 't_o'

A sample problem as described below has been solved using the above mentioned method and the results are shown in Figs (5 1-5 3).

IV) Sample Problem :

Consider a system in which the clutch is the multiple disc type with alternate steel and cork-coated plates System and clutch data are as below :

I_1	=	1 729	Newton-m-sec^2
I_2	=	5.186	Newton-m-sec^2
T_1	=	346	Newton-m
T_2	=	276	Newton-m
r_1	=	500	Rad./sec
r_2	=	200	Rad /sec
2l	=	0.002	m
T_o	=	80 °F	
k_1	=	23.1	W/m^2-°F/m
k_2	=	0.231	W/m^2-°F/m
P_1	=	76,800	Newton/m^3
c_1	=	32.56	Joule/Newton-°F

where subscript '1' refers to the clutch steel plate and '2'refers to the cork-coated friction plate

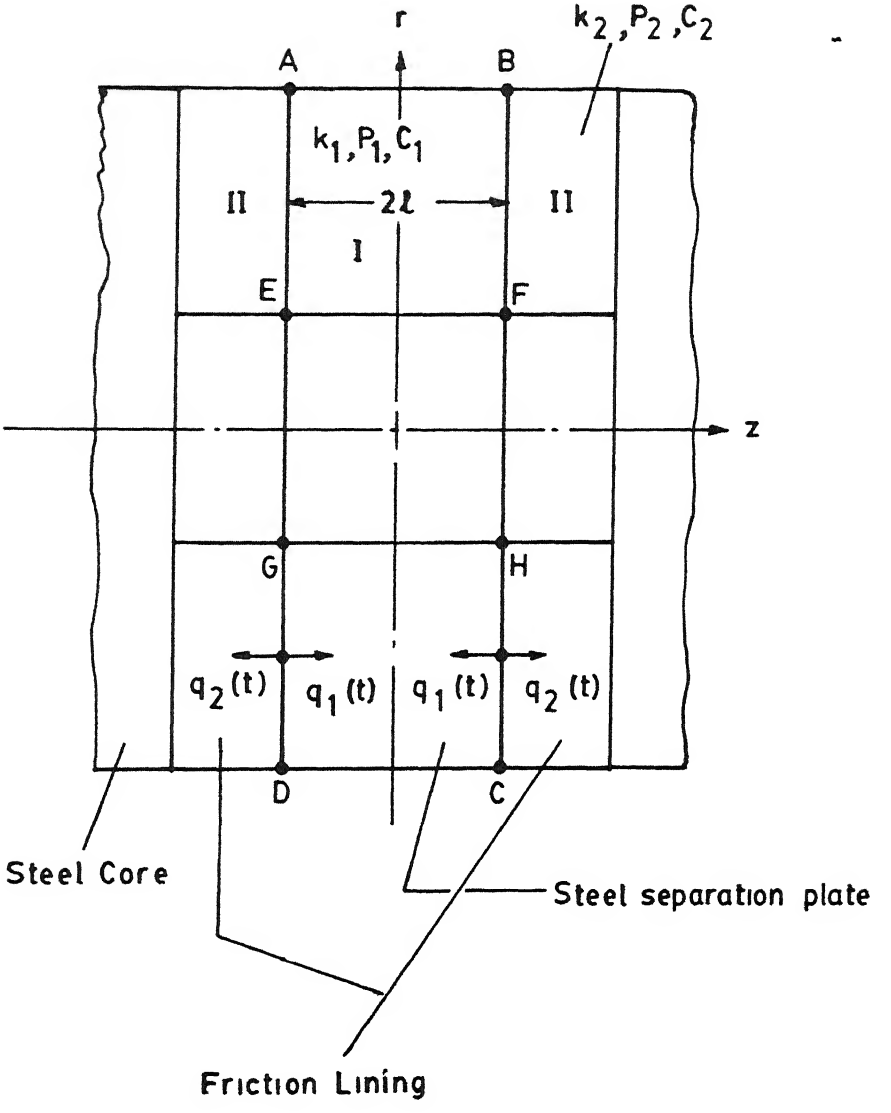

FIG. 7.1 Rubbing surfaces of a clutch plate

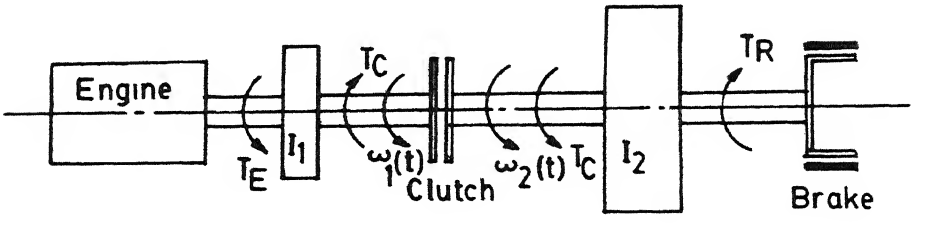

FIG 7 2 Typical Power Transmission System

REFERENCES

1. David Broek, "Elementary Engineering Fracture Mechanics", Sijthoff & Noordhof Int. Publishers (1978).

2. O L Bowie and C E. Freese, "Elastic Analysis for a Radial Crack in a Circular Ring", U S Ammre Monograph, MS-70-3, Watertown, MA (1970).

3. O L Bowie, "Analysis of an Infinite Plate Containing Radial Cracks Orignatings et the Boundary of an Internal Circular Hole", J Math and Phys. 35-60, (1965).

4 Francis I. Baratta, "Stress Intensity Factors for Internal Multiple Cracks in Thick-walled Cylinders Stressed by Internal Pressure Using Load Relief Factors", Engineering Fracture Mechanics, Vol. 10, pp. 691-697, (1978).

5. Kapp. J.A., "The Effect of Autofrettage on Fatigue Crack Propagation in Externally Flawed Thick Walled Disks", U.S. ARADCOM Tech Rep. ARCLB-TR-77025, Watervliet, NY (1977)

6. Peter G Tracy, "Elastic Analysis of Radial Cracks Emanating From the Outer and Inner Surfaces of a Circular Ring", Engineering Fracture Mechanics, Vol.11, pp.291-300,(1979)

7 S S.Shukla, "Numerical Investigation of the Radial Crack Problem" M.Tech Thesis, September 1989, I.I.T , Kanpur

8. Perl M & Arone R., "Stress Intensity Factors for a Radially Multicracked Partially Autofrettaged Pressurized Thick Cylinder", Trans ASME J Pres Vessel Tech., Vol. 110, pp. 147-154, (1988).

9. R S Barsoum, "On the Use of Isoparametric Finite Elements in Linear Fracture Mechanics", INJNME,Vol 1Ø,pp 25-37,(1976)

1Ø R D Henshell and K G. Shaw, "Crack Tip Finite Elements are Unnecessary", INJNME, Vol. 9, pp 495-5Ø7, (1976)

11. R.S Barsoum, "Further Application of Quadratic Isoparameteric Finite Elements to Linear Frcture Mechanics of Plate Bending and General Shells", Int J Fract , Vol. 11, pp 167-169, (1975)

12. R.S. Barsoum, "Triangular Quarter-Point Elements as Elastic and Perfectly Plastic Crack Tip Elements", INJNME Vol 11, pp 85-98, (1977)

13. C.E. Freese and D.M Tracy, "The Natural Isoparametric Triangle Versus Collapsed Quadrilateral for Elastic Crack Analysis", Int J. Fract., Vol. 12, pp 768-77Ø, (1976).

14 S L. Pu, M.A Hussain and W.E Lorensen, "Collapsed 12 node Triangular Elements as Crack Tip Elements for Elastic Fracture", Tech Rep ARLCB-TR-77Ø47, (1977).

15. Y. Yamada, Y. Ezawa and I. Nishiguchi, "Reconsiderations on Singularity or Crack Tip Elements", Int J Numer Methods Eng , Vol. 12, pp 1525-1544, (1979)

16. H.D. Bibbitt, "Some Properties of Singular Isoparametric Elements", Int. Numer. Methods Eng , Vol 11, pp. 18Ø-184, (1977).

17. L.A. Ying, "A Note on the Singularity and the Strain Energy of Singular Elements", Int. J Numer Methods Eng , Vol 18, pp. 31-39, (1982).

18. R S Barsoum, "Letter to the Editor", Int. J Numer. Methods Eng , Vol 18, pp 142Ø-1428, (1982)

19 R S Barsoum, "Triangular Quater Point Elements as Elastic and Perfectly Plastic Crack Tip Elements", Int. J. Numer. Methods Eng., Vol. 11, pp. 85-98, (1977).

20. P.P Lyan and A.R. Ingraffea, "Transition Elements to be Used with Quarter-Point Crack Tip Elements", IJNME, Vol. 11, pp 85-98, (1977).

21 M A. Hussain, J.D Vasilakis and L Pu, "Quadratic and Cubic Transition Elements", IJNME, Vol 16, pp 1397-1406, (1981)

22. A.R Ingraffea and C. Manu, "Stress Intensity FActor Computation in Three Dimension with Quarter - Point Elements', IJNME, Vol. 15, pp 1427- 1445, (1980)

23 R S Barsoum, "An Assessment of the Quarter-Point Elements in Pressue Vessel Fracture Analysis", Paper L6/5, Structural Mechanics in Reactor Technology, Conf., Paris, (1981)

24. L.P. Harrop, "The Optimum Size of Quarter-Point Crack Tip Element", IJNME, Vol. 17, pp. 1101-1103, (1982)

25 Vector E. Saouma and David Schwemmer, 'Numerical Evaluation of the Quarter-Point Crack Tip Element', IJNME, Vol 20, pp. 1920-1941, (1984).

26. K.J. Bathe and E.L. Wilson, "Numerical Methods in Finite Element Analysis.

27. Robert D Cook, "Concept and Applications of Finite Element Analysis", John Wiley & Sons, New York, (1981).

28 D.P S Chauhan, "An Experimental Study of Static and Dynamic Behaviour of Cyclically Symmetric Radial Cracks", M Tech Thesis , February 1990, I I T ,Kanpur

28a V. Ramamurti, "Computer Aided Design in Mechanical Engg.", Tata McGraw Hill Publication, New Delhi, (1984).

29 Z J. Jania, "Friction Clutch Transmissions" -- Part 3 - Thermal Capacities and Limitations", Machine Design, December 1958

30. J.R. Berger and J W Dally, "An overdeterministic Approach for Measuring K_I using Strain Gauges".

31 J.R. Berger, "An Improved Method of Boundary Collocation for the Analysis of Finite Body Opening Mode Fracture Problems". MS Thesis, Univ of Maryland (Aug 1986).

32 Jones, "Numerical Analysis'

33. "Fracture Investigation of a Rotating Disc".

34. L S.Srinath, "Experimental Stress Analysis".